Instituto Universitário de Lisboa

Department of Information Science and Technology

Synchronous Control of Double-Containers for Overhead Crane

Yongshuang Wang

A Dissertation presented in partial fulfillment of the Requirements for the Degree of

Master in Telecommunications and Computer Engineering

Supervisor:

Dr. Octavian Adrian Postolache, Associate Professor

ISCTE-IUL

Co-supervisor:

Dr.Weimin Xu, Associate Professor

Shanghai Maritime University

September, 2019

Resumo

O desenvolvimento e a vasta aplicação de pontes rolantes de duplo espalhamento tem melhorado a eficiência de carga e descarga dos terminais de contentores. No entanto devido ao facto das variações não lineares do tempo e a perturbação dos parâmetros do dispositivo de elevação de duplo espalhamento, é dificultado o controlo sincronizado e coordenado. Com o objetivo de resolver o problema do controlo síncrono das pontes rolantes de duplo espalhamento, este projeto usa o modelo matemático do guindaste de dupla propagação e propõe dois métodos de resolução. O controlo baseado no método do modo deslizante difuso. O controlo lógico difuso pode estimar eficazmente os parâmetros do sistema, reduzir a vibração do controlo do modo deslizante e melhorar o seu desempenho. O control de sincronização do acoplamento do desvio médio, combinado com o control do modo deslizante que pode controlar eficazmente o erro de velocidade entre os dois espalhadores, para que o seu trabalho possa continuar de forma síncrona. O outro controlador usa um controlo rápido e não singular do modo de deslizamento do terminal para garantir que o sistema possa convergir num tempo limitado. A combinação do control no modo deslizante do terminal e do algoritmo de super rotação pode melhorar a estabilidade do sistema.

Palavras-chave: ponte de rolamento; controlo síncrono; control de modo deslizante; controlo difuso

Abstract

The development and wide application of double spreaders overhead cranes have effectively improved the loading and unloading efficiency of the container terminals. However, due to the nonlinear time-varying characteristics and parameter perturbation of the lifting device of the double spreaders, the difficulty of synchronous and coordinated control of the double spreader overhead crane is increased. In order to solve the problem of synchronous control of double spreaders overhead cranes, this work establishes the mathematical model of the double spreaders overhead crane and proposes two main methods. The controller based on the fuzzy sliding mode method is established. Fuzzy logic control can effective estimate the parameters of the system, reduce the chattering of sliding mode control, and improve the performance of its control. Mean deviation coupling synchronization control combined with sliding mode control can effectively control the speed error between the two spreaders, so that they can keep working synchronously. The other controller is established which use fast non-singular terminal sliding mode control to ensure that the system can converge in a finite time. The combination of terminal sliding mode control and super twisting algorithm can enhance the stability of the system.

Keywords: overhead crane; synchronize control; sliding mode control; fuzzy control; tracking control

Acknowledgments

Firstly, I would like to express my sincere gratitude to my supervisor, Professor Octavian Postolache, for all the availability and support during the realization of this project.

I would also like to acknowledge my supervisor in China, Professor Weimin Xu, for his patience, motivation and immense.

I would also like to thank my colleagues, Mingming Zhang, Hang Xu, Dongchen Ni, Lin Ma, Yu Jin, Zeyu Ma, Peiyao Tang, for the stimulating discussions, for the sleepless nights we were working together before deadlines, and for all the fun we have had in the last year.

A special thanks to my boyfriend, Shaohua Ye, for his unconditional help, support and encouragement.

Finally, I must express my very profound gratitude to my parents, Tao Wang and Hong Zhou, for giving birth to me at the first place and supporting me spiritually throughout my life.

Content

List of Figures

List of Table

List of Acronyms

PID	Proportional-integral-derivative controller
SMC	Sliding Mode Control
TS Fuzzy	Takagi-Sugeno Fuzzy
T2FC	Type-2 Fuzzy Control
FSMC	Fuzzy Sliding Mode Control
TSMC	Terminal Sliding Mode Control
NFTSMC	Non-singular Fast Terminal Sliding Mode Control
IT2FTSMC	Interval Type-2 Fuzzy Terminal Sliding Mode Control
PI- NFTSMC/PI-TSM	Proportional-integral-Non-singular Fast Terminal Sliding Mode Control

Chapter 1 Introduction

1.1 Motivation

The double-container overhead crane is developed on the basis of a traditional overhead crane. The traditional overhead crane has a double-box lifting spreader. This type of spreader can handle one 40-feet or two 20-feet containers in one lifting operation. In order to improve the loading and unloading efficiency, the double-container overhead crane improved based on the traditional overhead crane is produced. In 2002, BROMMA produced a double-container overhead crane with load-locking mode[1]. The principle is to use a single electric motor, double-reel mechanism and a differential gearbox to achieve double spreaders can do the lifting movement at the same time(as shown in Figure 1.1).

Figure 1.1 The double containers of overhead crane at the working place

Subsequently, Shanghai Zhenhua Heavy Industry Co., Ltd. use double electric motors and double-reel structure to develop a new double-containers overhead crane (as shown in Figure 1.2) [2]. The characteristic of this kind of overhead crane is that it cannot only keep two spreaders synchronously loading and unloading goods during work, but also can complete the loading and unloading work separately after one

spreader stops working. Although the double spreader overhead crane has high work efficiency, there are still some safety hazards in the running process. For example, when the height or speed of the two spreaders are not synchronized during operation, when lifting or lowering the container, there may be a major safety accident such as a collision of the containers or a container falling into the truck[3]. There are many reasons for this accident.

Figure 1.2 The double containers of overhead crane is working in unlock mode

Nowadays, the operation of the overhead crane with double spreaders generally depends on the experienced driver. When the crane driver operates the overhead crane, because the driver's estimate of the position of the spreader may deviate significantly from the actual value, the height of the containers lifted by the driver is not accurate, resulting in the two spreaders not being able to keep running synchronously. The repeated changing synchronous error leads to metal fatigue of mechanical interlock device, which seriously affects the system stability, and causes safety accidents such as box collision and falling box[4]. Based on the above problems, it is stated that the double spreader and its load must maintain high synchronization accuracy during the

loading and unloading process, that is, the height position and running speed of the two spreaders should be the same.

In port operation, there are differences between the imposed speed and the real speed of the operated two containers. In these conditions appear the necessity to find some solutions regarding speed monitoring system that can reduce or eliminate this error. Another problem is other disturbance factors that conduct to speed difference between two containers [5].

A good solution is the development of a synchronization system that can reduce or eliminate this error, too. Therefore, it is necessary to design a synchronous tracking controller for the double lifting overhead crane to ensure the synchronous operation of the double spreaders.

1.2 Objectives

The main objectives of this MSc dissertation are to design a special overhead crane controller for the model of double containers of overhead crane using nonlinear control method. We should achieve three goals.

- According to the nonlinear and time-varying characteristics of overhead cranes, a reasonable mathematical model needs to be established.
- The algorithm suitable for the overhead crane system is selected to establish a synchronous controller to control the speed error between the two spreaders.
- Establish a tracking controller to control the error between the actual speed of the overhead crane and the preset speed.

This controller is capable of real-time control of the two spreaders of the overhead crane, allowing them to operate at the same position and speed. The entire overhead crane controller is divided into two parts, one is the tracking controller, and the other is the synchronous controller. The synchronous controller is the key to ensure that the two spreaders can run synchronously, and the tracking controller is the key to ensure that each spreader can operate at a preset speed. Firstly, for the synchronization problem, this work chooses the appropriate synchronization control strategy and introduces the

synchronization control error into the tracking controller. Secondly, the control method suitable for the overhead crane is selected to eliminate the synchronization error and tracking error of the system（as shown in Figure 1.3）.

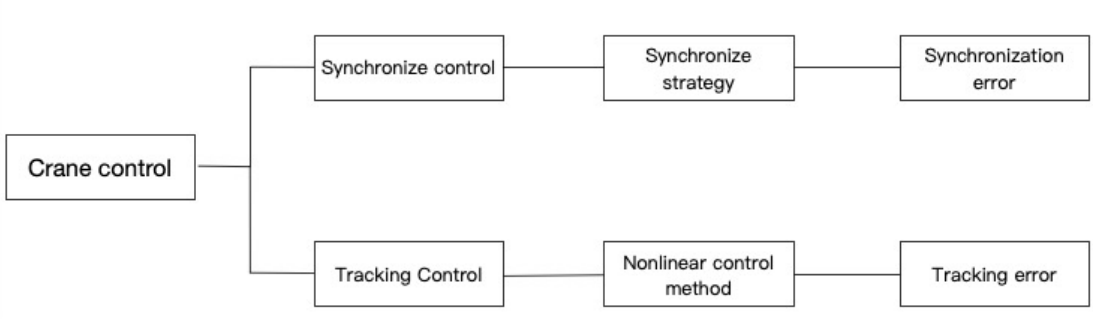

Figure 1.3 Classification of control targets

For the nonlinear, strong coupling, high-order, and time-varying parameters of overhead cranes, traditional control methods cannot control such systems well. Therefore, it is considered to use nonlinear control methods such as fuzzy control and sliding mode control (SMC) to control such systems to improve the steady state and dynamics of the system [6].

In the process of maintaining the double spreader synchronization of the overhead crane, the following points need to be considered, such as the system model is difficult to establish accurately, the model parameters change in real time, and the coupling of the motor affects. In view of this, the controller selects a combination of SMC and fuzzy control to solve the above problem. Finally, the designed double containers overhead crane sliding mode controller can achieve the following three main objectives.

1.3 Research Method

The research method used in this thesis includes literature study, theoretical approach and validation based on numerical simulation. After establishing the problem that needs to be solved, by reading a state-of-the-art scientific literature, we worked to find an optimal algorithm that can solve the problem. The synchronization problem of the

double containers overhead crane studied in this work can find some solutions for synchronous control reported in the literature. For the problem of double spreaders out-synchronization, we can find a suitable solution from multi-motor coupling strategies. When each spreader is unable to operate at a preset speed, by reading the literature, a nonlinear control method can be found to solve this problem. However, the double containers overhead crane model is different from other models in that when the overhead crane is working, the load driven by the motor is affected by gravity, and the motor is driven by the potential energy load. Therefore, we must pay great attention to this when establishing the system model of the double containers overhead crane. The specific control process is shown in the Figure 1.4.

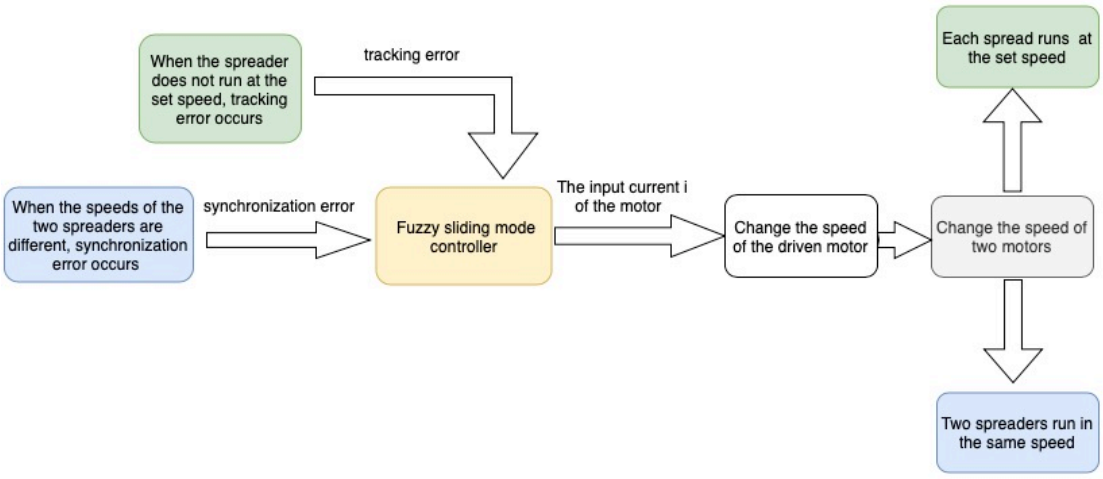

Figure 1.4 Control process block diagram

After the algorithm is established, it is proved by Lyapunov's law. Finally, the experimental method is used to verify the effectiveness of the algorithm. However, due to limited experimental conditions, our proposed control methods are validated through Matlab simulations that highlight the effectiveness of the proposed algorithm.

1.4 Structure of the dissertation

The double containers overhead crane system has the characteristics of strong coupling, nonlinearity and parameter uncertainty. In this work, an in-depth study of fuzzy control, SMC and other intelligent control and nonlinear control methods, a control method based on sliding mode and fuzzy control is proposed. While improving the accuracy of the model, it also greatly alleviates the chattering problem of the sliding mode in the approaching stage [7]. There are still some problems in SMC, such as chattering, input saturation and the inability to converge in a limited time. This work proposes a combination of PID (Proportional-integral-derivative controller) control and non-singular terminal SMC. This control method enhances the stability of the system and reduces the steady-state error of the system, while ensuring that the variables can converge in a limited time. The contents of each chapter of this work are as follows:

Chapter 2——The research status of the synchronous control of double spreaders overhead cranes and the research status of multi-motor synchronous control which is very similar to the double spreaders overhead crane control are expounded in detail.

Chapter 3——According to the goal of synchronous control of double spreader overhead cranes, combined with the actual situation of overhead crane operation, a reasonable model of overhead crane system is established. This chapter describes in detail the process of model building.

Chapter 4——A combination of fuzzy control and SMC is used to design a overhead crane controller with good performance for the control target. This chapter explains the specific structure of this controller.

Chapter 5——A method combining interval type 2 fuzzy control and fast terminal sliding mode is proposed to design the controller.

Chapter 6——The overhead crane model and controller are built by Matlab. The simulation verifies the effectiveness of the algorithm.

Chapter 7——The conclusions and future work are presented.

Chapter 2 State of the Art

The double spreaders of the overhead crane are driven by the motors during operation, and the movement synchronization of the double spreaders is essentially to keep the drive motor of the double spreaders synchronized. This chapter will introduce the research status of multi-motor synchronous control in recent years, as well as the research status of double spreader synchronous control. Meanwhile, some non-linear control methods used in synchronous control will be described.

2.1 Research Status of Multi-motor Synchronous Control

In recent years, with the development of industry, multi-motor synchronous control has also become a research hotspot. Multi-motor synchronous control systems have many applications in industrial manufacturing such as work making and textile. The multi-motor synchronous control system is mainly divided into two parts, one is the synchronous control strategy, and the other is the single motor tracking control method.

2.1.1 Synchronous control strategy

There are two main methods for synchronous control of multiple motors. In the case of physical connections, such as mechanical methods, they are widely used because of their simple structure. However, in this case, the mechanical structure is subject to large wear, so the control accuracy is not high, and the transmission range and distance are limited. If there is no physical connection, only the use of electrical control, there are mainly the following control structures: parallel control, master-slave control, cross-coupling control, virtual line-shafting control, deviation coupling control, ring coupling control, etc[8]. The above synchronous control strategy is divided into a coupled control and an uncoupled control, and the uncoupled control includes: parallel control, master-slave control, virtual line-shafting control. Coupling control includes: cross-

coupling control, deviation-coupling control, ring-coupling control. The classification of synchronization control strategies is shown in Figure 2.1.

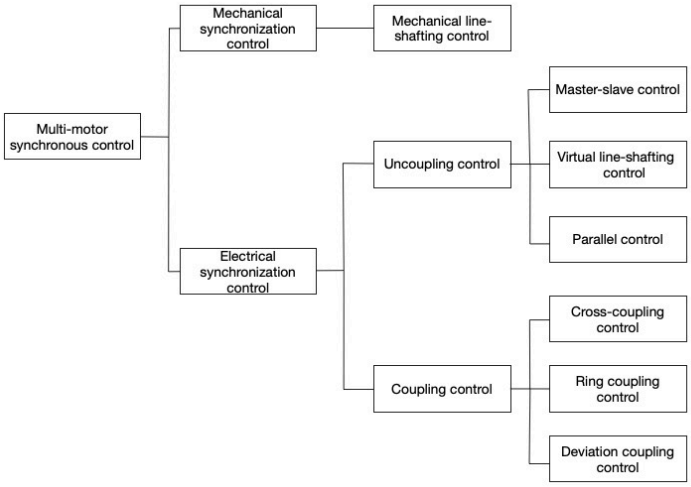

Figure 2.1 The classification of synchronous control strategy

The controller must consider three factors when controlling the motor.

1. Reference signal: Preset speed of each motor.

2. Tracking error: The speed difference between the reference speed and speed of the motor.

3. Synchronization error: The speed difference between two adjacent motors.

According to the characteristics and performance of different synchronous control strategies, the strategy suitable for the overhead crane is selected. The double spreaders of the overhead crane can keep the speed and position synchronized during operation.

2.1.2 Parallel coupling control

The principle of parallel coupling control is to give each motor the same preset speed signal to ensure that all motors can run at the same speed [9]. Its structure is shown in the figure 2.2.

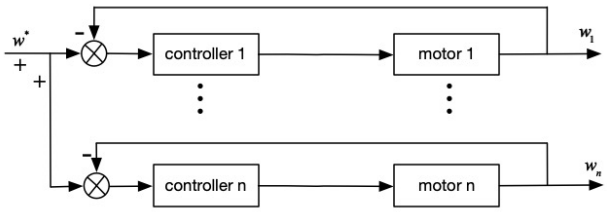

Figure 2.2 Parallel synchronous control

(Where w^* is reference signal, w_n is motor speed, n=1,2,3…)

However, since the motors are completely guaranteed to be independent, if any of the motors is disturbed, it cannot operate at the preset speed. In the case of disturbances, there is no guarantee that all motors will operate at the same speed. The structure of parallel synchronous control can only be used in industries where the accuracy of the synchronous speed of the motor is not high.

2.1.3 Master-slave control

The principle of master-slave synchronous control of the motor is to add a preset speed signal to the main motor, and other motors obtain the speed signal through the main motor[10]. Such a synchronous structure is simple (as shown in the figure 2.3), and each motor can be controlled by a separate controller without affecting each other.

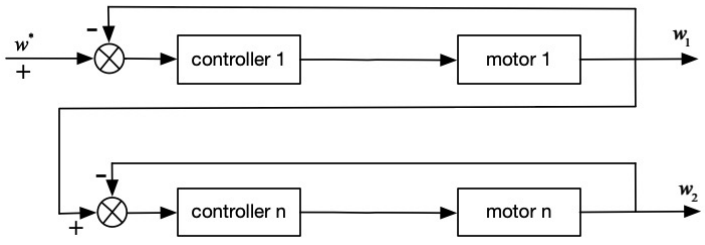

Figure 2.3 Master-slave synchronous control

(Where w^* is reference signal, w_n is motor speed, n=1,2,3…)

However, if the intermediate stage motor is affected by the disturbance, the output speed signal may not coincide with the speed signal transmitted by the main motor, so that the latter motor cannot run at the speed.

2.1.4 Virtual line-shafting control

The virtual line-shafting synchronous control is generated according to the evolution of the master-slave synchronous control. The torques of each axis are added, and the added results are fed back to the virtual line-shafting[11].

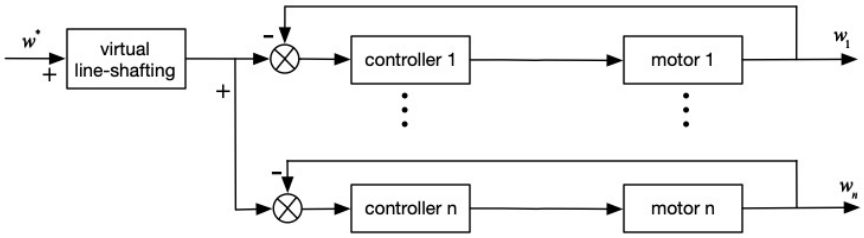

Figure 2.4 Virtual line-shafting synchronous control

(Where w^* is reference signal, w_n is motor speed, n=1,2,3…)

The virtual line-shafting is calculated to obtain the reference signals of each axis, and the signal is easily tracked, thus improving the synchronous control performance of the control system. Meanwhile, this control method also avoids the resonance of the mechanical system. The virtual internal axis system introduces inertia during control, making it difficult for the control system to track the input signal.

Although this method improves the synchronization performance of the system, it reduces the responsiveness of the input signal. The structure of the virtual master axis synchronization control mode is shown in Figure 2.4.

2.1.5 Cross-coupling control

The cross-coupling control strategy was proposed by Koren in 1980 [12]. The principle of its control is to compare the speed signals between the two motors and then

compensate according to the difference. The control structure is as shown in the Fig. 2.5. If the motor 1 and the motor 2 generate a speed difference, after the comparison calculation, the controller will compensate the two motors separately, so that the two motors can ensure the same speed during operation.

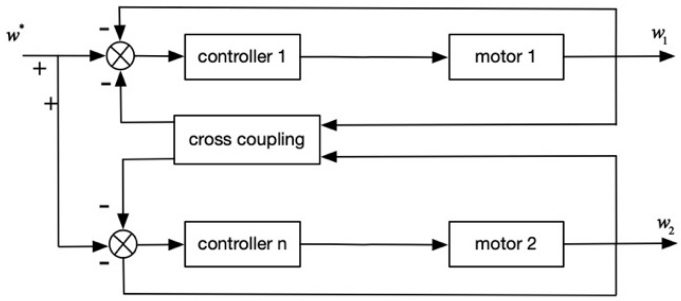

Figure 2.5 Cross-coupling control

(Where w^* is reference signal, w_n is motor speed, n=1,2,3…)

The biggest difference between this control method and the control method mentioned above is that if the motor is affected by disturbance during parallel control and master-slave control, the speed of motor operation cannot be consistent, but cross-coupling control can compensate for the influence of disturbance to solve this problem. The main feature of the cross-coupling control strategy is to compare the speed signals of the two motors to obtain a difference as an additional feedback signal. The feedback signal is used as a tracking compensation signal, so that the system can accept the load change of any one motor. Thereby obtaining good synchronization control accuracy. However, the disadvantage of this control method is that it is not suitable for more than two motors.

2.1.6 Deviation coupling control

Perez-Pinal et al. proposed a deviation coupling control structure in 2003[13]. The basic idea is to compare the speed signals of any two motors in a multi-motor system

and add the resulting speed deviation signal as compensation to the input signal of the motor. The structure of the deviation coupling synchronous control method is shown in Figure 2.6.

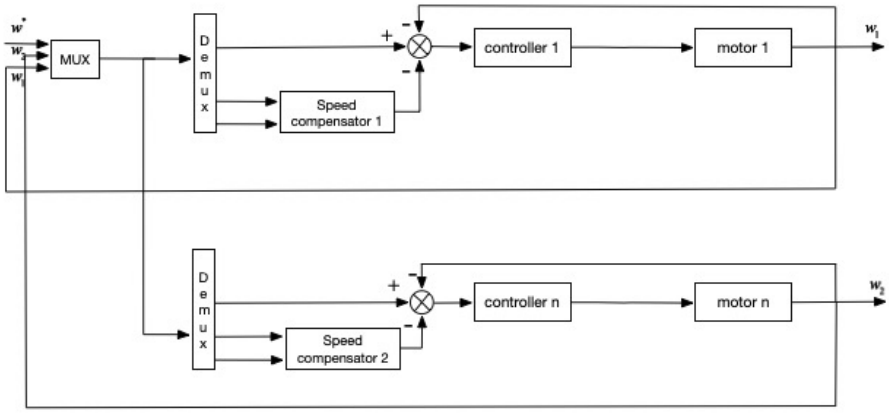

Figure 2.6 Deviation coupling control

(Where w^* is reference signal, w_n is motor speed, n=1,2,3…)

Because the method of deviation coupling control couples the motors of the system to form a closed-loop structure, when any motor is disturbed, other motors can adjust the speed in real time and accurately, thus achieving higher speed synchronization performance. Although the deviation coupling control method is applicable to the case where the number of motors in the system is greater than two, when the number of motors increases, the structure of the control system may be more complicated.

2.1.7 Ring coupling control

Liu Ran et al. proposed a ring coupling control method, which is based on parallel control[14]. The basic idea of the ring coupling control strategy is to give all motors the same reference signal and then give the motor compensation signal based on the speed difference of the adjacent motor. The specific control process is shown in figure 2.7.

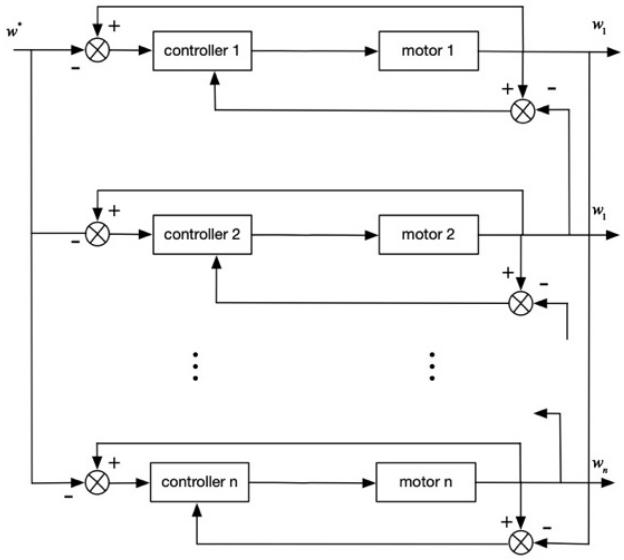

Figure 2.7 Ring coupling control

(Where w^* is reference signal, w_n is motor speed, n=1,2,3…)

The controller adjusts the speed of the motor according to the above three factors. Because the motors are coupled in pairs, they are called ring coupling control. The control strategy can not only ensure the synchronization performance of the system, but also greatly reduce the complexity of the control structure of the system.

However, it still has some shortcomings. Since the motor only considers the speed between two adjacent motors, it takes some time to complete the control of all the motors.

2.2 Research Status of tracking Control Method

The tracking control method is based on the nonlinear control method. For the characteristics of the model of the double-containers overhead crane, such as the uncertainty of the system model and the system is subject to external disturbances, the control method suitable for the model is selected[15]. The tracking algorithm is improved according to the requirements of the control object. The most commonly

used control methods in the literature are PID control, neural network control, fuzzy control, and SMC, etc.

PID control is integral, differential and proportional control[16]. However, PID control is less robust. For nonlinear systems such as overhead crane, they have the characteristics of nonlinearity and strong coupling. Therefore, the PID control method is not effective.

Neural network control has good self-learning ability and adaptability, but its self-learning requires more time. In systems with high real-time requirements, using neural network control, the response of the system will be delayed[17].

Fuzzy control is the use of fuzzy logic to achieve self-adjustment of controller parameters, so that the dynamic and static response of the motor is optimal. The fuzzy approximation property is used to approximate the uncertainty of the system to improve the anti-interference ability and robustness of the system[18].

Sliding mode variable structure control can control controlled objects without accurate model[19]. It adopts the control switching rule to generate the motion of the state trajectory according to the predetermined “sliding mode” by switching between different control actions, so that the system state reaches the desired point. However, this algorithm also has disadvantages.

This kind of control will inevitably have chattering, which means that the corresponding curve of the system will vibrate under the sliding mode switching line(as shown in figure 2.8) according to a certain amplitude and frequency. Such a phenomenon will have a negative effect on the system.

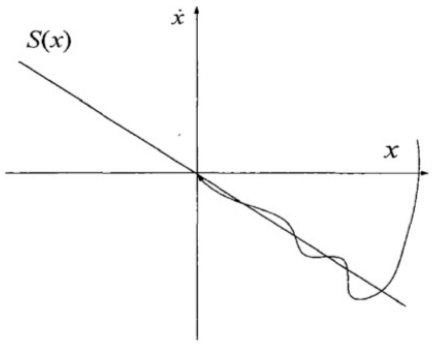

Figure 2.8 The diagram of sliding mode motion

(S is the surface of the sliding mode, x is the state variable)

For the double-containers overhead crane synchronization model, this work combines the advantages of fuzzy control and sliding mode control to control the system. The Takagi-Sugeno fuzzy control is used to estimate the uncertainty of the system effectively [20], which suppresses the chattering problem of the sliding mode control in the approaching stage. Although TS-fuzzy can solve the problem proposed in this work, because of its large amount of calculation, this algorithm will reduce the system's response ability.

2.2.1 Fuzzy Logic control

Fuzzy control is based on fuzzy set theory, fuzzy language and fuzzy logic. It is the application of fuzzy mathematics in control systems and is a kind of nonlinear intelligent control[21].

Fuzzy control is a method of controlling the control object by using human knowledge. It is usually expressed in the form of "if condition, then result", so it is also called language control. Fuzzy control is generally used for control object models that cannot be accurately established. This type of model can be well controlled using the experience and knowledge of skilled experts. Therefore, the method of using human intelligence to control is fuzzy control.

The core part of fuzzy control is the fuzzy controller. As shown in the figure 2.9, the basic structure of the fuzzy controller includes four parts: knowledge base, inference, fuzzification interface, defuzzification interface.

(1) Knowledge base

The knowledge base includes a fuzzy controller parameter library and a fuzzy control rule base. Fuzzy control rules are based on linguistic variables. The linguistic variables use fuzzy subsets such as "large", "medium", "small", etc., and each fuzzy subset uses a membership function to determine the extent to which the exact value on the basic domain belongs to the fuzzy subset. Therefore, in order to establish the fuzzy control rule, the exact value on the basic domain needs to be assigned to each fuzzy subset according to the membership function, so that the exact value is replaced by the linguistic variable value (large, medium, small, etc.).

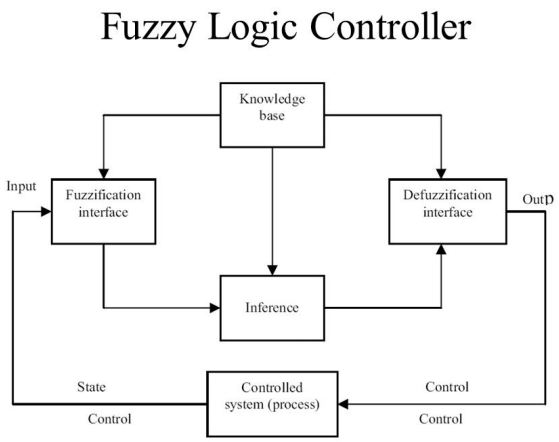

Figure 2.9 The structure of fuzzy control[22]

Because each variable has a different range of values, each of the basic domains should be mapped to a standardization domain with different correspondences. In general, the correspondence is taken as a quantization factor. In order to facilitate the processing, divide the standard domain into equal parts. Then we should fuzzify each domain and define fuzzy subsets, such as NB, PZ, PS, etc.

(2) Fuzzification

The fuzzification process is a process of converting the determined value of the fuzzy controller input variable into the corresponding fuzzy linguistic variable value, and the corresponding linguistic variable value is defined by the corresponding membership function. Through such a process of mapping the input variables to the appropriate corresponding domain, the precise input data is transformed into the appropriate linguistic variable value or the identifier of the fuzzy subset.

However, there are many types of membership functions, and the appropriate membership function is selected according to the characteristics of the input variables.

In the process of fuzzy control, the membership function plays a very important role.

Generally, the types of commonly used membership functions can be divided into the following three categories:

The most commonly used membership functions are the triangle function, the trapezoid function and the Gaussian function.

1. Triangle function

$$\mu_{A_i}(x)=\begin{cases}\dfrac{1}{b-a}(x-a), a\le x<b\\ \dfrac{1}{b-c}(u-c), b\le x\le c\\ 0, \quad else\end{cases} \tag{2.1}$$

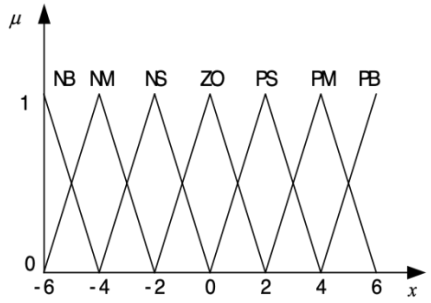

Figure 2.10 The two-dimensional diagram of the triangle membership function

Where NB, NM, NS, ZO, PS, PM, PB are the fuzzy set. NB=Big Nagetive, NM= Middle Nagetive, NS=Samll Nagetive, ZO=Zero, PS=Small Posive, PM= Middle Postive, PB=Big Postive. x is the domain of the fuzzy set, μ is the degree to which the input variable is related to each fuzzy set.

2. Trapezoid function

$$\mu_{A_i}(x)=\begin{cases}\dfrac{x-a}{b-a}, a\le x<b\\ 1, \quad b\le x\le c\\ \dfrac{d-x}{d-c}, c<x\le d\\ 0, \quad else\end{cases} \tag{2.2}$$

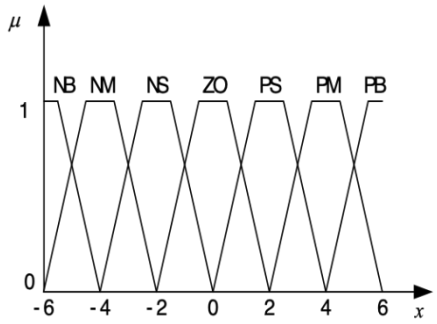

Figure 2.11 The two-dimensional diagram of the trapezoid membership function

3. Gaussian function

$$\mu_{A_i}(x)=e^{-\frac{(x-a_i)^2}{b_i^2}} \tag{2.3}$$

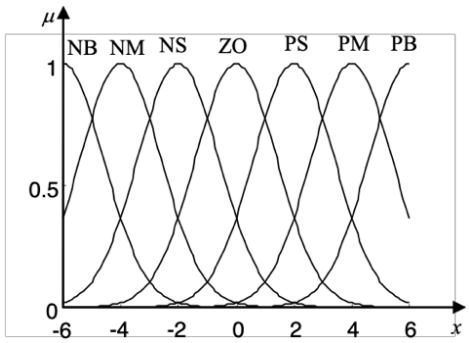

Figure 2.12 The two-dimensional diagram of the gaussian membership function

(3) Inference

According to the relationship between fuzzy variables, the fuzzy output variable is inferred. The example of fuzzy inference:

R1 : IF E is A1 AND EC is B1 THEN U is C1

R2 : IF E is A2 AND EC is B2 THEN U is C2

…… …… ……

Rn : IF E is An AND EC is Bn THEN U is Cn

(4) Defuzzification

The fuzzy subset obtained by inference is converted to an exact value to obtain the final control variable y. Two methods of defuzzification are currently used:

1、Maximum membership defuzzification. In the fuzzy subset obtained by inference, the average value of the standard domain elements with the largest degree of membership is selected as the precision result.

2、Center-average defuzzification. Through fuzzy inference, the membership function of the fuzzy subset of the output variables can be obtained. Take the graph enclosed by the membership function and the abscissa and find the center of gravity of the graph. The value in the standard domain corresponding to this center of gravity is taken as the result of the defuzzification.

2.2.2 Sliding mode variable structure control

Sliding mode variable structure control is a method of control proposed by Soviet scholars in the early 1960s. Sliding mode control is a special type of nonlinear control. Sliding mode control is a non-linear control technique that uses discontinuous control signals to adjust the characteristics of a nonlinear system, forcing the system to slip between the normal states of the two systems, and finally to a steady state. That is, it has a switching characteristic that changes the structure of the control system over time. This control feature can force the state of the system to be limited to movement on a certain submanifold. The control law may switch from one continuous control system to another continuous control system depending on the current position in the state space[23]. Therefore, the sliding model control belongs to the variable structure control.

Sliding modal control can still be designed in cases where the controlled object model is unknown, or the model is disturbed. This makes the sliding mode variable structure control have the advantages of strong robustness, fast response, no need for online recognition of the system [24], and simple physical implementation. Nowadays, the application research of SMC has made great progress, involving almost all control fields, such as: sliding mode control of aircraft and spacecraft, sliding mode control of electric and power systems, sliding mode control of robots, sliding mode control of intelligent transportation systems, sliding mode control of hybrid systems, etc.

The sliding mode variable structure control process is divided into two stages, the first stage is the approaching process before reaching the sliding mode, and the second stage is the sliding process after reaching the sliding mode surface(as shown in figure 2.13).

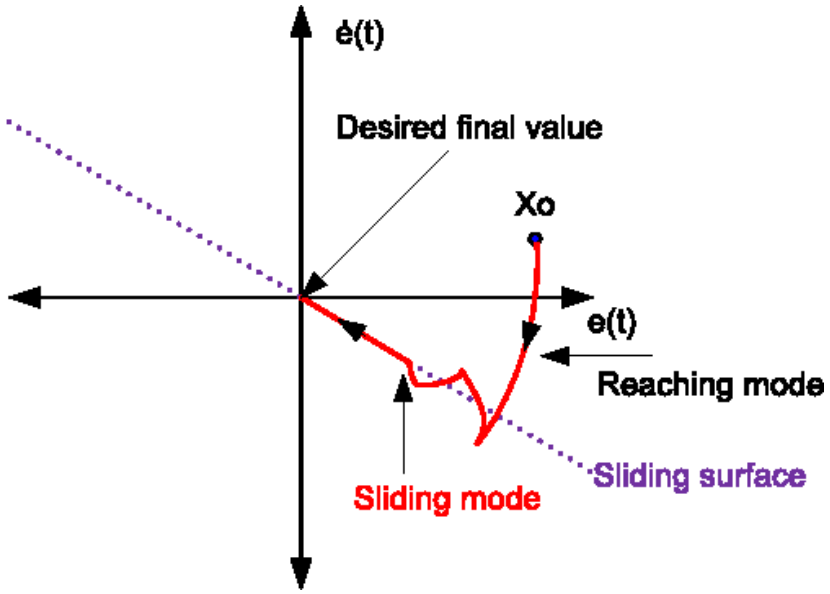

Figure 2.13 Detailed description of the sliding mode movement at each stage

(where X_O is a dynamic variable, e is the tracking error of the system state)[25]

The condition of the sliding mode variable structure design is that the sliding mode surface and its first derivative are zero. Equation 2.4 is an example of a normal sliding surface. The condition of the sliding mode variable structure design is that the sliding mode surface and its first derivative are zero. When the system is in the approaching process, the above characteristics will not be satisfied, and the robustness of the system cannot be guaranteed when it is disturbed.

$$s = ce \tag{2.4}$$

Where s is the switching surface, e is the tracking error of the system state. c is a variable parameter, which varies with the requirements of the system.

The design of the sliding surface is the core part of sliding mode variable structure control. The quality of the sliding surface design determines the performance of the system, and it also relates to the stability of the system. There are many design methods for sliding surface. Traditional sliding mode control includes time-varying sliding mode control, terminal sliding mode control, integral sliding mode control, and piecewise linear sliding mode control.

2.2.3 Time-varying sliding mode control

The time-varying sliding mode control is a variable structure controller with a full-sliding mode. Under the action of the controller, the arrival motion phase of the sliding mode control is eliminated, and the system is robust in the whole process of response. It overcomes the feature that the arriving process in traditional variable structure control is not robust[26]. The time-varying sliding mode control can be changed with the state or time of the system, so that the system is always in the sliding mode state, thereby eliminating the arriving process and improving the robustness of the system. Combined with intelligent control, how to design a time-varying sliding surface is an important part of sliding surface research.

2.2.5 Integral sliding mode control

When using the general sliding mode variable structure control to track the trajectory, if the system is subject to external disturbance, it may bring steady-state error and fail to achieve the required performance. Integral sliding mode control is to increase the integral term of the state variable in the linear sliding mode surface. Because the sliding mode surface contains the integral of the state variable, the chattering can be weakened and the steady state error can be reduced[27]. However, the integral term also has an additive effect, which may cause large overshoot or drive mechanism saturation when the initial state is large.

2.2.6 Terminal sliding mode control

Traditional sliding mode control uses a linear sliding surface. The benefit of this sliding surface is that the system response is completely insensitive to the system's uncertain parameters and to external disturbances. However, the disadvantage of conventional sliding mode control is that the convergence of the system state to the equilibrium point is asymptotic, rather than for a limited time[28]. Nowadays, the research of terminal sliding mode controller has attracted people's attention. It has some good characteristics, such as the system state can converge to zero in a limited time and has higher steady-state accuracy than the traditional linear sliding mode controller.

The overhead crane system has the characteristics of time-varying and non-linearity. During its operation, the parameters of the system will be perturbed, and the system will be subject to uncertain disturbance. So, the fuzzy sliding mode algorithm based on mean deviation coupling is been chosen to solve the above problems. The algorithm effectively suppresses the chattering problem of sliding mode control in the approaching stage and has a certain inhibitory effect on the uncertain disturbance.

Chapter 3 Overhead Crane Model and Controller Design

3.1 Mathematical model of double spreaders of overhead crane in two modes

The double-containers overhead crane consists of two independent spreader hoisting systems, which can be selected according to different working conditions. When the double spreader works in the independent working mode, the two spreaders can be lifted independently; when the double spreader works in the interlock mode, the two spreaders are lifted at the same time, and there is a strong coupling between them. The mathematical models in the two working modes are respectively established below.

3.1.1 Mathematical model in independent working mode

The double-container overhead crane consists of parallel runways, two trolleys, two hoists, the lifting component of a crane. As shown in Figure 3.1, trolleys and cranes run along their respective tracks. The trolley is equipped with two separate lifting motors and winding wheels. After the adjustment of the trolley and crane, the double spreaders are aligned with the position for loading and unloading the containers.

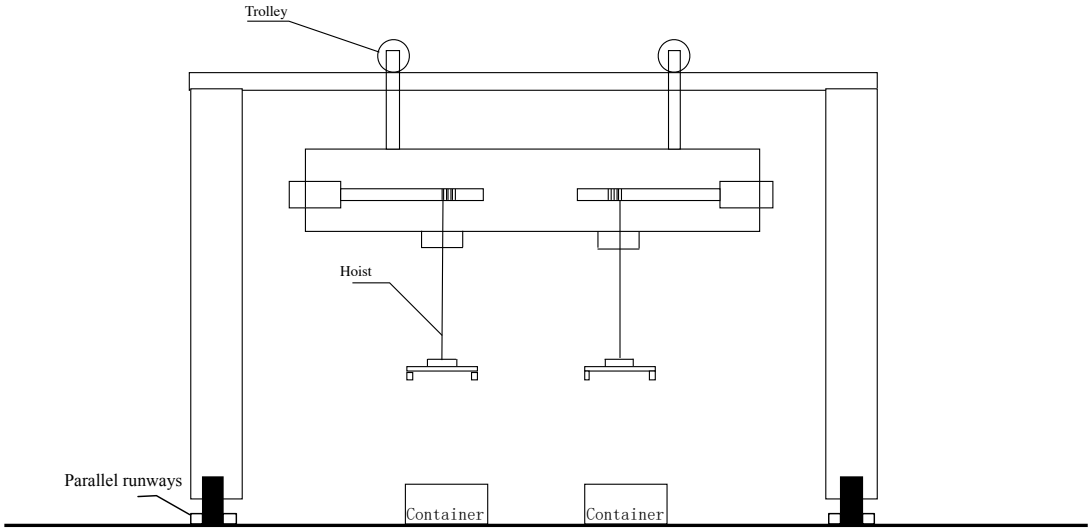

Figure 3.1 The structure diagram of double-container overhead crane

The double-container overhead crane consists of a system of double spreaders, spare wheel, lifting rope and drive motors (Figure 3.2). Each spreader system is equipped with a drive motor, a lifting rope and a spreader.

The spreader is driven by an induction motor. During the operation of an overhead crane, if two drive motors produce changes in system parameters, they will not be at the same angle or position. This causes the double spreaders to not run synchronously, which can cause the container to collide and is very dangerous. Therefore, it is important to keep the two spreaders running at the same time, that is, keep the two drive motors running synchronously.

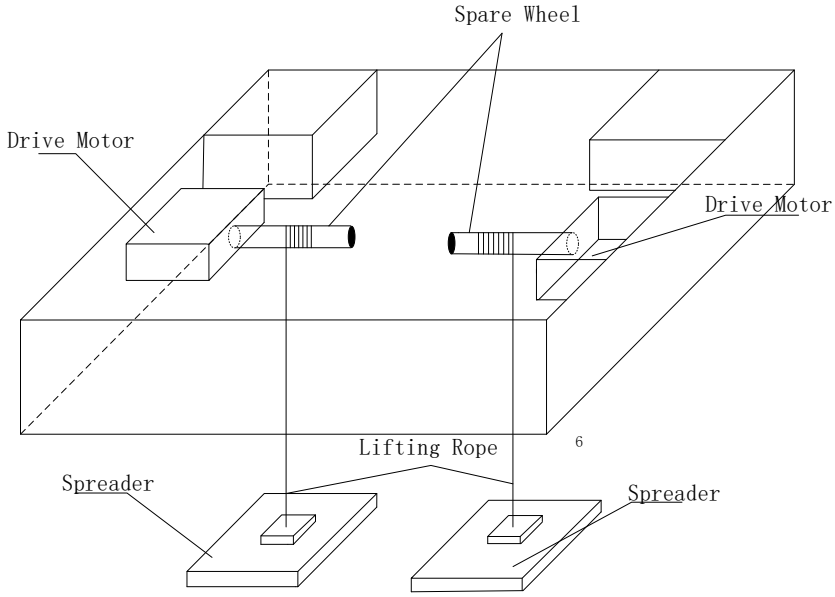

Figure 3.2 The structure diagram of double-container overhead crane

Taking the spreader i as an example, when the rotor field is oriented, the spreader i drives the motor to rotate synchronously, and the nonlinear mathematical model in the d-q coordinate system[29] can be written as:

$$\frac{d}{dt}\begin{bmatrix}\dot{\theta}\\ \psi_{dr}\\ i_{ds}\\ i_{qs}\end{bmatrix}=\begin{bmatrix}\mu(t)\psi_{dr}i_{qs}-\frac{1}{J}\left[B_m(\dot{\theta})\theta+G+\tau_f(\dot{\theta})+\tau_d(t)\right]\\ -\alpha(t)\psi_{dr}+\alpha(t)Mi_{qs}\\ -\gamma i_{ds}+\alpha(t)\beta(t)\psi_{dr}+n_p\dot{\theta}i_{qs}+\frac{\alpha(t)Mi_{qs}^2}{\psi_{dr}}\\ -\gamma i_{qs}+\beta(t)n_p\dot{\theta}\psi_{dr}-n_p\dot{\theta}i_{qs}+\frac{\alpha(t)Mi_{qs}i_{ds}}{\psi_{dr}}\end{bmatrix}+\frac{1}{\sigma L_s(t)}\begin{bmatrix}0&0\\0&0\\1&0\\0&1\end{bmatrix}\begin{bmatrix}u_{ds}\\u_{qs}\end{bmatrix} \tag{3.1}$$

Table 3.1 Model variable representation

Variable	Symbol
mechanical angular position	θ
d-axis rotor flux	ψ_{dr}
d-axis stator currents	i_{ds}
q-axis stator currents	i_{qs}
d-axis stator voltages	u_{ds}
q-axis stator voltages	u_{qs}
pole pair number	n_p
moment of inertia	J
nonlinear viscous drag coefficient	$B_m(\dot{\theta})$
external nonlinear perturbation torque	$\tau_d(t)$
the friction torque	$\tau_f(t)$
motor leakage inductance coefficient	$\mu_i(t), \beta_i(t),$ $\alpha_i(t), \gamma_i(t)$

The equation for the electromagnetically controlled torque T_c is described as:

$$T_c=\frac{3n_p\left(\psi_{dr}+\left(L_d-L_q\right)i_{ds}\right)i_{qs}}{2} \tag{3.2}$$

Where L_q and L_d are the inductances of the q-axis and the d-axis, respectively[30]. The model of the induction motor can be described as:

$$J\ddot{\theta}(t)+B_m\dot{\theta}(t)+G_i=T_c \tag{3.3}$$

In Equation (3.3), G is the gravity torque, which is related to the working mode of the spreader. When the double spreaders are in the independent working mode, G is described as follows:

$$G_i=m_igR \tag{3.4}$$

Where m_i is the sum of the mass of the spreader i and its load, g is the acceleration of gravity, and R is the radius of the wheels. It can be seen that when the double spreader is in the independent working mode, the load of each spreader is independent of each other and has no coupling effect.

By using the field-oriented mechanism with i_d^* =0, we can obtain:

$$T_c=K_Ti_{qs} \tag{3.5}$$

$$K_T=\frac{3n_p\psi_{dr}}{2} \tag{3.6}$$

In order to facilitate the design of the controller, the motor reference model is as follows:

$$J_r\ddot{\theta}_r(t)+B_{mr}\dot{\theta}_r(t)=K_{Tr}i_{qsi} \tag{3.7}$$

Where J_r is the moment of inertia, B_{mr} is the reference viscosity coefficient, θ_r is the reference rotation angle position, K_{Tr} is the reference electromagnetic torque coefficient, i_{qsi} is the reference control input.

Consider the dynamic equation of the induction motor described in Equation (3.5)(3.6) is:

$$J_r\ddot{\theta}_r(t)+B_{mr}\dot{\theta}_r(t)=T_c-T_L \tag{3.8}$$

Where T_L is the load torque. For the convenience of calculation, the reference model of the motor obtained by equation (1)(6) as follows:

$$\ddot{\theta}_i=A(t)\dot{\theta}_i+L(t)i_{qs} \tag{3.9}$$

Where $A(t) = -B_{mr}/J_r$, $L(t) = K_{Tr}/J_r$, and B_{mr} and K_{Tr} are parameters of the system that change with time.

3.1.2 Mathematical model in interlock mode

The interlock mode is to connect between the two spreaders with an interlocking lever. The function of the interlocking lever is to maintain the balance of the two spreaders when the two spreaders are at different speeds or different heights. Figure 3.3 shows the operation of the overhead crane in the interlock mode.

Figure 3.3 The double containers of overhead crane is working in interlock mode

In order to facilitate the analysis of the forces on the spreader, a simplified schematic diagram(as shown in figure 3.4) of the bridge crane interlocking model is presented.

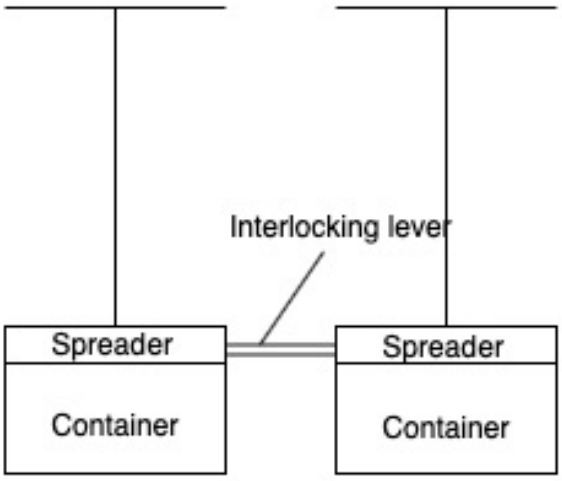

Figure 3.4 The structure diagram of interlock mode

Assume that the masses of the two spreaders and their loads are m_1 and m_2, the rope length AC of the spreader 1 is l_1, the length of the rope laid by the spreader 2 is l_2 , and the length of the connecting rod used for the interlock is L. The angle of the identifier is as shown.

The situation shown in Figure 3.5(a) is that $0 \le l_1 - l_2 < L$, rigid link has a force between the two spreader loads. The force of the rod against the mass points C and D is shown in Figure 3.5(b).

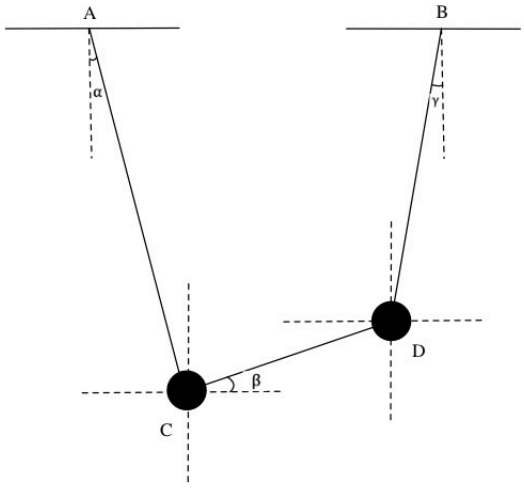

Figure 3.5(a) Schematic diagram of the positional relationship of the double spreaders

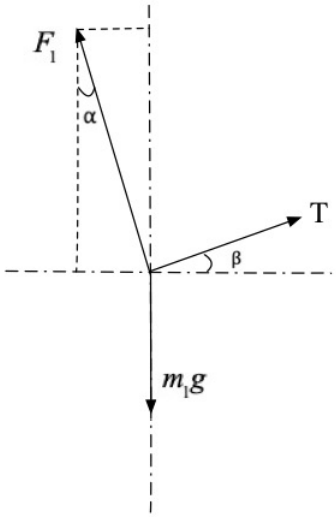

Figure 3.5(b) Schematic diagram of the positional relationship of the double spreaders

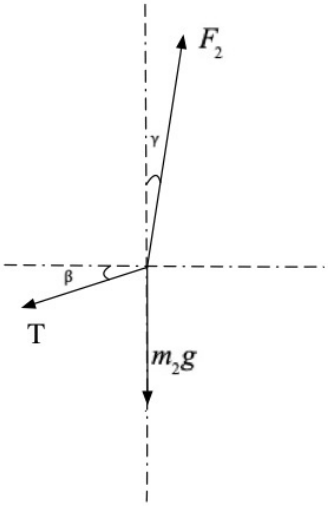

Figure 3.5(c) Schematic diagram of the positional relationship of the double spreaders

Where F_1 and F_2 are the tension of the two spreaders respectively.

According to Figure 3.5(b) the force analysis of the spreader can be carried out in the double spreader interlock mode. The gravity torque term G_i of the drive motor is expressed as follows:

$$G_i = \begin{cases} m_i gR + m_{i+1} gR, & l_i - l_{i+1} \le -L \\ m_i gR + m_{i+1} gR \left| \dfrac{l_i - l_{i+1}}{L} \right|, & -L < l_i - l_{i+1} \le 0 \\ m_i gR \left(1 - \left| \dfrac{l_i - l_{i+1}}{L} \right| \right), & 0 \le l_i - l_{i+1} < L \\ 0, & l_i - l_{i+1} \ge L \end{cases} \tag{3.10}$$

In Equation 3.8, the rope length l1 and the rope length l2 are variables which can be obtained by the corresponding rope length detecting means or by the encoder of the driving motor. Applying Equation (3.4) to the speed Equation (3.1) of the motor, the mathematical model of the overhead crane in the interlocking mode can be obtained.

3.2 Controller structure

In view of the subject of synchronous control of bridge cranes, the following problems need to be solved:

1、Since the precise mathematical model of the bridge crane is difficult to obtain, how to build a controller that does not rely on the model?

2、How to ensure that the system is not disturbed in the presence of external disturbances and internal uncertainties?

3、How to improve the synchronization performance of the overhead crane?

Aiming at the requirements of the above-mentioned problems, the fuzzy sliding mode algorithm based on average deviation coupling is proposed to solve the above problems. The algorithm effectively suppresses the chattering problem of sliding mode control in the approaching stage and has a certain inhibitory effect on the uncertain disturbance. Finally, the effectiveness of the algorithm is demonstrated by Matlab simulation.

3.3.1 Synchronization strategy

In the second chapter, several mainstream synchronous control strategies are introduced in detail. Parallel coupling control strategy cannot restore the motor to the preset speed when it is subjected to external disturbance. The master-slave control strategy control structure is simple, and the interference received by the main motor will be transmitted to the slave motor, but the reverse is not possible. In the virtual-shaft control strategy, the system input needs passing through the virtual axis to get the reference signal of motor, which results in the unequal between motor's reference signal and the system input signal. Cross-coupling strategy can only reflect the difference between adjacent motors[31] and cannot take care of the difference between all motor speeds. In view of this, the mean deviation coupling control strategy is a good solution to this problem. Compare to the ring coupling control strategy, the mean deviation coupling control reduce calculations and enables all motors to achieve speed synchronization faster.

Mean deviation coupling proposed in this work which can ensure the synchronization performance of multiple motors and reduce complexity of the control structure with the increasing number of motors[32]. This also solves the mentioned problems that need to improve synchronization performance.

3.3.2 Tracking control method

Tracking control for each spreader is the most important part of the entire controller. While the two spreaders are moving synchronously, each spreader must also be operated at a preset speed without being disturbed.

Through the modeling and analysis of the double-container overhead crane in the previous section, it can be clearly seen that the overhead crane is a kind of time-varying, strongly coupled, complex underactuated nonlinear system with various uncertain factors. It is difficult to establish a precise model to describe the double-container potential energy load synchronization system. It is almost impossible to use

mathematical models to completely reflect the controlled object. Even if the mathematical model of the controlled object is established, the model is also simplified on the controlled system. The double-container overhead crane model established in the above section is simplified. It can be seen that there is always a modeling error between the mathematical model of the controlled object and the actual model. Therefore, it is necessary to design a control method that relies less on model information or does not require model information to realize synchronous coordinated control of overhead cranes.

The sliding mode control chosen in this work is such a kind of nonlinear control method that does not depend on the model. Sliding mode control can overcome the uncertainty of the system, it has strong robustness to interference and unmodeled dynamics[33].

In the process of sliding mode control, when the state trajectory reaches the sliding mode surface, it is difficult to slide strictly along the sliding mode toward the equilibrium point. Instead, it approaches the equilibrium point back and forth across the two sides, thereby generating chattering[34].

In order to improve the control performance of sliding mode control, this work introduces fuzzy control. The fuzzy control is used to identify the model parameters online, so that the chattering of sliding mode control in the control process is reduced.

The structure of the whole controller is shown in Figure 3.6. The speed information of the two spreaders is sent to the mean deviation coupling controller. Then the sliding mode controller is designed according to the synchronization error and tracking error. The fuzzy controller is used to identify system parameters online and help the sliding mode control further control system.

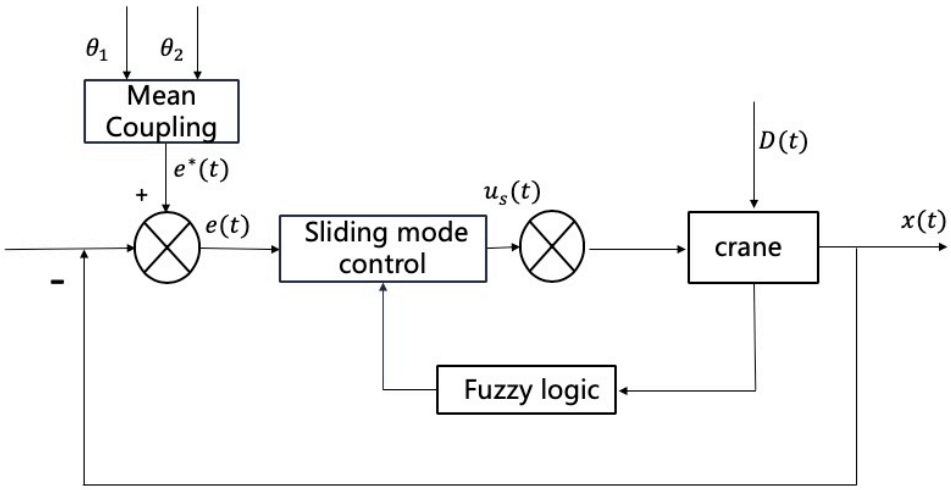

Figure 3.6 Schematic diagram of the controller

As shown in Figure 3.6, for the synchronization error between the two spreaders, this work uses the mean deviation coupling to define. It ensures the accuracy of the synchronization error processed in the controller. For the tracking error in the system, this method selects the combination of sliding mode control and fuzzy control, which further reduces the error of system response.

Chapter 4 Design of Time-Varying Sliding Mode Controller Based on T-S Fuzzy

4.1 Controller structure introduction

The system is mainly composed of fuzzy sliding mode controller and mean deviation coupling controller.

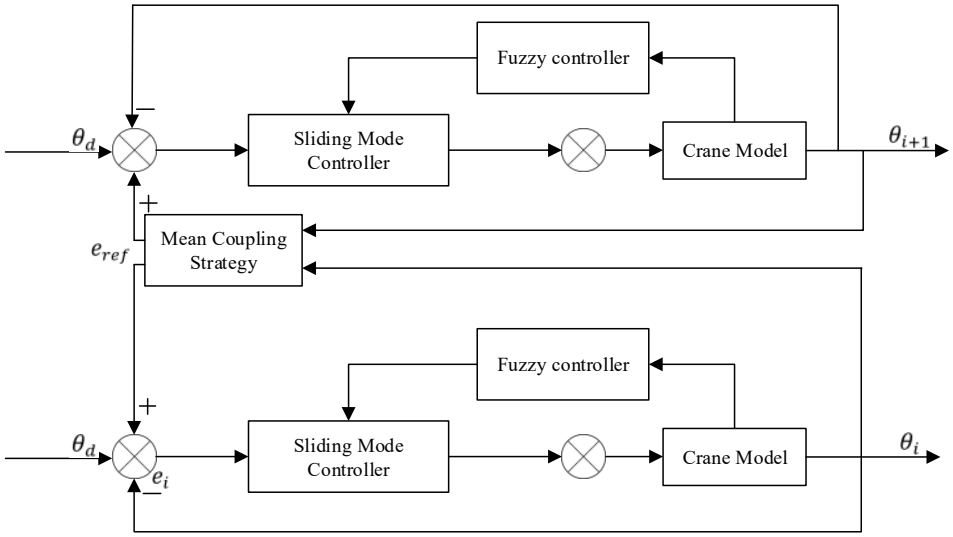

Figure 4.1 Schematic diagram of fuzzy sliding mode controller based on mean deviation coupling

The fuzzy control system is robust and insensitive to parameter perturbations. Thus, the basic idea of the control system is to use the fuzzy control method to fuzzify the control switching law and optimize the design of the control law, thereby further suppressing the chattering in the approaching stage of sliding mode control. The structure of the synchronous controller proposed in this work is shown in Figure 4.1.

4.2 Fuzzy sliding mode controller design

4.2.1 Time-varying sliding mode controller design

Define the two errors required to design the sliding surface, that is, the synchronization error between the two spreaders and the tracking error of the spreader

i. The following model uses the spreader i as an example. The mean deviation coupling synchronization error of the spreader i is:

$$e_i(t)=\theta_i(t)-\frac{\sum_{j=1}^{n}\theta_j(t)}{n} \tag{4.1}$$

The tracking error of the spreader i is defined as:

$$e_{ref,i}(t)=\theta_d(t)-\theta_i(t) \tag{4.2}$$

By the mean deviation coupling error and tracking error of the spreader i, the sliding surface is defined as:

$$s(t)=c_1\dot{e}_{ref}(t)+c_2e_{ref}(t)+c_3\dot{e}_i(t)+c_4e_i(t) \tag{4.3}$$

Where$c1$、$c2$、$c3$、$c4 \in R+$.

The full state control law of the spreader i is described as follows, where u_{swi} is the approach control law and u_{eqi} is the equivalent control law.

$$u=u_{sw}+u_{eq} \tag{4.4}$$

In order to suppress chattering, the exponential approach law is introduced as follows:

$$u_{sw}(t)=-\rho\,\mathrm{sgn}(s(t))-ks(t) \tag{4.5}$$

Where $\rho, k \in R+$, $sgn(s(t))$ is a sign function. For the convenience of calculation, mark $sgn(s(t))$ as $sgn(s)$. By adjusting the parameters k and ρ of the approach law, it can not only ensure the dynamic quality of approaching phase of the sliding mode, but also weaken the high-frequency chattering of the control signal. However, if the value of ρ is too large, the chattering will be aggravated[35].

In order to further ensure the quality of sliding mode control and reduce chattering, this work chooses the method of using saturation function instead of symbol function. The saturation function is defined as follows:

$$sat(S)=\begin{cases}1 & S>\zeta\\ \dfrac{S}{\zeta} & |S|<\zeta\\ -1 & S<-\zeta\end{cases} \tag{4.6}$$

Where $\xi\in$ R+.

Consider Equation (4.5) as:

$$u(t)_{sw}=-\rho sat\left(\frac{s(t)}{\zeta}\right)-ks(t) \tag{4.7}$$

Where $\rho\in$ R+, $k\in$ R+. The size of ρ determines the chattering of the sliding mode in the approaching phase, so ρ should not be too large. For the convenience of calculation, mark $sat(s(t)/\zeta)$ as $sat(s)$.

We can obtain:

$$\begin{aligned}\dot{s}&=c_1\ddot{e}_{ref}+c_2\dot{e}_{ref}+c_3\ddot{e}_i+c_4\dot{e}_i\\&=c_1\left(\ddot{\theta}_d-\ddot{\theta}_i\right)+c_2\left(\dot{\theta}_d-\dot{\theta}_i\right)+c_3\ddot{e}_i+c_4\dot{e}_i\\&=c_1\ddot{\theta}_d+c_2\dot{\theta}_d+c_3\ddot{e}_i+c_4\dot{e}_i-c_1\ddot{\theta}_i-c_2\dot{\theta}_i\end{aligned} \tag{4.8}$$

$$\dot{s}=-\rho sat(s)-ks \tag{4.9}$$

Substituting Equation (4.7) (4.8) into Equation (4.9), the control law can be expressed as:

$$\begin{aligned}u(t)=L_1^{-1}(\theta_i,t)\left[\gamma_i B_{mr}k_{Tr}\left(c_1\ddot{\theta}_d+c_2\dot{\theta}_d+c_3\ddot{e}_i+c_4\dot{e}_i+\rho sat(s)+ks\right)\right]-c_1\gamma_i B_{mr}k_{Tr}\dot{\theta}_i A(\theta_i,t)\\+c_2\gamma_i J_r k_{Tr}\ddot{\theta}_i\end{aligned} \tag{4.10}$$

Where $\gamma_i=\dfrac{1}{c_1k_{Tr}B_{mr}+c_2k_{Tr}J_r}$, control law $u(t)$ is the control current of the motor $i_{qs}(t)$.

In order to ensure the stability of the system, the Lyapunov method is used to prove. Consider the following Lyapunov function:

$$V_0=\frac{1}{2}s^2\geq 0 \tag{4.11}$$

$$\dot{V}_0 = \frac{1}{2} s\dot{s} \tag{4.12}$$

Substituting Equation (4.3) (4.10) into (4.10):

$$\begin{aligned} \dot{V}_0 &= s\dot{s} = s\left(c_1\ddot{\theta}_d + c_2\dot{\theta}_d + c_3\ddot{e}_i + c_4\dot{e}_i - c_1\ddot{\theta}_i - c_2\dot{\theta}_i\right) \\ &= s\left(-\rho sat\left(s\right) - ks\right) \\ &\le -\rho|s| - ks^2 \\ &\le 0 \end{aligned} \tag{4.13}$$

Through the proof of the above equations, it can be stated that the system is stable. The next step to consider is the solution in case the system is disturbed. The parameter perturbation of the system will affect the stability and robustness of the system. The fuzzy control is used to estimate the system parameters in the control rate online, which enhances the stability of the system.

4.2.2 Fuzzy Controller Design

The fuzzy system can approximate any continuous real function on the compact set with arbitrary precision. The fuzzy system is used to approximate the model parameters of the overhead crane and improve the output of the controller[36]. The fuzzy controller is used to estimate the system parameters $\hat{A}(t)$ and $\hat{L}(t)$ online, and the controller is built according to the following fuzzy rules:

$$\begin{aligned} &\text{IF } x_1 \text{ is } M_1^j \text{ , AND, ….,AND } x_n \text{ is } M_n^j \\ &\text{THEN } y \text{ is } N^i \quad (i = 1 \ldots m) \end{aligned} \tag{4.14}$$

Where x is the input variable; M is the fuzzy subset; y is the output. For this fuzzy system, consider the tracking error e and the tracking error rate e_c as the input of the fuzzy system, and the system parameters $A(t)$ and $L(t)$ are the output of the fuzzy system.

The fuzzy set considering the tracking error e and the tracking error rate e_c is [NB NM ZO PM PB][38].

Taking the central average defuzziation method, the output of the system is calculated as follows:

$$y(x)=\frac{\sum_{i=1}^{m} y^i \prod_{j=1}^{n} \mu_{A_j^i}(x_j)}{\sum_{i=1}^{m} \prod_{j=1}^{n} \mu_{A_j^i}(x_j)} \tag{4.15}$$

where $\mu_{A^i}(x)=\prod_{j=1}^{n} \mu_{A_j^i}(x_j)$

$\mu_{A^i}(x)$ is a membership function, considering the Gaussian function as the membership function of the system. The membership function of the input is shown in figure 4.2.

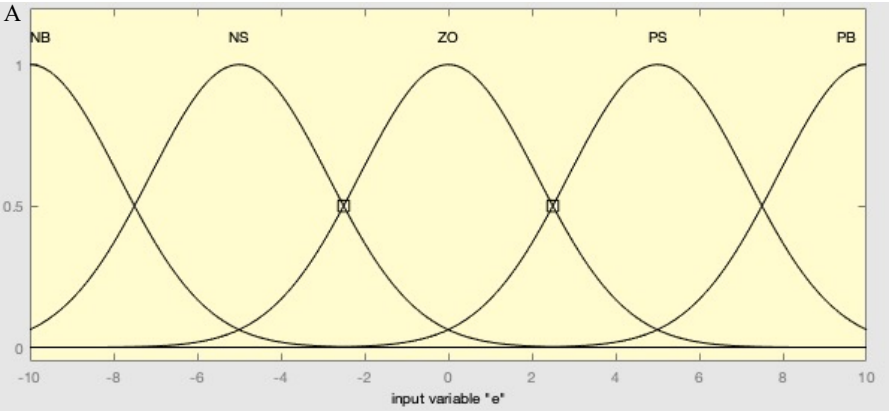

Figure 4.2 Two-dimensional diagram of membership function

(where e is the tracking error, A is the degree to which the input variable is related to each fuzzy set)

Equation (4.15) can also be written:

$$y(x)=\delta^T \phi(x) \tag{4.16}$$

Where $\delta=\left[y^1,\ldots,y^m\right]^T$ is an adaptive vector,

$\phi(x)=\left[\phi^1(x),\ldots,\phi^m(x)\right]^T$ is a fuzzy vector.

The relationship between input and output is shown in figure 4.3.

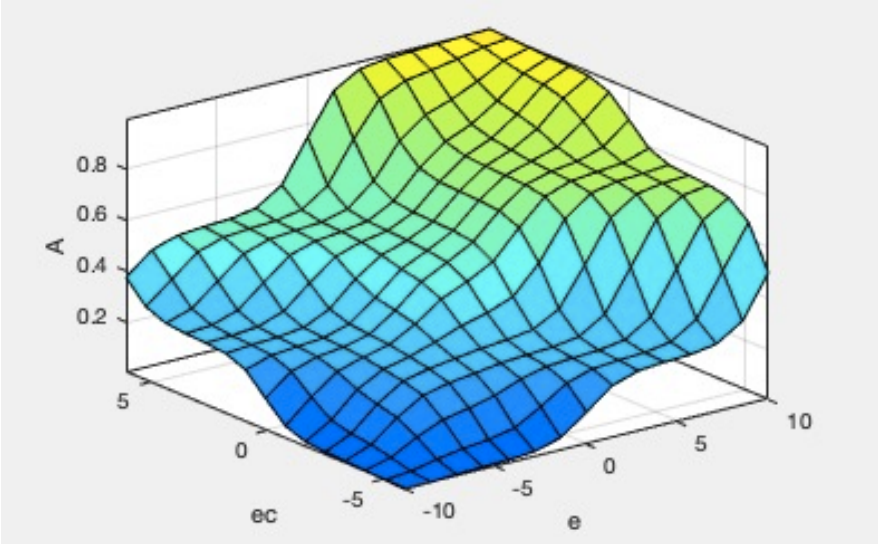

Figure 4.3 3D schematic diagram of membership function

(where e is the tracking error, ec is the rate of change of the tracking error, A is the degree to which the input variable is related to each fuzzy set)

Consider the estimated quantities of A and L as follows:

$$\hat{A}\left(\theta_i,\delta_A\right)=\delta_A^T\phi\left(\theta_i\right) \tag{4.17}$$

$$\hat{L}_1\left(\theta_i,\delta_L\right)=\delta_L^T\phi\left(\theta_i\right) \tag{4.18}$$

Substituting Equation (4.17) (4.23) into (4.10):

$$\begin{aligned} i_{qs}\left(t\right)=&\left(\hat{L}_1\left(\theta_i,t\right)\right)^{-1}\left[\gamma_i B_{mr}k_{Tr}\left(c_1\ddot{\theta}_d+c_2\dot{\theta}_d+c_3\ddot{e}_i+c_4\dot{e}_i+\rho_{ad}sat\left(s\right)+ks\right)\right]\\ &-c_1\gamma_i B_{mr}k_{Tr}\dot{\theta}_i\hat{A}\left(\theta_i,t\right)+c_2\gamma_i J_r k_{Tr}\ddot{\theta}_i \end{aligned} \tag{4.19}$$

Define the minimum estimation error as follows:

$$\beta\left(\theta_i\right)=c_1\dot{\theta}_i\left(A\left(\theta_i,t\right)-\hat{A}\left(\theta_i,\delta_A^*\right)\right)+\frac{1}{\gamma_i B_{mr}k_{Tr}}\left(L_1\left(\theta_i,t\right)-\hat{L}_1\left(\theta_i,\delta_L^*\right)\right)i_{qs}\left(t\right) \tag{4.20}$$

Where β has an upper bound.

The update of parameter $\dot{\delta}_A$, $\dot{\delta}_L$ is as follows:

$$\dot{\delta}_A=c_1\dot{\theta}_i s\left(\theta_i\right)\phi\left(\theta_i\right) \tag{4.21}$$

$$\dot{\delta}_L = \frac{1}{\gamma_i B_{mr} k_{Tr}} s(\theta_i)\phi(\theta_i) i_{qs}(t) \tag{4.22}$$

The optimization parameters for δ_L^*, δ_A^* are defined as follows:

$$\delta_L^* = \arg\min_{\delta_L \subset \chi_L} \left(\sup \left| L_1(\theta_i, t) - \hat{L}_1(\theta_i, \delta_L^*) \right| \right) \tag{4.23}$$

$$\delta_A^* = \arg\min_{\delta_A \subset \chi_A} \left(\sup \left| A(\theta_i, t) - \hat{A}(\theta_i, \delta_A^*) \right| \right) \tag{4.24}$$

Consider the following Lyapunov function[38]:

$$V_1 = \frac{1}{2} s(\theta)^2 + \frac{1}{2} \eta_A^T \eta_A + \frac{1}{2} \eta_L^T \eta_L \tag{4.25}$$

From Equation (4.8) (4.17) (4.18) (4.20), $\dot{s}$ can be expressed as follows:

$$\dot{s}(x) = c_1 \dot{\theta}_i \left(\hat{A}(\theta_i, \delta_A^*) - \hat{A}(\theta_i, \delta_A) \right) + \frac{1}{\gamma_i B_{mr} k_{Tr}} i_{qs} \left(\hat{L}_1(\theta_i, \delta_L^*) - \hat{L}_1(\theta_i, \delta_L) \right) - \rho_{ad} sat(s) - ks + \beta(\theta_i) \tag{4.26}$$

Define η_A, η_L as follows:

$$\eta_A = \delta_A^* - \delta_A \tag{4.27}$$

$$\eta_L = \delta_L^* - \delta_L \tag{4.28}$$

$$\begin{aligned}\dot{V}_1 &= s\left(\frac{1}{\gamma_i B_{mr} k_{Tr}} i_{qs}\left(\hat{L}_1\left(\theta_i,\delta_L^*\right)-\hat{L}_1\left(\theta_i,\delta_L\right)\right)+c_1\dot{\theta}_i\left(\hat{A}\left(\theta_i,\delta_A^*\right)-\hat{A}\left(\theta_i,\delta_A\right)\right)\right.\\ &\quad\left.+\beta\left(\theta_i\right)-ks-\rho sat\left(\frac{s}{\alpha}\right)\right)+\eta_A^T\dot{\eta}_A+\eta_L^T\dot{\eta}_L\\ &= s\left(\frac{1}{\gamma_i B_{mr} k_{Tr}} i_{qs}\left(\hat{L}_1\left(\theta_i,\delta_L^*\right)-\hat{L}_1\left(\theta_i,\delta_L\right)\right)+c_1\dot{\theta}_i\left(\hat{A}\left(\theta_i,\delta_A^*\right)-\hat{A}\left(\theta_i,\delta_A\right)\right)-\rho sat\left(\frac{s}{\alpha}\right)-ks+\beta\left(\theta_i\right)\right)\\ &\quad-c_1\dot{\theta}_i\eta_A^T s\phi\left(\theta\right)-\frac{1}{\gamma_i B_{mr} k_{Tr}}\eta_L^T s\phi\left(\theta_i\right)i_{qs}\left(t\right)\\ &= s\left(c_1\dot{\theta}_i\left(\left(\delta_A^*\right)^T\phi\left(\theta_i\right)-\delta_A^T\phi\left(\theta_i\right)\right)-\rho sat\left(\frac{s}{\alpha}\right)-ks+\beta\left(\theta_i\right)+\frac{1}{\gamma_i B_{mr} k_{Tr}} i_{qs}\left(\left(\delta_L^*\right)^T\phi\left(\theta_i\right)-\delta_L^T\phi\left(\theta_i\right)\right)\right)\\ &\quad-c_1\dot{\theta}_i\eta_A^T s\phi\left(\theta\right)-\frac{1}{\gamma_i B_{mr} k_{Tr}}\eta_L^T s\phi\left(\theta\right)i_{qs}\left(t\right)\end{aligned}$$

(4.29)

$$\begin{aligned}&= s\left(c_1\dot{\theta}_i\eta_A^T\phi\left(\theta_i\right)+\frac{1}{\gamma_i B_{mr} k_{Tr}} i_{qs}\eta_L^T\phi\left(\theta_i\right)-\rho sat\left(\frac{s}{\alpha}\right)-ks+\beta\left(\theta_i\right)\right)\\ &\quad-c_1\dot{\theta}_i\eta_A^T s\phi\left(\theta\right)-\frac{1}{\gamma_i B_{mr} k_{Tr}}\eta_L^T s\phi\left(\theta\right)i_{qs}\left(t\right)\\ &= -\rho sat\left(\frac{s}{\alpha}\right)-ks+\beta\left(\theta_i\right)s\\ &\le\left(-\frac{\rho}{\alpha}-k+\beta\left(\theta_i\right)\right)|s|\end{aligned}$$

According to the fuzzy control theorem, it can be seen that the amount of β is infinitely close to zero. ρ update as: $\rho=\varepsilon_0\left(-k+\beta\left(\theta_i\right)\right)\alpha$. When $\varepsilon_0>1$, $\dot{V}_1<0$ According to Lyapunov's law, the designed fuzzy sliding mode control system is globally asymptotically stable.

In this chapter, a time-varying sliding mode controller based on TS-fuzzy is established. The TS-fuzzy effectively estimates the parameters of the system. This controller successfully solves the problem that the system can still guarantee operation under the condition of parameter perturbation. The Lyapunov definition proves the

stability of the system. Further, in the following chapters, more simulation results will prove the superiority of this controller.

Chapter 5 Design of T-S Fuzzy Sliding Mode Controller Based on interval type 2 fuzzy method

5.1 Controller structure introduction

In this work, the proposed controller can eliminate or reduce the influence of disturbance on the system. In addition, the problems in the controller of Chapter 4 have been improved accordingly, and the performance of the system has been improved.

In the traditional sliding mode variable structure control, the linear sliding mode surface is often selected. After the system reaches the sliding mode, the tracking error gradually converges to zero. By selecting the sliding mode surface parameter matrix, the progressive convergence speed can be arbitrarily adjusted. However, adjustment does not guarantee that the state tracking error converges to zero in a finite time [39]. Converging to zero in a finite time is a very good characteristic. In order to achieve this goal, a new terminal sliding mode control(TSMC) strategy is proposed. However, in the traditional terminal sliding mode control, the system converges slowly and has a singular phenomenon. Literature 40 proposes a non-singular fast terminal sliding mode control strategy, which not only ensures that the system converges in a finite time, but also improves the convergence speed and solves the non-singular phenomenon. In order to enhance the robustness of sliding mode control and reduce the steady-state error, PID control is combined with terminal sliding mode control to further improve the robustness of the system[41].

The universal approximation algorithm in fuzzy control used in Chapter 4, but the fuzzy set has limitations when dealing with the uncertainty of the model. The membership values in the exact set are given fuzzification values. Such fuzzy sets are called type-1 fuzzy sets. In order to enhance the ability of traditional fuzzy systems to deal with uncertainty, the traditional fuzzy sets are extended to give the degree of ambiguity of the membership values in the set[42]. The fuzziness enhancement of fuzzy sets, this extended general fuzzy set is called a type 2 fuzzy set. The use of two-

type fuzzy control can further improve the accuracy of system identification. At the same time, the two-type fuzzy is used to estimate the nonlinear uncertainty of the system and improve the robustness of the system[43].

The specific structure of the controller proposed in Chapter 5 is shown in figure 5.1.

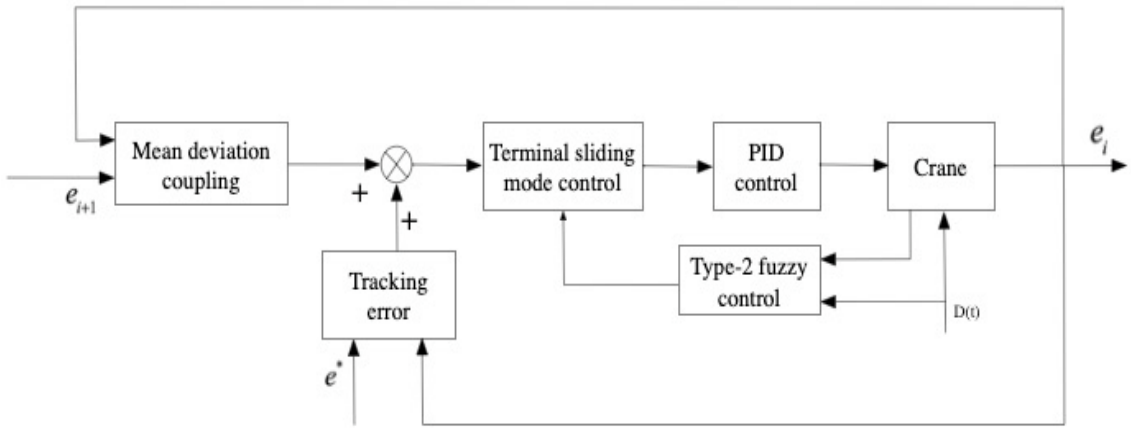

Figure 5.1 The schematic diagram of TSMC based on interval two-type fuzzy

Consider the model of the spreader with perturbation as follows:

$$J\ddot{\theta}_i + B_m\dot{\theta}_i + G_i = k_T i_{qsi} - \varsigma_f - \varsigma_d \tag{5.1}$$

Where ζ_f is the friction torque, ζ_d is the external disturbance, G_i is the potential energy load.

The standard model of the motor is as follows:

$$J_r\ddot{\theta}_i + B_{mr}\dot{\theta}_i = k_{Tr} i_{qsi} - d_i \tag{5.2}$$

$$d_i = G_i + \varsigma_f + \varsigma_d - \triangle k_T i_{qsi} \tag{5.3}$$

Where $\triangle k_T = k_T - k_{Tr}$, d_i is the polymerization disturbance. And the uncertainties are bounded to be $\Delta k_T \in \left[\Delta k_{T,L}, \Delta k_{T,H}\right]$, the subscripts L and H denote lower and upper uncertainty values.

For the convenience of calculation, the Equation (5.2) can be rewritten as follows:

$$\ddot{\theta}_i = -\frac{B_{mr}}{J_r}\dot{\theta}_i + \frac{k_{Tr}}{J_r}i_{qsi} - \frac{1}{J_r}d_i \tag{5.4}$$

Where $A(\theta,t) = -\frac{B_{mr}}{J_r}$, $L_1(\theta,t) = \frac{k_{Tr}}{J_r}$, $L_2(\theta,t) = -\frac{1}{J_r}$.

Simplified Equation (5.4), we can obtain:

$$\ddot{\theta}_i = A(t)\dot{\theta}_i + L_1(t)i_{qsi} + L_2(t)d_i \tag{5.5}$$

The polymerization disturbance d_i is a complex nonlinear term for the time t, the rotational speed ω_i. d_i has an unknown finite upper bound, that is $d_{i,\max} = \sup\left|d_i(\omega_i,t)\right| < +\infty$. Both $A(t)$ and $L_1(t)$ are functions that vary according to time, and their values must be non-negative.

5.2 PI and fast non-singular terminal sliding mode control

Nonlinear non-singular terminal sliding mode (NTSM) controllers can effectively control nonlinear dynamic systems. Such nonlinear dynamic systems have parametric uncertainties. NTSM manifold is proposed to overcome the singularity problem. NTSM can ensure that the system reaches the equilibrium point with limited convergence in sliding mode[44]. In this work, a layered terminal sliding mode control is adopted. The non-singular terminal sliding mode is defined as follows:

$$s_1 = e_{ref} + \chi_1 \dot{e}_{ref}^{p/q} \tag{5.6}$$

$$s_2 = e_i + \chi_2 \dot{e}_i^{p/q} \tag{5.7}$$

Where $\chi_1, \chi_2 \in R^+$, $e_i(t) = \theta_i(t) - \frac{\sum_{j=1}^{n}\theta_j(t)}{n}$, $e_{ref}(t) = \theta_d(t) - \theta_i(t)$,the parameters p and q must be positive odd integers, meanwhile p and $q$need to

satisfy $p<\mathrm{q}$. This sliding surface can converge to $e_{ref}=0,\ e_i=0$ in a limited time.

The finite time t_e is expressed as follows:

$$t_e=\frac{q}{\chi_1(q-p)}\left|e(0)\right|^{\frac{q-p}{q}} \tag{5.8}$$

Where e is e_{ref} or e_i. The reaching time t_e can be adjusted by $\chi_1,\ q,\ p$.

In order to get the system to reach the equilibrium point faster and avoid singularity, a non-singular fast terminal sliding mode model is introduced.

When the system is in the sliding mode stage and $s=0$, there is:

$$\dot{e}_{ref}=\left[\frac{1}{\chi_1}\left(-e_{ref}\right)\right]^{q/p} \tag{5.9}$$

$$\dot{e}_i=\left[\frac{1}{\chi_2}\left(-e_i\right)\right]^{q/p} \tag{5.10}$$

Since the index of e_{ref} and e_i in Equation (5.9) (5.10) are less than one. In the region far from the equilibrium point, the state derivative is smaller than the linear sliding surface of the same parameter, which causes the system state to converge slowly, far below the exponential convergence rate.

From the above analysis, the main reason for the slow convergence of the non-singular terminal sliding mode is that the index of e_{ref} and e_i in the sliding surface are less than one. That is, if the higher-order exponents of e_{ref} and e_i on the right side of Equation (5.9) (5.10) can be increased, the absolute value of the state derivative can be effectively increased in the region far from the equilibrium point. This will effectively improve the convergence speed of the terminal sliding mode control[45].

Based on the above theory, the mathematical function of the non-singular fast terminal sliding mode is now defined as follows:

$$s_1=e_{ref}+\frac{1}{\chi_1}\dot{e}_{ref}^{p/q}+\frac{1}{\chi_3}e^{g/h}{}_{ref}=0 \tag{5.11}$$

$$s_2 = e_i + \frac{1}{\chi_2}\dot{e}_i^{p/q} + \frac{1}{\chi_4}e_i^{g/h} = 0 \tag{5.12}$$

Where $\ddot{e}_{ref} = \ddot{\theta}_d(t) - \ddot{\theta}_i(t)$, $\ddot{e}_i = \ddot{\theta}_i(t) - \frac{\sum_{j=1}^{n}\ddot{\theta}_j(t)}{n}$, $\chi_1, \chi_2, \chi_3, \chi_4 \in R^+$, $p, q, g, h \in N$,and p, q, g, h are odd numbers. When $e = 0$, $\dot{e} \neq 0$, and $1 < p/q < 2$, $g/h > p/q$.

The derivative of the sliding surface s_1 , s_2 are calculated as follows:

$$\frac{ds_1}{dt} = \dot{e}_{ref} + \frac{p}{q\chi_1}\dot{e}_{ref}^{p/q-1}\ddot{e}_{ref} + \frac{q}{h\chi_3}e_{ref}^{g/h-1}\dot{e}_{ref} \tag{5.13}$$

$$\frac{ds_2}{dt} = \dot{e}_i + \frac{p}{q\chi_2}\dot{e}_i^{p/q-1}\ddot{e}_i + \frac{q}{h\chi_4}e_i^{g/h-1}\dot{e}_i \tag{5.14}$$

The PID controller (proportional-integral-derivative controller) is composed of a proportional unit P, an integral unit I, and a differential unit D. The basis of PID control is proportional control[46]; integral control can eliminate steady-state error, but this may increase overshoot; differential control can speed up the response of large inertia system and weaken overshoot. The PI non-singular fast terminal sliding mode controller(NFTSMC) proposed in this chapter is the advantage of using PI to reduce the steady-state error and overshoot of the system, and further enable the non-singular fast terminal sliding mode to control the system[47]. The key to using PI control is to adjust the two coefficients of PI to make PI control play its role.

Now propose PI-NFTSMC surface as follows:

$$s_{PI-TSM} = \varpi_1 s^* + \varpi_2 \int s^* \tag{5.15}$$

Where ϖ_1, ϖ_2 are PID coefficients, and $\varpi_1, \varpi_2 \in R$. The s in the formula is s_1 and s_2 .

Due to the large amount of calculation, the controllers for tracking error and synchronization error are designed separately.

Note:

(1) s_1 is the sliding mode surface of the tracking control, and s_2 is the sliding mode surface of the synchronous control.

(2) The coefficients designed in the two sliding surfaces of s_1 and s_2 are consistent.

(3) i_{qsi} is the input current of the drive motor. For the sake of understanding, the next chapter will replace i_{qsi} with u_i.

5.2.1 Tracking error controller design

The second derivative of the tracking error is calculated as follows:

$$\ddot{e}_{ref} = \ddot{\theta}_d - A(t)\dot{\theta}_i - L_1(t)u_i - L_2(t)d_i \tag{5.15}$$

The tracking controller's PID non-singular fast terminal sliding surface is defined as follows:

$$s_{PI-TSM1} = \varpi_1 s_1 + \varpi_2 \int s_1 \tag{5.16}$$

From Equation (5.13)(5.15), we can obtain the derivative of the sliding surface s_1

$$\begin{aligned}\frac{ds_1}{dt} &= \left(\dot{\theta}_d - \dot{\theta}_i\right) + \frac{p}{q\chi_1}\left(\dot{\theta}_d - \dot{\theta}_i\right)^{p/q-1}\left(\dot{\theta}_d - A(t)\dot{\theta}_i - L_1(t)u_i - L_2(t)d_i\right) \\ &\quad + \frac{g}{h\chi_3}\left(\theta_d - \theta_i\right)^{g/h-1}\left(\dot{\theta}_d - \dot{\theta}_i\right) \\ &= \frac{p}{q\chi_1}\left(\dot{\theta}_d - \dot{\theta}_i\right)^{p/q-1}\left(\dot{\theta}_d - A(t)\dot{\theta}_i - L_1(t)u_i - L_2(t)d_i\right) \\ &\quad + \left(\frac{g}{h\chi_3}\left(\theta_d - \theta_i\right)^{g/h-1} + 1\right)\left(\dot{\theta}_d - \dot{\theta}_i\right)\end{aligned} \tag{5.17}$$

According to Equation (5.11) (5.16), the sliding surface $s_{PI-TSM1}$ of the tracking controller is obtained as:

$$\begin{aligned} s_{PI-TSM1} &= \varpi_1 s_1 + \varpi_2 \int s_1 \\ &= \varpi_1 \left(e_{ref} + \frac{1}{\chi_1} \dot{e}_{ref}^{p/q} + \frac{1}{\chi_3} e^{g/h}{}_{ref} \right) + \varpi_2 \int \left(e_{ref} + \frac{1}{\chi_1} \dot{e}_{ref}^{p/q} + \frac{1}{\chi_3} e^{g/h}{}_{ref} \right) \end{aligned} \tag{5.18}$$

From Equation (5.18), we can obtain the derivative of the sliding surface $s_{PI-TSM1}$:

$$\begin{aligned} \dot{s}_{PI-TSM1} &= \varpi_1 \frac{d}{dt} \left(e_{ref} + \frac{1}{\chi_1} \dot{e}_{ref}^{p/q} + \frac{1}{\chi_3} e^{g/h}{}_{ref} \right) + \varpi_2 \left(e_{ref} + \frac{1}{\chi_1} \dot{e}_{ref}^{p/q} + \frac{1}{\chi_3} e^{g/h}{}_{ref} \right) \\ &= \varpi_1 \left(\dot{e}_{ref} + \frac{p}{q\chi_1} \dot{e}_{ref}^{p/q-1} \ddot{e}_{ref} + \frac{g}{h\chi_3} e_{ref}^{g/h-1} \dot{e}_{ref} \right) + \varpi_2 \left(e_{ref} + \frac{1}{\chi_1} \dot{e}_{ref}^{p/q} + \frac{1}{\chi_3} e^{g/h}{}_{ref} \right) \\ &= \varpi_1 \dot{e}_{ref} \left(\frac{g}{h\chi_3} e_{ref}^{g/h-1} + 1 \right) + \varpi_1 \left(\frac{p}{q\chi_1} \dot{e}_{ref}^{p/q-1} \ddot{e}_{ref} \right) + \varpi_2 \left(e_{ref} + \frac{1}{\chi_1} \dot{e}_{ref}^{p/q} + \frac{1}{\chi_3} e^{g/h}{}_{ref} \right) \end{aligned} \tag{5.19}$$

From Equation (5.17) (5.19), the derivative of the sliding mode surface $s_{PI-TSM1}$ can be further refined as:

$$\begin{aligned} \dot{s}_{PI-TSM1} &= \varpi_1 \dot{e}_{ref} \left(\frac{g}{h\chi_3} e_{ref}^{g/h-1} + 1 \right) + \varpi_1 \left(\frac{p}{q\chi_1} \dot{e}_{ref}^{p/q-1} \ddot{e}_{ref} \right) + \varpi_2 \left(e_{ref} + \frac{1}{\chi_1} \dot{e}_{ref}^{p/q} + \frac{1}{\chi_3} e^{g/h}{}_{ref} \right) \\ &= \varpi_1 \dot{e}_{ref} \left(\frac{g}{h\chi_3} e_{ref}^{g/h-1} + 1 \right) + \varpi_1 \left(\frac{p}{q\chi_1} \dot{e}_{ref}^{p/q-1} \left(\ddot{\theta}_d - A(t) \dot{\theta}_i - L_1(t) u_i - L_2(t) d_i \right) \right) \\ &\quad + \varpi_2 \left(e_{ref} + \frac{1}{\chi_1} \dot{e}_{ref}^{p/q} + \frac{1}{\chi_3} e^{g/h}{}_{ref} \right) \\ &= \Omega_{ref}(e_{ref}) + \kappa_{ref}(e_{ref}) + \varpi_1 \left(\frac{p}{q\chi_1} \dot{e}_{ref}^{p/q-1} \left(\ddot{\theta}_d - A(t) \dot{\theta}_i - L_1(t) u_i - L_2(t) d_i \right) \right) \end{aligned} \tag{5.20}$$

Where $\Omega_{ref}(e_{ref}) = \varpi_1 \dot{e}_{ref} \left(\frac{g}{h\chi_3} e_{ref}^{g/h-1} + 1 \right)$, $\kappa_{ref}(e_{ref}) = \varpi_2 \left(e_{ref} + \frac{1}{\chi_1} \dot{e}_{ref}^{p/q} + \frac{1}{\chi_3} e^{g/h}{}_{ref} \right)$.

The switching law uses a symbol function, we can get the expression of u_{ref} by the following formula.

$$\dot{s}_{PI-TSM1} = -\rho_1 \operatorname{sgn}\left(s_{PI-TSM1}(t) \right) - \psi_1 s_{PI-TSM1} \tag{5.21}$$

$$\Omega_{ref}\left(e_{ref}\right)+\kappa_{ref}\left(e_{ref}\right)+\varpi_1\left(\frac{p}{q\chi_1}\dot{e}_{ref}^{p/q-1}\left(\ddot{\theta}_d-A(t)\dot{\theta}_i-L_1(t)u_i-L_2(t)d_i\right)\right)$$
$$=-\rho_1\,\mathrm{sgn}\left(s_{PI-TSM1}(t)\right)-\psi_1 s_{PI-TSM1} \tag{5.22}$$

Where ρ_1 is the gain of switching control law, and $\rho_1,\psi_1\in R$. By adjusting the value of ρ_1, the chattering of the sliding mode can be effectively suppressed. However, if the value of ρ_1 is too large or too small, the performance of the system will be deteriorated.

The equivalent control law of the tracking controller is:

$$u_{ref,eq}=L_1^{-1}(t)\left(-A(t)\dot{\theta}_i+\ddot{\theta}_d-\frac{q\chi_1\left(-\Omega_{ref}\left(e_{ref}\right)-\kappa_{ref}\left(e_{ref}\right)\right)}{\varpi_1 p\dot{e}_{ref}^{p/q-1}}\right) \tag{5.23}$$

The control law u_{ref} of the system is the sum of the equivalent control law and the switching law, and the form is as follows:

$$u_{ref}=u_{ref,sw}+u_{ref,eq} \tag{5.24}$$

The control law of the tracking controller is calculated as follows:

$$u_{ref}=L_1^{-1}(t)\left(-A(t)\dot{\theta}_i+\ddot{\theta}_d-\frac{q\chi_1\left(-\rho_1\,\mathrm{sgn}\left(s_{PI-TSM1}\right)-\psi_1 s_{PI-TSM1}-\Omega_{ref}\left(e_{ref}\right)-\kappa_{ref}\left(e_{ref}\right)\right)}{\varpi_1 p\dot{e}_{ref}^{p/q-1}}\right) \tag{5.25}$$

In the field of automatic control, Lyapunov stability can be used to describe the stability of a power system. If the trajectory of any initial condition of the power system near the equilibrium state can be maintained near the equilibrium state, then the system can be said to be Lyapunov stable. Lyapunov stability theory can be applied to the analysis of the stability of linear systems and nonlinear systems, stationary systems and time-varying systems. It is a more general stability analysis method.

The design of the controller proposed in this work uses Lyapunov's theorem to prove the stability of the system.

Theorem 5.1: Consider the double spreader overhead crane system described in Equation (5.15), and the sliding mode surface $s_{PI-TSM1}$ based on PI and non-singular fast terminal sliding mode theory proposed in Equation(5.20). If the switching law proposed in Equation (5.21) and the tracking controller in Equation (5.25) are used, and with:

$$\rho_1 \geq L_2(t) d_{i,\max} \tag{5.26}$$

then, the stability of the system and the convergence of the sliding surface are guaranteed.

Proof: Consider the following Lyapunov function:

$$V_0 = \frac{1}{2}\left(s_{PI-TSM1}\right)^2 \tag{5.27}$$

Appendix1: In order to facilitate the proof, the first-order nonlinear inequality is given as follows[48]:

$$\dot{V}(x) + aV(x) + bV^c(x) \leq 0 \tag{5.28}$$

where $V(x)$ is a positive Lyapunov function, $a, b > 0$ and $0 < c < 1$.

According to Equation (5.20) (5.27), the following proofs can be obtained:·

$$\begin{aligned}
\dot{V}_0 &= s_{PI-TSM1}\dot{s}_{PI-TSM1} \\
&= s_{PI-TSm1}\left(\Omega_{ref}\left(e_{ref}\right) + \kappa_{ref}\left(e_{ref}\right) + \varpi_1\left(\frac{p}{q\chi_1}\dot{e}_{ref}^{p/q-1}\left(\ddot{\theta}_d - A(t)\dot{\theta}_i - L_1(t)u_{ref} - L_2(t)d_i\right)\right)\right) \\
&= s_{PI-TSM1}\left(-\rho_1 \operatorname{sgn}\left(s_{PI-TSM1}\right) - \psi_1 s_{PI-TSM1} - \frac{pL_2(t)}{q\chi_1}\dot{e}_{ref}^{p/q-1}d_i\right) \\
&\leq -\rho_1\left|s_{PI-TSM1}\right| - \psi_1\left(s_{PI-TSM1}\right)^2 - \frac{pL_2(t)}{q\chi_1}\dot{e}_{ref}^{p/q-1}d_i s_{PI-TSM1} \\
&\leq -\rho_1\left|s_{PI-TSM1}\right| - \psi_1\left(s_{PI-TSM1}\right)^2 + \tau_1 s_{PI-TSM1}
\end{aligned} \tag{5.29}$$

where $\tau_1 = -\frac{p\rho_1}{q\chi_1}\dot{e}_{ref}^{p/q-1}$.

There are two cases for the Lyapunov Equation (5.29).

Case1: We can rewrite Equation (5.29) into the following form:

$$\dot{V}_0 \le -\left(\psi_1 - \frac{\tau_1}{s}\right)\left(s_{PI-TSM1}\right)^2 - \rho_1\left|s_{PI-TSM1}\right| \tag{5.30}$$

Hence, if $\psi_1 - \frac{\tau_1}{s} > 0$ and $\dot{e}_{ref}^{p/q-1} \neq 0$. According to the inequality proposed in the appendix1, there exits $\vartheta_1, \vartheta_2 > 0$ to make the following formula

$$\begin{aligned} \dot{V}_0 &\le -\vartheta_1\left(s_{PI-TSM1}\right)^2 + \vartheta_2\left|s_{PI-TSM1}\right| \\ &\le 0 \end{aligned} \tag{5.31}$$

It can be seen from Equation (5.31) that the tracking controller designed in this section is stable in the sense of Lyapunov.

Case 2: From Equation (5.29), we can get

$$\dot{V}_0 \le -\psi_1\left(s_{PI-TSM1}\right)^2 - \left[\rho_1 - \frac{\tau_1}{s_{PI-TSM1}}\right]\left|s_{PI-TSM1}\right| \tag{5.32}$$

Similarly, if $\rho_1 - \frac{\tau_1}{s_{PI-TSM1}} > 0$ and $\dot{e}_{ref}^{p/q-1} \neq 0$, $\dot{V}_0 \le 0$ .This shows that the system is stable under Lyapunov's theorem

Consequently, the finite time tracking of the double spreader overhead crane system described in Equation (5.5) can be achieved, due to the implementation of PI non-singular fast terminal sliding mode surface $s_{PI-TSM1}$ described in Equation (5.18). Therefore, based on the Lyapunov criterion, the stability and convergence of the system is guaranteed. This completes the proof 5.1.

When $s_{PI-TSM1}$ in Equation (5.18) converges to zero, s_1 also converges to zero. From this sliding surface of the Equation (5.11) $s_1 = e_{ref} + \frac{1}{\chi_1}\dot{e}_{ref}^{p/q} + \frac{1}{\chi_3}e^{g/h}{}_{ref} = 0$, it can be seen that when the system state is close to the equilibrium point, if the high-order term of e_{ref} is ignored, the Equation (5.11) is similar to Equation (5.6), that is, its convergence speed is similar to that of the conventional terminal sliding mode.

However, when the system state is far from the equilibrium point, the high-order term of e_{ref} in Equation (5.11) plays a major role, and its convergence speed is faster than that of the ordinary terminal sliding mode. The non-singular fast terminal sliding mode not only has a fast convergence speed, but also has a limited convergence time. The specific convergence time is calculated as follows[47]:

$$t_{s,ref} = \frac{\frac{p}{q}\left|e_{ref}\right|^{1-\frac{p}{q}}}{\chi_1\left(\frac{p}{q}-1\right)} \cdot \Lambda\left(\frac{p}{q}, \frac{\frac{p}{q}-1}{(\lambda-1)\frac{p}{q}}; 1+\frac{\frac{p}{q}-1}{\left(\frac{g}{h}-1\right)\frac{p}{q}}; -\chi_1\left|e_{ref}(0)\right|^{\frac{g}{h}-1}\right) \tag{5.32}$$

Where Λ is Gauss' hypergeometric function.

In this section, the non-singular fast terminal sliding mode method is selected to make the tracking system stable for a limited time. The convergence time of the system is shown in Equation 5.32. This work combines PI and NFTSMC to create a new sliding surface to improve the robustness of the tracking system.

5.2.2 Synchronization error controller design

The main function of the synchronous controller is to eliminate the synchronization error between the two spreaders. First, it is necessary to define the form of the synchronization error. Combining the mean deviation coupling algorithm defined in Equation (4.1) with the double spreaders model in Equation (5.5), the second derivative of the synchronization error can be obtained.

$$\begin{aligned}\ddot{e}_i &= \ddot{\theta}_i - \frac{\sum_{j=1}^{n}\ddot{\theta}_j(t)}{n} \\ &= A(t)\dot{\theta}_i + L_1(t)u_i + L_2(t)d_i - \frac{\sum_{j=1}^{n}}{n}\left(A(t)\dot{\theta}_j + L_1(t)u_j + L_2(t)d_j\right) \\ &= A(t)\left(\dot{\theta}_i - \frac{\sum_{j=1}^{n}\dot{\theta}_j}{n}\right) + L_1(t)\left(u_i - \frac{\sum_{j=1}^{n}u_j}{n}\right) + L_2(t)\left(d_i - \frac{\sum_{j=1}^{n}d_j}{n}\right) \\ &= A(t)\dot{e}_i + L_1(t)u_i^* + L_2(t)\left(d_i - \frac{\sum_{j=1}^{n}d_j}{n}\right)\end{aligned} \tag{5.33}$$

Where $u_i^* = u_i - \frac{\sum_{j=1}^{n}u_j}{n}$.

The synchronization controller's PI non-singular fast terminal sliding surface is defined as follows:

$$\begin{aligned}s_{PI-TSM2} &= \varpi_1 s_2 + \varpi_2 \int s_2 \\ &= \varpi_1\left(e_i + \frac{1}{\chi_2}\dot{e}_i^{p/q} + \frac{1}{\chi_4}e_i^{g/h}\right) + \varpi_2\int\left(e_i + \frac{1}{\chi_2}\dot{e}_i^{p/q} + \frac{1}{\chi_4}e_i^{g/h}\right)\end{aligned} \tag{5.34}$$

We can further get the derivative of $s_{PI-TSM2}$ as:

$$\begin{aligned}\dot{s}_{PI-TSM2} &= \varpi_1\frac{d}{dt}\left(e_i + \frac{1}{\chi_2}\dot{e}_i^{p/q} + \frac{1}{\chi_4}e^{g/h}{}_i\right) + \varpi_2\left(e_i + \frac{1}{\chi_2}\dot{e}_i^{p/q} + \frac{1}{\chi_4}e^{g/h}{}_i\right) \\ &= \varpi_1\left(\dot{e}_i + \frac{p}{q\chi_2}\dot{e}_i^{p/q-1}\ddot{e}_i + \frac{g}{h\chi_4}e_i^{g/h-1}\dot{e}_i\right) + \varpi_2\left(e_i + \frac{1}{\chi_2}\dot{e}_i^{p/q} + \frac{1}{\chi_4}e^{g/h}{}_i\right) \\ &= \varpi_1\dot{e}_i\left(\frac{g}{h\chi_4}e_i^{g/h-1} + 1\right) + \varpi_1\left(\frac{p}{q\chi_2}\dot{e}_i^{p/q-1}\ddot{e}_i\right) + \varpi_2\left(e_i + \frac{1}{\chi_2}\dot{e}_i^{p/q} + \frac{1}{\chi_4}e^{g/h}{}_i\right)\end{aligned} \tag{5.35}$$

According to Equation (5.33) (5.35), the derivative of $s_{PI-TSM2}$ can be organized as follows:

$$\begin{aligned}\dot{s}_{PI-TSM2} &= \varpi_1\dot{e}_i\left(\frac{g}{h\chi_4}e_i^{g/h-1}+1\right)+\varpi_1\left(\frac{p}{q\chi_2}\dot{e}_i^{p/q-1}\ddot{e}_i\right)+\varpi_2\left(e_i+\frac{1}{\chi_2}\dot{e}_i^{p/q}+\frac{1}{\chi_4}e^{g/h}{}_i\right)\\ &= \varpi_1\dot{e}_i\left(\frac{g}{h\chi_4}e_i^{g/h-1}+1\right)+\varpi_1\left(\frac{p}{q\chi_2}\dot{e}_i^{p/q-1}\left(A(t)\dot{e}_i+L_1(t)u_i^*+L_2(t)\left(d_i-\frac{\sum_{j=1}^{n}d_j}{n}\right)\right)\right)\\ &\quad+\varpi_2\left(e_i+\frac{1}{\chi_2}\dot{e}_i^{p/q}+\frac{1}{\chi_4}e^{g/h}{}_i\right)\\ &= \Omega_i(e_i)+\kappa_i(e_i)+\varpi_1\left(\frac{p}{q\chi_2}\dot{e}_i^{p/q-1}\left(A(t)\dot{e}_i+L_1(t)u_i^*+L_2(t)\left(d_i-\frac{\sum_{j=1}^{n}d_j}{n}\right)\right)\right)\end{aligned} \tag{5.36}$$

Where $\Omega_i(e_i)=\varpi_1\dot{e}_i\left(\frac{g}{h\chi_4}e_i^{g/h-1}+1\right)$, $\kappa_i(e_i)=+\varpi_2\left(e_i+\frac{1}{\chi_2}\dot{e}_i^{p/q}+\frac{1}{\chi_4}e^{g/h}{}_i\right)$.

The exponential approach law is chosen as the switching law, and the control law is calculated as follows:

$$\begin{aligned}&\Omega_i(e_i)+\kappa_i(e_i)+\varpi_1\left(\frac{p}{q\chi_2}\dot{e}_i^{p/q-1}\left(A(t)\dot{e}_i+L_1(t)u_i^*+L_2(t)\left(d_i-\frac{\sum_{j=1}^{n}d_j}{n}\right)\right)\right)\\ &\qquad=-\rho_2\,\mathrm{sgn}\left(s_{PI-TSM2}(t)\right)-\psi_2 s_{PI-TSM2}\end{aligned} \tag{5.37}$$

where $\rho_2,\psi_2\in R$.

The equivalent control law of the synchronous controller is:

$$\begin{aligned}u_i^* &= L_1^{-1}(t)\\ &\left(-A(t)\dot{\theta}_i+\frac{q\chi_2\left(-\Omega_i(e_i)-\kappa_i(e_i)\right)}{\varpi_1 p\dot{e}_i^{p/q-1}}\right)\end{aligned} \tag{5.38}$$

The control law u_i^* of the system is the sum of the equivalent control law and the switching law, and the form is as follows

$$u_i^* = u_{i,sw} + u_{i,eq} \tag{5.39}$$

The control law of the synchronous controller is calculated as follows:

$$u_i^* = L_1^{-1}(t) \left(-A(t)\dot{\theta}_i + \frac{q\chi_2\left(-\rho_2 \operatorname{sgn}\left(s_{PI-TSM2}\right) - \psi_2 s_{PI-TSM2} - \Omega_i\left(e_i\right) - \kappa_i\left(e_i\right)\right)}{\varpi_1 p \dot{e}_i^{p/q-1}} \right) \tag{5.40}$$

Theorem 5.2: Consider the double spreader bridge crane system described in 5.5, and the sliding mode surface $s_{PI-TSM2}$ based on PI and non-singular fast terminal sliding mode theory proposed in Equation (5.34). If using NFTSMC based on mean deviation coupling via Equation (5.33) (5.34), and with

$$\rho_2 \geq L_2(t) d_{i,\max} \tag{5.41}$$

then, the stability of the system and the convergence of the sliding surface are guaranteed.

Proof: Consider the following Lyapunov function:

$$V_1 = \frac{1}{2}\left(s_{PI-TSM2}\right)^2 \tag{5.42}$$

$$
\begin{aligned}
\dot{V}_1 &= s_{PI-TSM2}\dot{s}_{PI-TSM2} \\
&= s_{PI-TSM2}\left(\Omega_i(e_i)+\kappa_i(e_i)+\varpi_1\left(\frac{p}{q\chi_2}\dot{e}_i^{p/q-1}\left(A(t)\dot{\theta}_i+L_1(t)u_i^*+L_2(t)\left(d_i-\frac{\sum_{j=1}^{n}d_j}{n}\right)\right)\right)\right) \\
&= s_{PI-TSM2}\left(-\rho_2\,\mathrm{sgn}(s_{PI-TSM2})-\psi_2 s_{PI-TSM2}+\frac{pL_2(t)}{q\chi_2}\dot{e}_i^{p/q-1}\left(d_i-\frac{\sum_{j=1}^{n}d_j}{n}\right)\right) \\
&\le -\rho_2|s_{PI-TSM2}|-\psi_2(s_{PI-TSM2})^2+\frac{pL_2(t)}{q\chi_2}\dot{e}_i^{p/q-1}\left(d_i-\frac{\sum_{j=1}^{n}d_j}{n}\right)s_{PI-TSM2} \\
&\le -\rho_2|s_{PI-TSM2}|-\psi_2(s_{PI-TSM2})^2+\frac{p\rho_2}{q\chi_2}\dot{e}_i^{p/q-1}s_{PI-TSM2} \\
&\le -\rho_2|s_{PI-TSM2}|-\psi_2(s_{PI-TSM2})^2+\tau_2 s_{PI-TSM2}
\end{aligned}
\tag{5.43}
$$

where $\tau_2=\dfrac{p\rho_2}{q\chi_2}\dot{e}_i^{p/q-1}$

Similar to the proof process of tracking controller stability, we can also divide the Equation (5.43) into two cases.

Case 1: From Equation (5.43), we can get

$$
\dot{V}_1 \le -\left(\psi_2-\frac{\tau_2}{s}\right)(s_{PI-TSM2})^2-\rho_2|s_{PI-TSM2}| \tag{5.44}
$$

Hence, if $\psi_2-\dfrac{\tau_2}{s}>0$ and $\dfrac{p\rho_2}{q\chi_2}\dot{e}_i^{p/q-1}\neq 0$, $\dot{V}_1\le 0$.

Case 2: Rewrite Equation (5.43) as follow:

$$
\dot{V}_1 \le -\psi_2(s_{PI-TSM2})^2-\left[\rho_2-\frac{\tau_2}{s_{PI-TSM2}}\right]|s_{PI-TSM2}| \tag{5.45}
$$

Similarly, if $\rho_2-\dfrac{\tau_2}{s_{PI-TSM2}}>0$ and $\dfrac{p\rho_2}{q\chi_2}\dot{e}_i^{p/q-1}\neq 0$, $\dot{V}_1\le 0$.

Consequently, the finite time tracking of the double spreader overhead crane system described in Equation (5.5) can be achieved, due to the implementation of PI non-singular fast terminal sliding mode surface $s_{PI-TSM2}$ described in Equation (5.34). Therefore, based on the Lyapunov criterion, the stability and convergence of the system is guaranteed. This completes the proof 5.2.

Similar to the tracking controller proposed in the previous section, the synchronous error controller proposed in this section still uses non-singular fast terminal sliding mode. This type of sliding mode control has the advantage of enabling the system to converge for a limited time. The finite time calculation formula for the control of the synchronous controller is as follows:

$$t_{s,i}=\frac{\frac{p}{q}\left|e_i\right|^{1-\frac{p}{q}}}{\chi_2\left(\frac{p}{q}-1\right)}\cdot\Lambda\left(\frac{p}{q},\frac{\frac{p}{q}-1}{\left(\lambda-1\right)\frac{p}{q}};1+\frac{\frac{p}{q}-1}{\left(\frac{g}{h}-1\right)\frac{p}{q}};-\chi_2\left|e_i\left(0\right)\right|^{\frac{g}{h}-1}\right) \tag{5.46}$$

Where Λ is Gauss' hypergeometric function.

This section also uses the combination of PID and non-singular fast terminal sliding mode to build a synchronous controller. The next section further solves the problem that the switching law gain of the sliding mode control is too large or too small. It optimizes the structure of controller.

5.3 Super-Twisting algorithm

When the variable structure control reaches the switching plane, the switching between the two structures is controlled by the action of the control law to keep the system near the sliding surface or the equilibrium point. Due to the time lag of the switching device and the inertia of the controlled object, after the system state reaches the sliding surface or the equilibrium point, it does not remain on them. Instead, it makes a round-trip movement around the sliding surface or around the balance point. This phenomenon is called variable structure chattering.

The commonly used method to avoid chattering is to replace the discontinuous symbol function with a continuous saturation function, although this method can control continuity and eliminate chattering. Meanwhile, it also limits the sliding trajectory of the sliding system not toward the sliding surface, so that the trajectory in the vicinity thereof loses its robustness to interference.

The super-twisting algorithm can be used to replace the saturation function scheme, which can avoid the chattering problem without affecting the tracking performance[49]. The super-twisting sliding mode control scheme moves the trajectory of the system in the phase plane in a twisting mode during control. Meanwhile, this control method allows the system to asymptotically converge or the origin for a limited time.

It can be known from Equation (5.21) (5.37) that if we want to ignore the influence of the disturbance on the system, the gain of the switching law should be set very large. The result of this is that the chattering in the control process is too large, which affects the performance of the controller. In order to solve this problem, in the super-twisting algorithm, the adaptive parameter $\hat{k}_1$, $\hat{k}_3$ can be set to reduce the chattering of the system. This approach makes the system less susceptible to interference and ensures system performance. According to Equation (5.21), the super-twisting sliding mode control is proposed as follows:

$$\begin{cases} \dot{s}_{PID-TSM1} = -\hat{k}_1 \left| s_{PI-TSM1} \right|^{1/2} \operatorname{sgn}\left(s_{PI-TSM1}\left(t\right) \right) + \upsilon_1 \\ \dot{\upsilon}_1 = -\hat{k}_3 \operatorname{sgn}\left(s_{PI-TSM1}\left(t\right) \right) \end{cases} \tag{5.47}$$

Equation (5.47) is the super-twisting sliding mode control design of the tracking controller.

According to Equation (5.20) (5.47),

$$\begin{aligned} & -\hat{k}_1 \left| s_{PI-TSM1} \right|^{1/2} \operatorname{sgn}\left(s_{PI-TSM1}\left(t\right) \right) + \upsilon_1 \\ & = \Omega_{ref}\left(e_{ref}\right) + \kappa_{ref}\left(e_{ref}\right) + \varpi_1 \left(\frac{p}{q\chi_1} \dot{e}_{ref}^{p/q-1} \left(\ddot{\theta}_d - A\left(t\right)\dot{\theta}_i - L_1\left(t\right)u_{ref} - L_2\left(t\right)d_i \right) \right) \end{aligned} \tag{5.48}$$

$$u_{ref} = L_1^{-1}(t)\left(-A(t)\dot{\theta}_i + \ddot{\theta}_d\right) - L_1^{-1}(t)\left(\frac{q\chi_1\left(-\hat{k}_1\left|s_{PI-TSM1}\right|^{1/2}\operatorname{sgn}\left(s_{PI-TSM1}(t)\right)+\upsilon_1-\Omega_{ref}\left(e_{ref}\right)-\kappa_{ref}\left(e_{ref}\right)\right)}{\varpi_1 p\dot{e}_{ref}^{p/q-1}}\right) \tag{5.49}$$

The system's Lyapunov equation can be defined as follows[50]:

$$V_{ref} = \frac{1}{2}e_{ref}^2 \tag{5.50}$$

The derivative of V_{ref} is calculated as follows:

$$\begin{aligned}\dot{V}_{ref} &= \frac{1}{2}\left(\frac{\partial V_{ref}}{\partial e_{ref}}\frac{\partial e_{ref}}{\partial \theta_i}\frac{\partial \theta_i}{\partial u_{ref}}\right)\left[\frac{\partial u_{ref}}{\partial \hat{k}_1}\frac{\partial \hat{k}_1}{\partial t}+\frac{\partial u_{ref}}{\partial \upsilon_1}\frac{\partial \upsilon_1}{\partial t}\right] \\ &= \left(e_{ref}\frac{\partial \theta_i}{\partial u_{ref}}\right)\left[\frac{\partial u_{ref}}{\partial \hat{k}_1}\frac{\partial \hat{k}_1}{\partial t}+\frac{\partial u_{ref}}{\partial \upsilon_1}\frac{\partial \upsilon_1}{\partial t}\right]\end{aligned} \tag{5.51}$$

From Equation (5.47), we can get:

$$\frac{\partial \upsilon_1}{\partial t} = -\hat{k}_3\operatorname{sgn}\left(s_{PI-TSM1}(t)\right) \tag{5.52}$$

From Equation (5.49), we can get:

$$\frac{\partial u_{ref}}{\partial \hat{k}_1} = \frac{L_1^{-1}(t)q\chi_1}{\varpi_1 p\dot{e}_{ref}^{p/q-1}}\left|s_{PI-TSM1}\right|^{1/2}\operatorname{sgn}\left(s_{PI-TSM1}(t)\right) \tag{5.53}$$

With Equation (5.52) (5.53), Equation (5.51) can be further simplified as follows:

$$\begin{aligned}\dot{V}_{ref} &= \left(e_{ref}\frac{\partial \theta_i}{\partial u_{ref}}\right)\left[\frac{\partial u_{ref}}{\partial \hat{k}_1}\frac{\partial \hat{k}_1}{\partial t}+\frac{\partial u_{ref}}{\partial \upsilon_1}\frac{\partial \upsilon_1}{\partial t}\right] \\ &= \frac{L_1^{-1}(t)q\chi_1}{\varpi_1 p\dot{e}_{ref}^{p/q-1}}\left|s_{PI-TSM1}\right|^{1/2}\operatorname{sgn}\left(s_{PI-TSM1}(t)\right)\dot{\hat{k}}_1\left(e_{ref}\frac{\partial \theta_i}{\partial u_{ref}}\right) \\ &\quad + \frac{L_1^{-1}(t)q\chi_1}{\varpi_1 p\dot{e}_{ref}^{p/q-1}}\dot{\hat{k}}_3\operatorname{sgn}\left(s_{PI-TSM1}(t)\right)\left(e_{ref}\frac{\partial \theta_i}{\partial u_{ref}}\right)\end{aligned} \tag{5.54}$$

According to the Lyapunov stability theorem, $\dot{V}_{ref}$ should be less than zero to ensure the stability of the system. Based on this, it can be known that $\hat{k}_1$ and $\hat{k}_3$ should be updated as follows:

$$\dot{\hat{k}}_1 = \frac{\varpi_1 p \dot{e}_{ref}^{p/q-1} k_0}{L_1^{-1}(t) q \chi_1} s_{PI-TSM1}(t) \operatorname{sgn}\left(e_{ref} \frac{\partial \theta_i}{\partial u_{ref}} \right) \tag{5.55}$$

where k_0 is a constant coefficient, and $k_0 \in R$.

$$\dot{\hat{k}}_3 = \frac{\varpi_1 p \dot{e}_{ref}^{p/q-1}}{L_1^{-1}(t) q \chi_1} s_{PI-TSM1}(t) \operatorname{sgn}\left(e_{ref} \frac{\partial \theta_i}{\partial u_{ref}} \right) \tag{5.56}$$

Similar to the tracking controller, for the synchronous controller, the switching control law is proposed as follows:

$$\begin{cases} \dot{s}_{PID-TSM2} = -\hat{k}_2 \left| s_{PI-TSM2} \right|^{1/2} \operatorname{sgn}\left(s_{PI-TSM2}(t) \right) + \upsilon_2 \\ \dot{\upsilon}_2 = -\hat{k}_4 \operatorname{sgn}\left(s_{PI-TSM2}(t) \right) \end{cases} \tag{5.57}$$

Where $\hat{k}_2$ and $\hat{k}_4$ are adaptive parameters, the purpose of setting these two parameters is to reduce the chattering phenomenon in the control process.

From Equation (5.37) (5.57), the control law of the synchronous controller can be defined as follows:

$$-\hat{k}_2 \left| s_{PI-TSM2} \right|^{1/2} \operatorname{sgn}\left(s_{PI-TSM2}(t) \right) + \upsilon_2 =$$

$$\Omega_i(e_i) + \kappa_i(e_i) + \varpi_1 \left(\frac{p}{q \chi_2} \dot{e}_i^{p/q-1} \left(A(t) \dot{e}_i + L_1(t) u_i^* + L_2(t) \left(d_i - \frac{\sum_{j=1}^{n} d_j}{n} \right) \right) \right)$$

$$u_i^* = L_1^{-1}(t) \left(-A(t) \dot{\theta}_i + \frac{q \chi_2 \left(-\hat{k}_2 \left| s_{PI-TSM2} \right|^{1/2} \operatorname{sgn}\left(s_{PI-TSM2}(t) \right) + \upsilon_2 - \Omega_i(e_i) - \kappa_i(e_i) \right)}{\varpi_1 p \dot{e}_i^{p/q-1}} \right) \tag{5.59}$$

The system's Lyapunov equation can be defined as follows:

$$V_i = \frac{1}{2} e_i^2 \tag{5.60}$$

The derivative of V_i is calculated as follows:

$$\begin{aligned} \dot{V}_i &= \frac{1}{2}\left(\frac{\partial V_i}{\partial e_i}\frac{\partial e_i}{\partial \theta_i}\frac{\partial \theta_i}{\partial u_i^*} \right)\left[\frac{\partial u_i}{\partial \hat{k}_2}\frac{\partial \hat{k}_2}{\partial t} + \frac{\partial u_i^*}{\partial \sigma \upsilon_2}\frac{\partial \upsilon_2}{\partial t} \right] \\ &= \left(e_i \frac{\partial \theta_i}{\partial u_i^*} \right)\left[\frac{\partial u_i^*}{\partial \hat{k}_2}\frac{\partial \hat{k}_2}{\partial t} + \frac{\partial u_1^*}{\partial \upsilon_2}\frac{\partial \upsilon_2}{\partial t} \right] \end{aligned} \tag{5.61}$$

Similar to Equation (5.52) (5.53) can be simplified as follows:

$$\begin{aligned} \dot{V}_i &= \left(e_i \frac{\partial \theta_i}{\partial u_i^*} \right)\left[\frac{\partial u_i^*}{\partial \hat{k}_2}\frac{\partial \hat{k}_2}{\partial t} + \frac{\partial u_i^*}{\partial v_2}\frac{\partial v_2}{\partial t} \right] \\ &= -\frac{L_1^{-1}(t) q \chi_2}{\varpi_1 p \dot{e}_i^{p/q-1}} \left| s_{PI-TSM2} \right|^{1/2} \operatorname{sgn}\left(s_{PI-TSM2}(t) \right) \dot{\hat{k}}_2 \left(e_o \frac{\partial \theta_i}{\partial u_1^*} \right) \\ &\quad - \frac{L_1^{-1}(t) q \chi_2}{\varpi_1 p \dot{e}_i^{p/q-1}} \dot{\hat{k}}_4 \operatorname{sgn}\left(s_{PI-TSM1}(t) \right) \left(e_i \frac{\partial \theta_i}{\partial u_i^*} \right) \end{aligned} \tag{5.62}$$

Similar to Equation (5.55) (5.56), the update laws for $\hat{k}_2$ and $\hat{k}_4$ are defined as follows:

$$\dot{\hat{k}}_2 = \frac{\varpi_1 p \dot{e}_i^{p/q-1} k_0}{L_1^{-1}(t) q \chi_2} s_{PI-TSM2}(t) \operatorname{sgn}\left(e_i \frac{\partial \theta_i}{\partial u_i^*} \right) \tag{5.63}$$

$$\dot{\hat{k}}_4 = \frac{\varpi_1 p \dot{e}_i^{p/q-1}}{L_1^{-1}(t) q \chi_2} s_{PI-TSM2}(t) \operatorname{sgn}\left(e_i \frac{\partial \theta_i}{\partial u_i^*} \right) \tag{5.64}$$

In sliding mode control, most of the switching laws used are *sgn* function or *sat* function. This work uses super-twisting algorithm to replace the traditional switching law, which effectively improves the chattering phenomenon of sliding mode. Equation (5.55) (5.56) (5.63) (5.64) give an adaptive method of gain value in the super-twisting algorithm, which can keep the system stable.

5.4 Interval Type 2 Fuzzy Control

The combination of fuzzy control and sliding mode control can reduce the dependence of the control system on the controlled object model. Although fuzzy sliding mode control has many advantages, the commonly used one-type fuzzy control algorithm also has many problems. For example, in the face of system modeling difficulties and minimizing uncertainty, the uncertainty of the corresponding membership function will be generated. It is difficult to directly deal with the uncertainty of its own fuzzy rules by using a type of fuzzy set represented by the exact membership function.

The type 2 fuzzy logic system is a new system tool. The Type 2 fuzzy logic system is a new system tool. It was proposed in 1998 by a working group led by Professors Jerry Mendal and Professor Liang Qilian of the Department of Electrical Engineering of the University of Southern California[51]. This group applied Type 2 fuzzy logic to time-varying channel equalization, which worked very well.

Traditional fuzzy systems are constructed based on fuzzy sets, using corresponding fuzzy logic inference and precision to achieve specific system functions. However, fuzzy sets have limitations when dealing with the uncertainty of real objects. The membership values in the exact set are given fuzzification values. Such fuzzy sets are called type-one fuzzy sets[52]. In order to enhance the ability of traditional fuzzy systems to describe and deal with uncertainties, the traditional fuzzy sets are extended to further give the degree of ambiguity of the membership values in the set, so that the set ambiguity of the description is enhanced. This extended general fuzzy set is called a type-2 fuzzy set. A system based on type-1 fuzzy set is called type-1 fuzzy logic system, and system based on type-2 fuzzy set is called type-2 fuzzy logic system (Type-2 FLS)[53].

It can be seen from Figure 5.2 that compared with the type-1 fuzzy system, the type-2 fuzzy further refines the fuzzy subset in the fuzzy output, which improves the accuracy of the fuzzy algorithm.

Figure 5.2 shows the control process of T2FC. Firstly, Input values are converted to fuzzy variables by fuzzy sets. The input values are reasoned by the fuzzy rule. After the calculation of the membership function, the fuzzy variable of the output can be obtained. After defuzzification, we can get the output value.

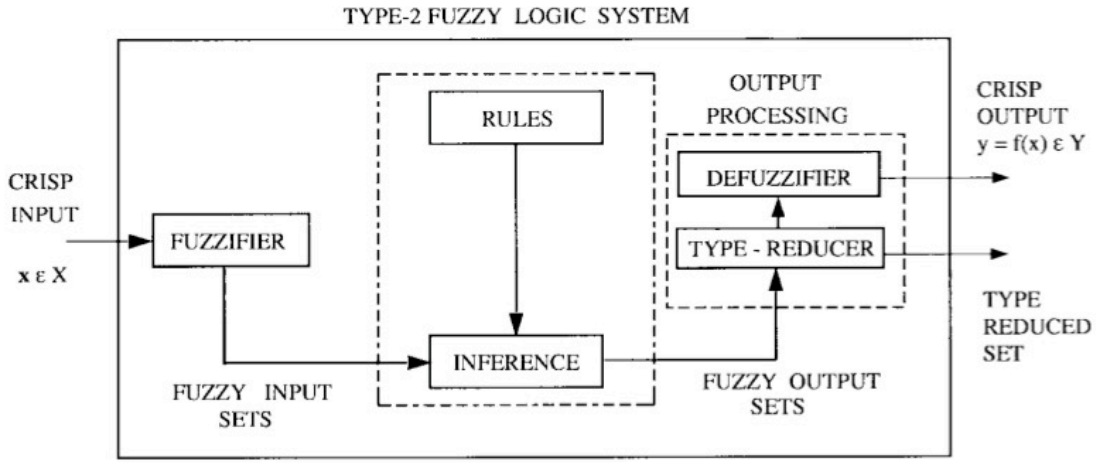

Figure 5.2 The schematic diagram of the type 2 fuzzy controller[54]

There are many types of fuzzy control methods. In order to reduce the complexity of the calculation, the interval type-2 fuzzy method is used to estimate the uncertainty of the system online. The sub-degree membership of the fuzzy set of interval type-2 fuzzy system is only 0 or 1.

Firstly, this work selects $A(t)$ and $L_1(t)$ in the system as the input of the model system, and fuzzifies it. We use the singleton fuzzification method to fuzzify these two variables, which ensures that each variable has a corresponding fuzzy value after it has been fuzzified.

Define the fuzzy set of T2-FS as $\tilde{Q}$, x is the input primary variable of T2-FLS and $x \in X_0$. X_0 is the domain. $u_{\tilde{Q}}(x)$ is the membership of x , u is the secondary variable, and $u \in J_x, J_x \in [0,1]$. $f_x(u)$ is the secondary of membership. $\tilde{Q}$ can be expressed as follows:

$$\tilde{Q} = \int_{x \in X_0} u_{\tilde{Q}} / x = \int_{x \in X_0} \left[\int_{u \in J_x} f_x(u) / u \right] / x \tag{5.65}$$

Where u is the fuzzy set in $[0,1]$, not the specific value in $[0,1]$. When $f_x(u) = 1$, $\forall u \in J_x \subseteq [0,1]$. The sub-member function is an interval type 2 membership function. We can re-represent as $\tilde{Q}$ follows:

$$\tilde{Q} = \int_{x \in X_0} u_{\tilde{Q}} / x = \int_{x \in X_0} \left[\int_{u \in J_x} 1 / u \right] / x \tag{5.66}$$

Gaussian interval type T2-FS membership function consists of an adjustable uncertainty center value m_1, m_1 and an adjustable standard deviation σ, as shown in equation

$$\mu_{\tilde{Q}} = \exp\left[-\frac{1}{2}\left(\frac{x-m}{\sigma} \right)^2 \right]_{m \in [m_1, m_2]} \tag{5.67}$$

Where $\tilde{Q}$ is the interval type-2 set, x is the input variable of T2-FLS, and x' is a value of x. Figure shows the Gaussian interval type T2-FS (Type-2 Fuzzy Set) with an uncertain center. As we can be seen from the figure, T2-FS is a fuzzy set region that describes the uncertainty of the membership function. With type-1 fuzzy membership function, that is, the Gaussian membership function is the boundary. The upper bound of the domain is represented by UMF, and the lower bound of the domain is represented by LMF. This domain is called the foot-print of uncertain (FOU). It is represented by the gray part of Figure. The UMF and LMF of the interval type-2 fuzzy membership function are denoted by $\overline{\mu}_{\tilde{A}}(x')$ and $\underline{\mu}_{\tilde{A}}(x')$, respectively, which are μ_1 and μ_2 in Figure 5.3.

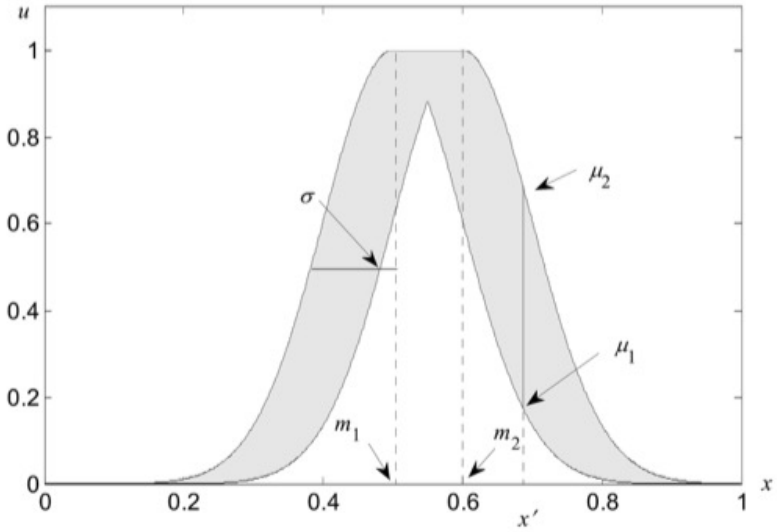

Figure 5.3 Two-dimensional diagram of membership function of type 2 fuzzy control[55]

Where μ_1 is the upper membership function, μ_2 is the lower membership function.

According to the characteristics of the overhead crane system, a multi inputs single output interval type-2 fuzzy logic system is considered, and we suppose that it has *z* antecedents and *W* rules, the corresponding *j*th rule is depicted as follows[56]:

$$R^i : IF\ x_1\ is\ \tilde{Q}_1^j\ and\ x_2\ is\ \tilde{Q}_2^j, \ldots, x_1\ is\ \tilde{Q}_z^j\ THEN\ y\ is\ \tilde{P}^j$$

Where $x \in X_0$, y is the output of the interval type-2 fuzzy system. $\tilde{Q}^j$ and $\tilde{P}^j$ are interval type-2 fuzzy sets of input values and output values. $j = 1,2,...,W$ is the number of fuzzy rules, W is a positive integer.

The fuzzy inference engine and the rule base are combined to specify a mapping relationship between an input typ-2 fuzzy set and an output type-2 fuzzy set. In this process, the type-2 fuzzy set will have intersection and union operations. The fuzzy inference engine outputs a type-2 fuzzy set, which is degraded to obtain a type-1 fuzzy set. After defuzzification, a clear output is obtained.

The fuzzy system input variable x is processed by singleton fuzzification method. The reduced-order fuzzy set is obtained based on the product inference engine and Center-of-sets (COS).

$$Y_{\cos}\left(Y^1,...,Y^W,A^1,...,A^W\right)=\left[y_l,y_r\right]=\int_{y^l}\cdots\int_{y^W}\cdots\int_{f^1}\cdots\int_{f^W}\left(1/\frac{\sum_{j=1}^{W}f^j y^j}{\sum_{j=1}^{W}f^j}\right) \tag{5.68}$$

Where $Y_{\cos}$ is the set of intervals determined by the left and right endpoints y_l, y_r; $y^j \in Y^j=\left[y_l^j,y_r^j\right]$ represents the central interval set of $\tilde{P}^j$; $f^j \in \tilde{Q}^j=\left[\underline{f}^j,\overline{f}^j\right]$, where

$$\underline{f}^j=\underline{\mu}_{\tilde{A}^j}\left(x\right) \tag{5.69}$$

$$\overline{f}^j=\overline{\mu}_{\tilde{A}^j} \tag{5.70}$$

Therefore, for $\forall y \in Y_{\cos}$, y can be expressed as follows:

$$y=\frac{\sum_{j=1}^{W}f^j y^j}{\sum_{j=1}^{W}f^j} \tag{5.71}$$

Where y is the monotonically increasing function of y^j. Furthermore, y_l is the minimum value of y_l^j, y_r is the maximum value of y_r^j, and the magnitude of y_l and y_r depends on the value of $\underline{f}^j$, $\overline{f}^j$.Therefore, the leftmost endpoint l and the rightmost endpoint r are represented by fuzzy-base-function(FBF) as follows:

$$y_l=\frac{\sum_{j=1}^{W}f_l^j y_l^j}{\sum_{j=1}^{W}f_l^j}=\sum_{j=1}^{W}y_l^j\xi_l^j \tag{5.72}$$

$$y_r=\frac{\sum_{j=1}^{W}f_r^j y_r^j}{\sum_{j=1}^{W}f_r^j}=\sum_{j=1}^{W}y_r^j\xi_r^j \tag{5.73}$$

$$\xi_l^j=\frac{f_l^j}{\sum_{j=1}^{W}f^j} \tag{5.74}$$

$$\xi_r^j = \frac{f_r^j}{\sum_{j=1}^{W} f^j} \tag{5.75}$$

The FBF vector is defined as $\boldsymbol{\xi}_l = \left[\xi_l^1, \xi_l^2, ..., \xi_l^W\right]$, $\boldsymbol{\xi}_r = \left[\xi_r^1, \xi_r^2, ..., \xi_r^W\right]$, $\boldsymbol{\xi}_r = \left[\xi_r^1, \xi_r^2, ..., \xi_r^W\right]$, $\boldsymbol{y}_l^T = \left[y_l^1, y_l^2, ..., y_l^W\right]$, $\boldsymbol{y}_r^T = \left[y_r^1, y_r^2, ..., y_r^W\right]$.

Equation (5.72) and (5.73) can be rewritten as:

$$y_l = \frac{\sum_{j=1}^{W} f_l^j y_l^j}{\sum_{j=1}^{W} f_l^j} = \sum_{j=1}^{W} y_l^j \xi_l^j = \boldsymbol{y}_l^T \boldsymbol{\xi}_l \tag{5.76}$$

$$y_r = \frac{\sum_{j=1}^{W} f_r^j y_r^j}{\sum_{j=1}^{W} f_r^j} = \sum_{j=1}^{W} y_r^j \xi_r^j = \boldsymbol{y}_r^T \boldsymbol{\xi}_r \tag{5.77}$$

For illustrating the results, a brief description of the calculation method of y_r is given here. Without loss of generality, assume that y_r^i is in ascending order, that is $y_r^1 \le y_r^2 \le \cdots \le y_r^W$.

Step 1: Define $f_r^j = \frac{\underline{f}^j + \overline{f}^j}{2}$, $j = 1,2,...,W$, where and b are both calculated by Equation, let $y_r' = y_r$;

Step 2: According to the actual situation of the system, choose the value of R $\left(1 \le R \le W-1\right)$, so that $y_r^R \le y_r' \le y_r^{R+1}$;

Step 3: When $j \le R$, $f_r^j = \underline{f}^j$. When $j > R$, $f_r^j = \overline{f}^j$. Use this rule to calculate y_r, let $y_r = y_r''$;

Step 4: If $y_r' \ne y_r''$, proceed to step 5. If $y_r' = y_r''$, stop the calculation. Let $y_r = y_r''$;

Step 5: Set $y_r' = y_r''$ and return to step 2.

It can be seen that the above algorithm is to find the values $\underline{f}^j$ and $\overline{f}^j$ on both sides separated by R. Therefore, Equation (5.77) can be expressed as follows:

$$y_r = \frac{\sum_{j=1}^{R} \underline{f}^j y_r^j + \sum_{j=R+1}^{W} \overline{f}^j y_r^j}{\sum_{j=1}^{R} \underline{f}^j + \sum_{j=R+1}^{W} \overline{f}^j} = \sum_{j=1}^{R} \underline{a}_r^j y_r^j + \sum_{j=R+1}^{W} \overline{a}_r^j y_r^j = \left[\underline{\boldsymbol{A}}_r \ \overline{\boldsymbol{A}}_r \right] \begin{bmatrix} \underline{y}_r \\ \overline{y}_r \end{bmatrix} = \boldsymbol{\xi}_r^T \boldsymbol{\Theta}_r \tag{5.78}$$

Where $\underline{a}_r^j = \dfrac{\underline{f}^j}{D_r}$, $\overline{a}_r^j = \dfrac{\overline{f}^j}{D_r}$, $D_r = \left(\sum_{j=1}^{R} \underline{f}^j + \sum_{j=R+1}^{W} \overline{f}^j \right)$, $\underline{\boldsymbol{A}}_r = \left[\underline{a}_r^1, \underline{a}_r^2, ..., \underline{a}_r^R \right]$,

$\overline{\boldsymbol{A}}^r = \left[\overline{a}_r^{R+1}, \overline{a}_r^{R+2}, ..., \overline{a}_r^W \right]$, $\underline{y}_r = \left[y_r^1, y_r^2, ..., y_r^R \right]^T$, $\overline{y}_r = \left[y_r^{R+1}, y_r^{R+2}, ..., y_r^W \right]^T$,

$\boldsymbol{\xi}_r^T = \left[\underline{\boldsymbol{A}}_r \ \overline{\boldsymbol{A}}_r \right]$, $\boldsymbol{\Theta}_r^T = \left[\underline{\boldsymbol{y}}_r \ \overline{\boldsymbol{y}}_r \right]$.

The method of calculating y_l and y_r is similar, and the differences are as follows:

1 In step 2, select the appropriate value of L $\left(1 \le L \le W-1\right)$ so that $y_l^L \le y_l' \le y_l'^{L+1}$;

2 In step 3, when $j \le L$, $f_l^j = \underline{f}^j$. When $j > L$, $f_l^j = \underline{f}^j$.

$$y_l = \frac{\sum_{j=1}^{L} \underline{f}^j y_l^j + \sum_{j=L+1}^{W} \overline{f}^j y_l^j}{\sum_{j=1}^{R} \underline{f}^j + \sum_{j=L+1}^{W} \overline{f}^j} = \sum_{j=1}^{L} \underline{a}_l^j y_l^j + \sum_{j=L+1}^{W} \overline{a}_l^j y_l^j = \left[\underline{\boldsymbol{A}}_l \ \overline{\boldsymbol{A}}_l \right] \begin{bmatrix} \underline{y}_l \\ \overline{y}_l \end{bmatrix} = \boldsymbol{\xi}_l^T \boldsymbol{\Theta}_l \tag{5.79}$$

Where $\underline{a}_l^j = \dfrac{\underline{f}^j}{D_l}$, $\overline{a}_l^j = \dfrac{\overline{f}^j}{D_l}$, $D_l = \left(\sum_{j=1}^{L} \underline{f}^j + \sum_{j=L+1}^{W} \overline{f}^j \right)$, $\underline{\boldsymbol{A}}_l = \left[\underline{a}_l^1, \underline{a}_l^2, ..., \underline{a}_l^L \right]$,

$\overline{\boldsymbol{A}}^l = \left[\overline{a}_l^{L+1}, \overline{a}_l^{L+2}, ..., \overline{a}_l^W \right]$, $\underline{y}_l = \left[y_l^1, y_l^2, ..., y_l^L \right]^T$, $\overline{y}_l = \left[y_l^{L+1}, y_l^{L+2}, ..., y_l^W \right]^T$,

$\boldsymbol{\xi}_l^T = \left[\underline{\boldsymbol{A}}_l \ \overline{\boldsymbol{A}}_l \right]$, $\boldsymbol{\Theta}_l^T = \left[\underline{\boldsymbol{y}}_l \ \overline{\boldsymbol{y}}_l \right]$.

Then the exact output variable after the defuzzification of interval T2-FLS is

$$y(x) = \frac{y_l + y_r}{2} = \frac{1}{2}\left(\boldsymbol{\xi}_l^T \boldsymbol{\Theta}_l + \boldsymbol{\xi}_r^T \boldsymbol{\Theta}_r \right) = \frac{1}{2} \left[\boldsymbol{\xi}_l^T \ \boldsymbol{\xi}_r^T \right] \begin{bmatrix} \boldsymbol{\Theta}_l \\ \boldsymbol{\Theta}_r \end{bmatrix} = \boldsymbol{\xi} \boldsymbol{\Theta}^T \tag{5.80}$$

Where $\boldsymbol{\xi} = \frac{1}{2}\left[\boldsymbol{\xi}_l^T \ \boldsymbol{\xi}_r^T\right]$, $\boldsymbol{\Theta} = \left[\boldsymbol{\Theta}_l \ \boldsymbol{\Theta}_r\right]$.

The estimation of $A(t)$ and $L_1(t)$ can be obtained by Equation (5.80):

$$\hat{A}\left(\theta_i, \delta_A\right) = \delta_A \boldsymbol{\Theta}^T \tag{5.81}$$

$$\hat{L}_1\left(\theta_i, \delta_L\right) = \delta_L \boldsymbol{\Theta}^T \tag{5.82}$$

From Equations (5.81) (5.82), and (5.49) (5.59), it can be concluded that the tracking control u_{ref} and the synchronization control u_i^* are as follows:

$$\begin{aligned} u_{ref} = {} & \hat{L}_1^{-1}(t)\left(-\hat{A}(t)\dot{\theta}_i + \ddot{\theta}_d\right) \\ & - \hat{L}_1^{-1}(t)\left(\frac{q\chi_1\left(-\hat{k}_1\left|s_{PI-TSM1}\right|^{1/2}\operatorname{sgn}\left(s_{PI-TSM1}(t)\right) + \upsilon_1 - \Omega_{ref}\left(e_{ref}\right) - \kappa_{ref}\left(e_{ref}\right)\right)}{\varpi_1 p \dot{e}_{ref}^{p/q-1}}\right) \end{aligned} \tag{5.83}$$

$$\begin{aligned} u_i^* = {} & \hat{L}_1^{-1}(t) \\ & \left(-\hat{A}(t)\dot{\theta}_i + \frac{q\chi_2\left(-\hat{k}_2\left|s_{PI-TSM2}\right|^{1/2}\operatorname{sgn}\left(s_{PI-TSM2}(t)\right) + \upsilon_2 - \Omega_i\left(e_i\right) - \kappa_i\left(e_i\right)\right)}{\varpi_1 p \dot{e}_i^{p/q-1}}\right) \end{aligned} \tag{5.84}$$

Through the interval type-2 fuzzy control method, the parameters of the system are estimated. Combined with the terminal sliding mode control method, the chattering phenomenon of sliding mode control is improved. Meanwhile, the super-helical algorithm improves the problem of excessive switching law gain and makes the system more stable. According to the simulation results in the following sections, the superiority of the proposed algorithm is further explained.

Chapter 6 Simulation and Result

6.1 Simulink

Simulink is a visual simulation tool in MATLAB. Meanwhile, it is a block diagram design environment based on MATLAB. Simulink implements dynamic system modeling, a software package for simulation and analysis. It is widely used in the modeling and simulation of linear systems, nonlinear systems, digital control and digital signal processing. Simulink can be used to construct complex systems without the need for a lot of writing programs, but with a simple and intuitive mouse operation [57].

This work uses Simulink to simulate the proposed control algorithm and model, we can analyze the superiority of the algorithm based on the simulation results. The figure6.1 is the simulation interface of the fuzzy sliding mode algorithm proposed in this work. The packaged controller in the simulation is the construction of the algorithm, and the packaged motor is the construction of the overhead crane model. The final outputs are the synchronization error, the tracking error, the output torque of the motor, the speed of the motor and the position of the motor.

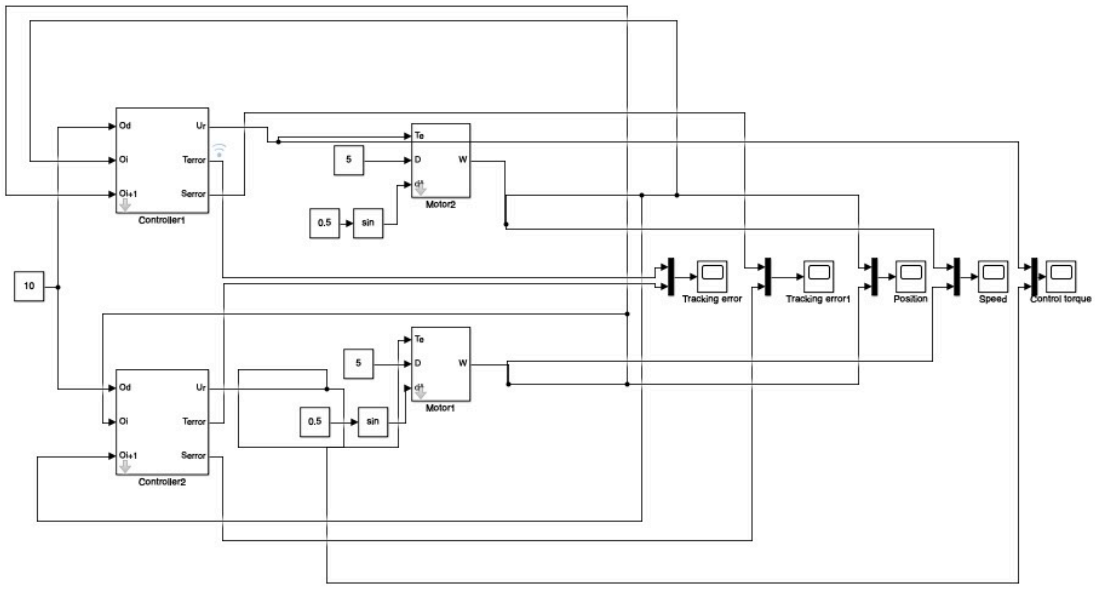

Figure 6.1 The interface of the simulation

The model of the controlled bridge crane, that is, the model of the motor, can be known from Equation (3.8). Fig.6.2 shows the structure of the motor in the simulation. This model is built according to Equation (3.8).

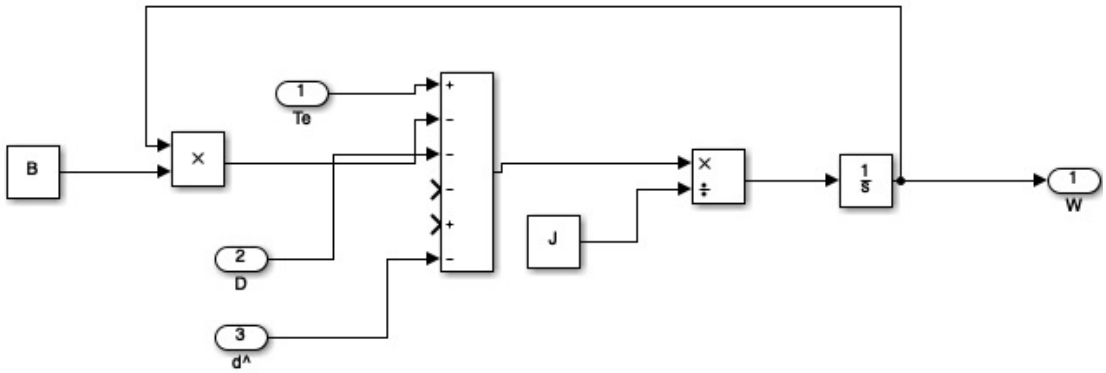

Figure 6.2 Construction of the motor model in the simulation

The structure of the controller is shown in Figure 6.3. This controller is built according to the method proposed in Chapter 4.

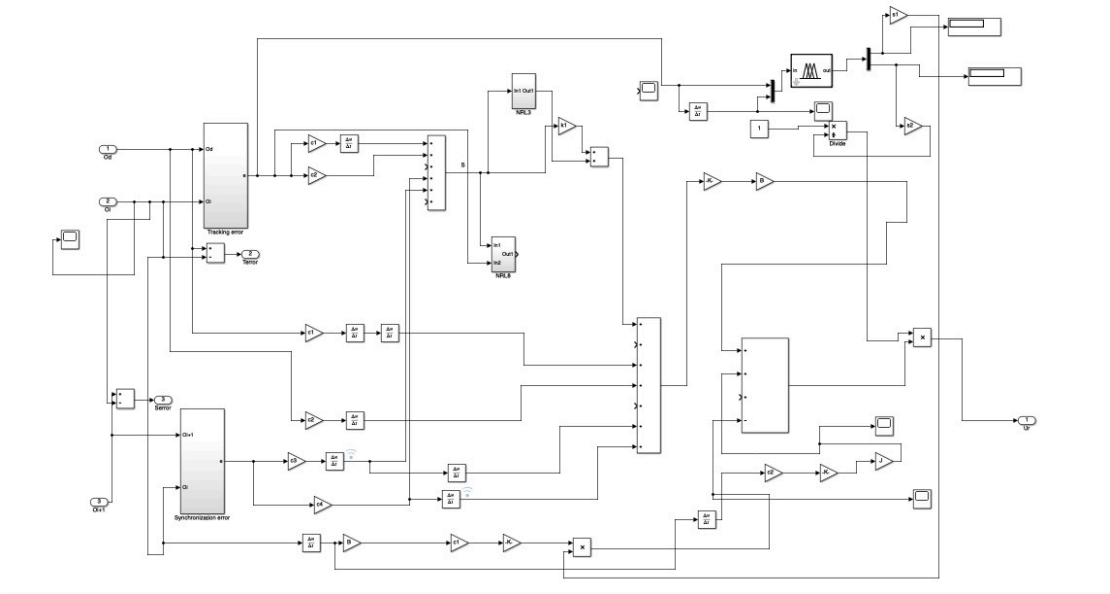

Figure 6.3 Construction of the controller in the simulation

According to the above simulation of the controller and the motor model, the simulation of the overhead crane system is completed. According to different control

methods, the structure of the controller is modified. The simulation results are compared, that is, the size of the synchronization error and tracking error and the stability of the system, and the superiority of the control method is evaluated.

6.2 Fuzzy sliding mode control results

In order to illustrate the performance of the fuzzy sliding mode control method, the simulation results of the traditional sliding mode control are compared with the simulation results of the FSMC proposed in this work.

Case 1: Sliding mode control based on double-container overhead crane system with or without fuzzy control. The load G_1 of the container 1 is set to 5 N/m, the load $G_2$of the container 2 is set to 5 N/m, and the desired angle is $\theta_d = 10rad$ [58].

Some important parameters of the controller are set as Table 6.1.

Table 6.1 Parameter values in the simulation

	J	**B**	**K**
Motor 1	0.0016	0.008	100
Motor 2	0.0008	0.005	100

Set the controller according to the values in Table 6.1. Figures 6.4 and 6.5 are the tracking error and synchronization error generated by the system using the traditional sliding mode method.

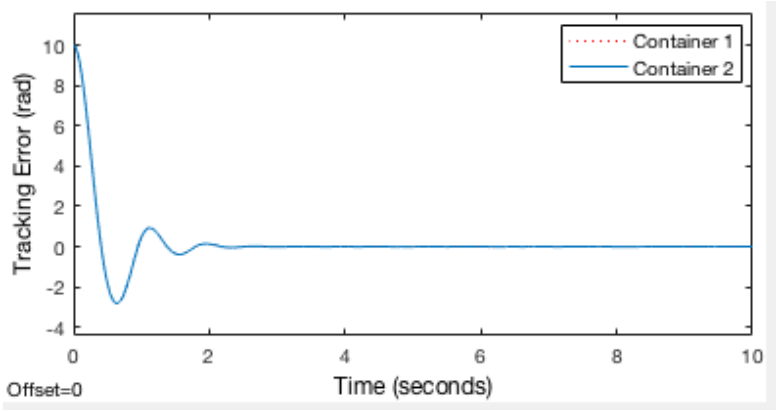

Figure 6.4 Tracking error under traditional sliding mode control

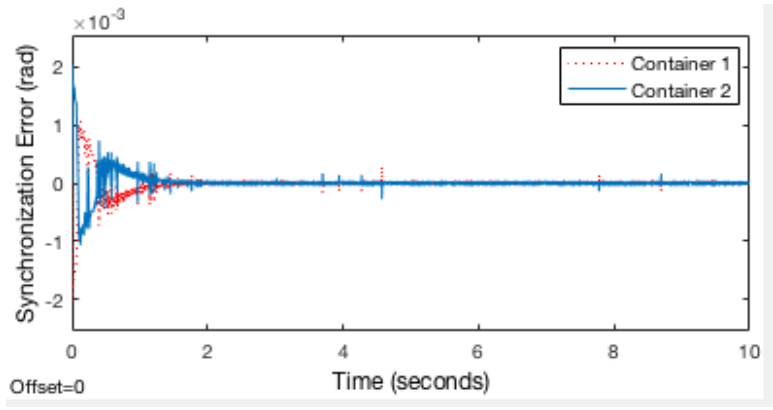

Figure 6.5 Synchronization error under traditional sliding mode control

Set the controller according to the values in Table 6.1. Figures 6.5 and 6.6 are the tracking error and synchronization error generated by the system in the case of using the combination of fuzzy control and sliding mode control to control the system.

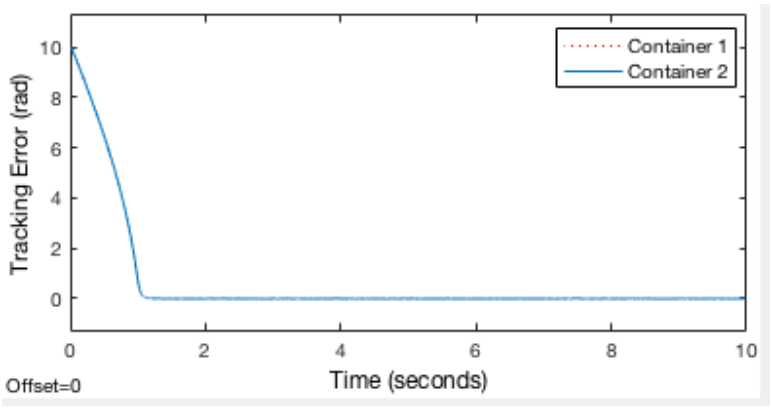

Figure 6.6 Tracking error under FSMC

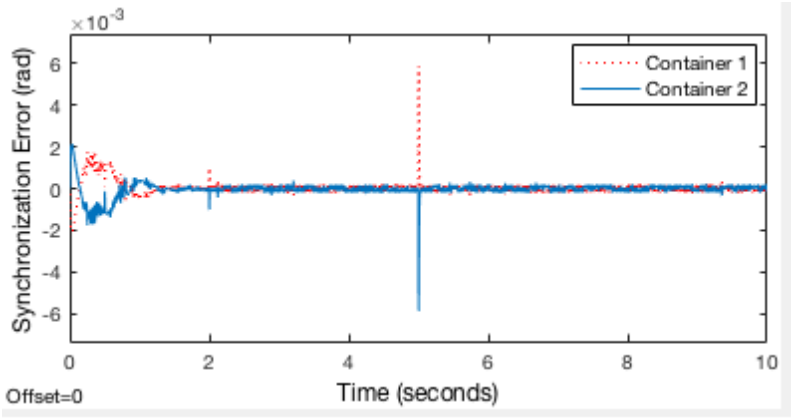

Figure 6.7 Synchronization error under FSMC

Table 6.2 Comparison of simulation results

	Tracking error convergence time(second)	**Synchronization error(rad)**	**Overshoot in the control process**
SMC	2.2s	$2 * 10^{-4}$	30%
FSMC	1.1s	$0.3 * 10^{-4}$	0%

It can be seen from Fig. 6.4 that after the overhead crane system is controlled by the traditional sliding mode, when the drive motor of the overhead crane reaches the specified value, the tracking error of the system has a 30% overshoot, which indicates that the system is unstable. The synchronization error converges to around $2 * 10^{-4}$.

It can be seen from Fig. 6.5 that after the overhead crane system is controlled by the fuzzy sliding mode, the tracking error has no overshoot and smoothly converges to infinity at 1s. The synchronization error converges to around $0.3 * 10^{-4}$.

The overhead crane system is controlled by two methods, and the following conclusions can be drawn from the simulation results. The tracking error in Fig. 6.6 does not produce overshoot, and Fig. 6.4 shows that the tracking error has a 30% overshoot. The fuzzy control method successfully estimates the parameters of the system and makes the system more stable in the control process. Meanwhile, the fuzzy

sliding mode method proposed in this work is more effective in reducing the synchronization error than the traditional sliding mode method.

Case 2 When the system parameters change, the robustness of the system is reflected by the synchronization error of the drive motors of the two spreaders. This simulation compares the robustness of the system with or without fuzzy control. The load G_1 of the container 1 is set to 2 N/m, the load G_2 of the container 2 is set to 2 N/m, and the desired angle is $\theta_d = 10rad$.

Set the controller according to the values in Table 6.1. Figures 6.8 is the synchronization error generated by the system in the case of using the traditional sliding mode control to control the system. At 0.5s, the viscosity coefficient B of the drive motor of the spreader is abruptly changed to two-thirds of the original, that is, $B` = \frac{2B}{3}$.

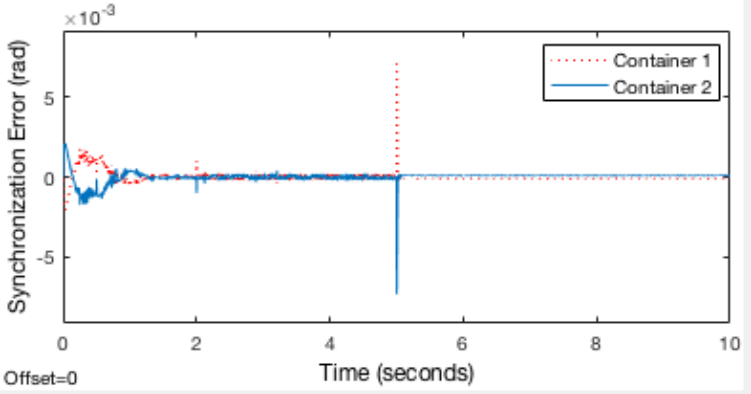

Figure 6.8(a) Synchronization error under parameter variation

Fig. 6.8(a) shows the synchronization error of the double spreader based on the traditional sliding mode control. After 0.5 s, the value of the synchronization error has changed.

Set the controller according to the values in Table 6.1. Figures 6.8 is the synchronization error generated by the system in the case of using the combination of

fuzzy control and sliding mode control to control the system. At 0.5s, the viscosity coefficient B of the drive motor of the spreader is abruptly changed to two-thirds of the original, that is, $B` = \frac{2B}{3}$.

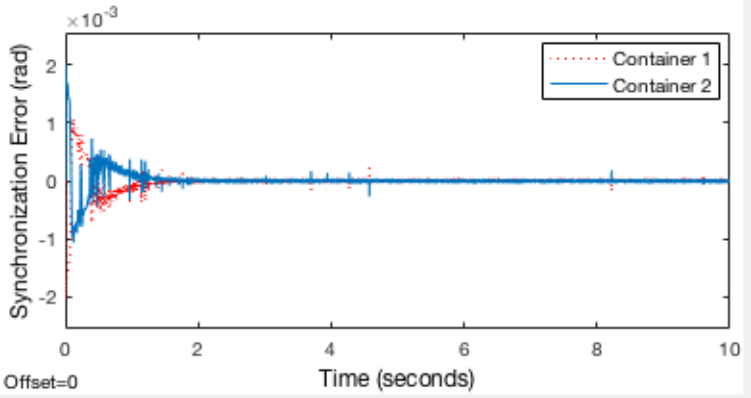

Figure 6.8(b) Synchronization error under parameter variation

Fig. 6.8(b) shows the synchronization error of the double spreader based on FSMC. It can be seen that the system has little change before and after 0.5s.

It can be seen from Figures 6.8(a) and 6.8(b) that when the parameters of the system are perturbed, the system under FSMC is less affected. The traditional sliding mode control is greatly affected. This shows that the system under the fuzzy sliding mode control method is robust.

6.3 Interval type-2 fuzzy terminal sliding mode control results

In order to illustrate the performance of the interval type-2 fuzzy terminal sliding mode control (IT2FTSMC) method, the simulation results of the traditional terminal sliding mode control are compared with the simulation results of the interval IT2FTSMC proposed in this work.

Case 1: This simulation is built in independent working mode, as shown in Eq. (3.8). The load G_1 of the container 1 is set to 5 N/m, the load G_2 of the container 2 is set to 5 N/m, and the desired angle is $\theta_d = 10rad$.

Set the controller according to the values in Table 6.1. Figures 6.9 and 6.10 are the tracking error and synchronization error generated by the system using the traditional terminal sliding mode method.

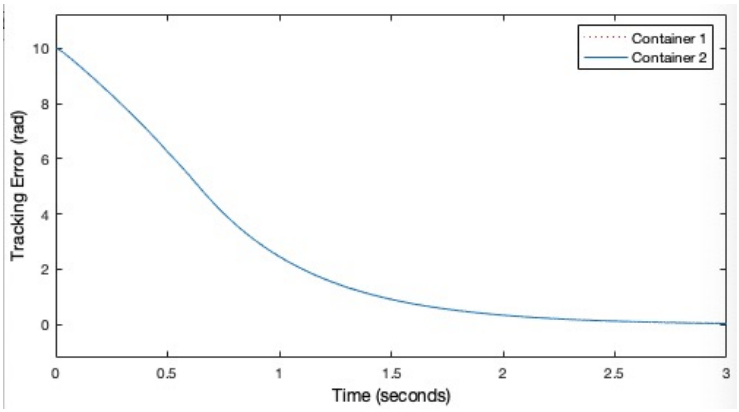

Figure 6.9 Tracking error under traditional terminal sliding mode control

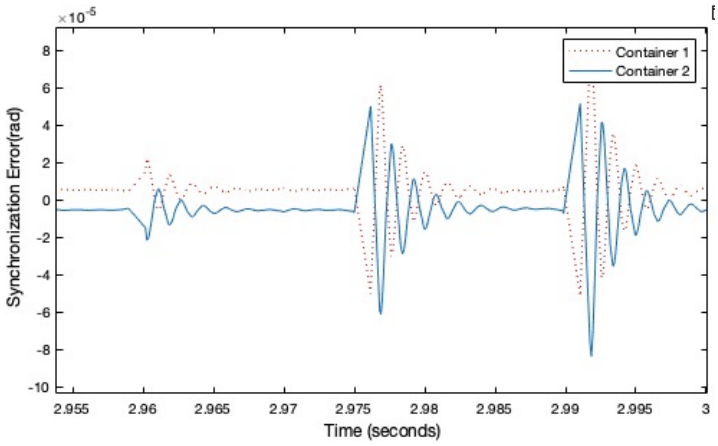

Figure 6.10 Synchronization error under traditional terminal sliding mode control

It can be seen from Figure 6.9 that under the control of the traditional terminal sliding mode, the tracking error converges to zero in about 2s. The synchronization error finally converges to $0.25 * 10^{-5}\ rad$, but it always vibrates in the range of $\pm 8 * 10^{-5}\ rad$.

Set the controller according to the values in Table 6.1. Figures 6.5 and 6.6 are the tracking error and synchronization error generated by the system in the case of using

the combination of interval type-2 fuzzy control and PID terminal sliding mode control to control the system.

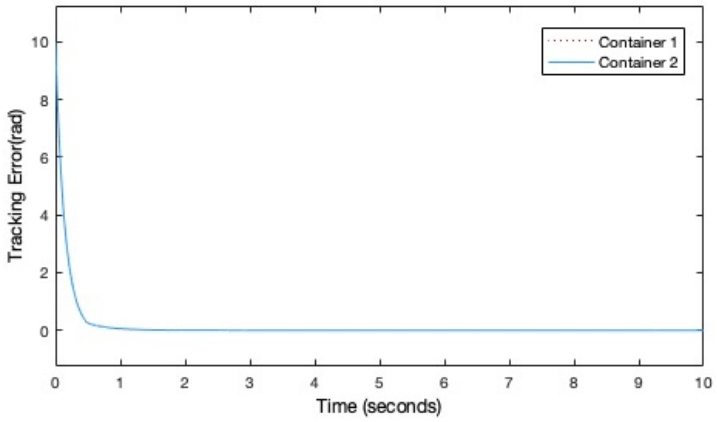

Figure 6.11 Tracking error under the IT2FTSMC

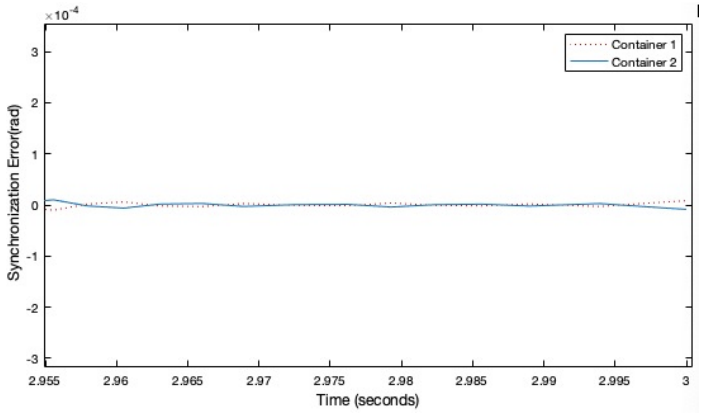

Figure 6.12 Synchronization error under IT2FTSMC

It can be seen from Figure 6.11 that under the IT2FTSMC, the tracking error converges to zero in about 0.4s. The synchronization error finally converges to $0.6 * 10^{-5}\ rad$.

Table 6.3 Comparison of simulation results

	Tracking error convergence time(second)	**Synchronization error(rad)**
TSMC	2s	$0.8 * 10^{-5}$
IT2FTSMC	0.4s	$0.6 * 10^{-5}$

Comparing Tables 6.2 and 6.3, it can be seen that the control performance of the terminal sliding mode is better. Using the improved terminal sliding mode proposed in this work, the control speed of the tracking control is faster. During the synchronous control process, the system is more stable and the control precision is higher.

Case 2: This simulation is built in interlock working mode, as shown in Eq. (3.10). The load G_1 of the container 1 is set to 5 N/m, the load G_2 of the container 2 is set to 5 N/m, and the desired angle is $\theta_d = 10rad$.

Set the controller according to the values in Table 6.1. Figures 6.13(a) is the synchronization error generated by the system using the traditional terminal sliding mode method.

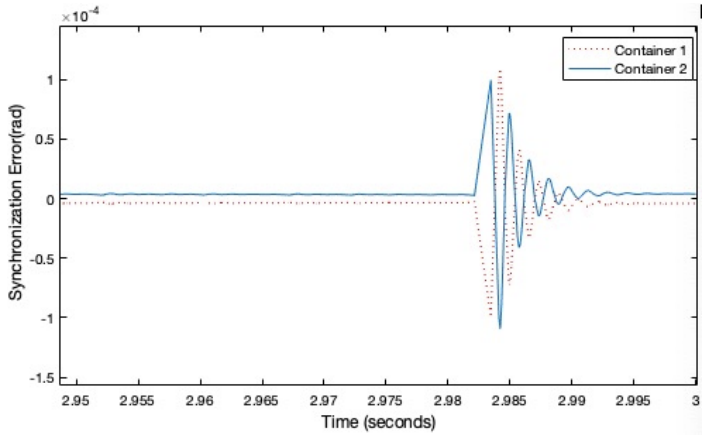

Figure 6.13 Synchronization error under traditional terminal sliding mode control

Figure 6.13 is the synchronization error of the system in the interlock working mode. The synchronization error vibrates in the range of $\pm 1 * 10^{-4}\ rad$.Compared with the synchronization error shown in Figure 6.10, the amplitude of the vibration is larger.

Set the controller according to the values in Table 6.1. Figures 6.14 is the synchronization error generated by the system in the case of using the combination of interval type-2 fuzzy control and PID terminal sliding mode control to control the system.

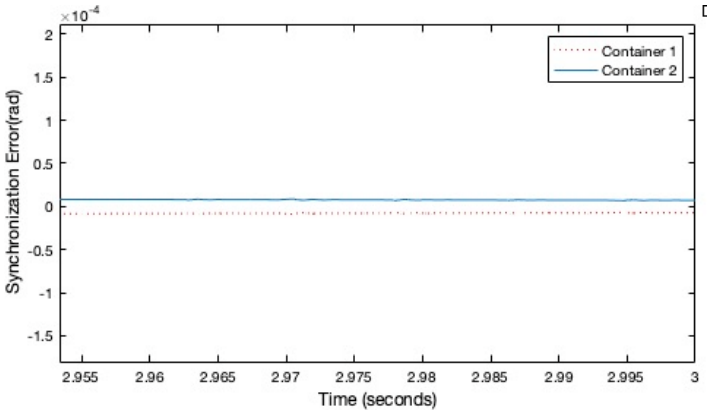

Figure 6.14 Synchronization error under IT2FTSMC

Figure 6.14 is the synchronization error of the system in the interlock working mode. It can be seen from the figure that the synchronization error can finally converge to $1 * 10^{-5}\ rad$. Compared with Figure 6.12, although the synchronization error is increased, the system can finally be controlled within a stable range. This shows that the system is robust.

Chapter 7 Conclusion and Future Work

7.1 Conclusions

This work has designed two different controller for the double spreaders of overhead crane model, so that the overhead crane can run synchronously.

Using the characteristics of a permanent magnet synchronous motor, a double spreader model of the overhead crane was established. Meanwhile, an effective physical analysis of the model was carried out for overhead cranes under different working modes. Considering friction, internal disturbance and other factors, this work successfully designs two suitable controllers to control this model.

This work is based on the tracking control and synchronization control in the overhead crane synchronization problem. For the synchronous control problem, the mean deviation coupling method is adopted in this work. For the tracking control problem, the first controller is based on the sliding mode theory and fuzzy logic control. Because the sliding mode control produces the chattering phenomenon in the control phase, it seriously affects the robustness of the system and the effectiveness of the control. The fuzzy control method is used to estimate the parameters of the system effectively, which reduces the influence of parameter perturbation on the system and reduces the chattering phenomenon of sliding mode control.

The second controller is based on the non-singular fast terminal sliding mode method. The super-twisting algorithm, the type-2 fuzzy control and the non-singular fast terminal sliding mode control are combined to establish the controller. It effectively control the overhead crane system. The non-singular fast terminal sliding mode control solves the problem of slow convergence of the system. The type-2 fuzzy control used in this controller further accurate system model. The super-twisting algorithm makes the system more stable and reliable.

Finally, the effectiveness of the controller is proved by simulation and Lyapunov theorem.

7.2 Contributions

This dissertation‘s ,main contributions are:

- A reliable mathematical model of the double spreader overhead crane is established.
- A fuzzy sliding mode controller is established to improve the response capability of the system and reduce the synchronization error.
- A interval type-2 fuzzy terminal sliding mode controller is established to improves the responsiveness of the system and ensures stability of the system.

The developed work and the initial results were included in the article and the poster in Appendix A, which were accepted and presented at the IEEE ATEE 2019 the 11th International Symposium on Advanced Topics in Electrical Engineering, March 28-30, Bucharest, Romania. The article has been published in IEEEXplorer.

Yongshuang Wang. and Postolache O., “Fuzzy Sliding Mode Synchronous Control of Double-Container for Overhead Crane”, ATEE 2019, Bucharest, Romania 2019 the 11th International Symposium on Advanced Topics in Electrical Engineering.

7.3 Future Work

The proposed controller in this work has been tested by simulation showing good performances expressed by small errors. But exist also some drowbacks, for instance, the effect of friction on the motor is not considered. There are still some areas for improvement.

In the process of external disturbances removing, can be considered disturbance observers or other control methods that will be study in the future.

In order to solve the problem of eliminating tracking error in this work control methods as reinforcement learning or neural network can be considered.

References

[1] Q. F. Bao and M. H. Jin. “Application Practice and Exploration of Double 40-foot Container Bridge Crane.” *Containerization*, 2008(02):1-4.

[2] X. L. Wang and H. M. Fu. “The technology of overhead crane and its application in automated container terminal.” *Lifting the transport machinery*, 2018(01):142-146.

[3] C. Hu. “Discussion on Automatic Leveling Control of Double Lifting Height of overhead Crane” *Lifting the transport machinery*, 2015(03):92-94.

[4] P. Xu and W. M. Xu. “Synchronous control of double-container in overhead crane system.” *Control Theory & Applications*,2013,30(10):1300-1308.

[5] X. Lai and D. Zhu. “Synchronization Control of Double Container Crane Based on Sliding Mode Control.” *Control Engineering*, 2007(s3).145-147.

[6] Bouarroudj, Noureddine. “A hybrid fuzzy fractional order PID sliding-mode controller design using PSO algorithm for interconnected nonlinear systems.” *Journal of Control Engineering and Applied Informatics* 17.1 (2015): 41-51.

[7] Hashim, Ahmad Yusairi Bani, Lokman Abdullah, and Nur Aidawaty Rafan. “Design of Sliding Mode Controller Using Smoothening Method for Chattering Suppression in Machine Tools.” *Intelligent Manufacturing and Mechatronics: Proceedings of the 2nd Symposium on Intelligent Manufacturing and Mechatronics-Sympo SIMM* 2019, 8 July 2019, Melaka, Malaysia. Springer, 2019.

[8] Perez-Pinal, et al. “Comparison of multi-motor synchronization techniques.” *Industrial Electronics Society, 2004. IECON 2004. 30th Annual Conference of IEEE*, 2004.

[9] Vulliez, Margot, Said Zeghloul, and Oussama Khatib. “Design strategy and issues of the Delthaptic, a new 6-DOF parallel haptic device.” *Mechanism and Machine Theory* 128 (2018): 395-411.

[10] Ling, Yun, H. Chen, and F. Li. “Speed Synchronization System of Master-Slave Motor Based on Repetitive Control.” *Applied Mechanics & Materials* 644-650(2014):523-526.

[11] Zhang, C, et al. “Virtual line-shafting control for permanent magnet synchronous motor systems using sliding-mode observer.” *Control Theory & Applications Iet* 9.3(2015):456-464.

[12] Koren, Y., and C. C. Lo. “Variable-Gain Cross-Coupling Controller for Contouring.” *Annals of the Cirp* 40.1(1991):371-374.

[13] Perez-Pinal, F. J, G. Calderon, and I. Araujo-Vargas. “Relative coupling strategy.” *IEEE International Electric Machines & Drives Conference2003*.

[14] Liu, Ran, et al. “Research on Multi-Motor Synchronization Control Based on the Ring Coupling Strategy for Cutterhead Driving System of Shield Machines.” *Applied Mechanics & Materials* 52-54(2011):65-72.

[15] Chen, He, Yongchun Fang, and Ning Sun. "Optimal trajectory planning and tracking control method for overhead cranes." *IET Control Theory & Applications* 10.6 (2016): 692-699.

[16] Dantas, Amanda Danielle O. da S., et al. "PID control for electric vehicles subject to control and speed signal constraints." *Journal of Control Science and Engineering* 2018 (2018).

[17] Liu, Yan-Jun, et al. "Neural network control-based adaptive learning design for nonlinear systems with full-state constraints." *IEEE transactions on neural networks and learning systems* 27.7 (2016): 1562-1571.

[18] S. Dzung, H. Duy, and T. Seo, "Nonlinear adaptive control based on fuzzy sliding mode technique and fuzzy-based compensator," *ISA Trans.*, vol. 70, pp. 309–321, 2017.

[19] Bu, Wenshao, Xiaofeng Zhang, and Fangzhou He. "Sliding mode variable structure control strategy of bearingless induction motor based on inverse system decoupling." *IEEJ Transactions on Electrical and Electronic Engineering* 13.7 (2018): 1052-1059.

[20] Vaidyanathan, Sundarapandian, and Ahmad Taher Azar. "Takagi-Sugeno fuzzy logic controller for Liu-Chen four-scroll chaotic system." *International Journal of Intelligent Engineering Informatics* 4.2 (2016): 135-150.

[21] De Silva, Clarence W. Intelligent control: fuzzy logic applications. CRC press, 2018.

[22] https://images.app.goo.gl/vfveGJx7eqtAdvUq5

[23] Tan, Siew-Chong, Yuk-Ming Lai, and Chi-Kong Tse. "Introduction to Sliding Mode Control." *Sliding Mode Control of Switching Power Converters. CRC Press*, 2018. 17-34.

[24] Yang, Bo, et al. "Robust sliding-mode control of wind energy conversion systems for optimal power extraction via nonlinear perturbation observers." *Applied Energy* 210 (2018): 711-723.

[25] https://images.app.goo.gl/ZVNfmRdi5ZbT7cpt8

[26] Yorgancioglu, Ferhun, and H. Komurcugil. "Decoupled sliding-mode controller based on time-varying sliding surfaces for fourth-order systems." *Expert Systems with Applications* 37.10(2010):6764-6774.

[27] Cui, Rongxin, et al. "Extended State Observer-Based Integral Sliding Mode Control for an Underwater Robot With Unknown Disturbances and Uncertain Nonlinearities." *IEEE Transactions on Industrial Electronics*64.8(2017):6785-6795.

[28] Du, Haibo, et al. "Discrete-Time Fast Terminal Sliding Mode Control for Permanent Magnet Linear Motor." *IEEE Transactions on Industrial Electronics* PP.99(2018):1-1.

[29] Feng, Yong, et al. "Speed Control of Induction Motor Servo Drives Using Terminal Sliding-Mode Controller." *Advances in Variable Structure Systems and Sliding Mode Control—Theory and Applications. Springer, Cham*, 2018.

341-356.

[30] L. B. Li, L. L. Sun, S. Z. Zhang, and Q. Q. Yang, “Speed. tracking and synchronization of multiple motors using ring coupling control and adaptive sliding mode control,” *ISA Trans.*, vol. 58, pp. 635–649, 2015.

[31] Zhao, D. Z. , C. W. Li , and J. Ren . “Speed synchronization of. multiple induction motors with adjacent cross-coupling control.” *IET Control Theory & Applications* 4.1(2010):119.

[32] L. Li, L. Sun, and S. Zhang, “Mean deviation coupling synchronous control for multiple motors via second-order adaptive sliding mode control,” *ISA Trans.*, vol. 62, pp. 222–235, 2016.

[33] Zhao, Wei , X. M. Ren , and S. Wang . “Parameter Estimation-Based Time-Varying Sliding Mode Control for Multi-Motor Driving Servo Systems.” *IEEE/ASME Transactions on Mechatronics* (2017):1-1.

[34] A. Sabanovic, “Variable Structure Systems With Sliding Modes in Motion Control—A Survey,” in *IEEE Trans. Indus. Infor.*, vol. 7, no. 2, pp. 212-223, May 2011.

[35] H. Ji, X. Liu, Z. Song, and Y. Zhao, “Time-varying sliding mode guidance scheme for maneuvering target interception with impact angle constraint,” *Journal of the Franklin Institute*., , pp,9192-9208 ,2017.

[36] Mao, Xiang , H. Zhang , and D. Han. “T-S fuzzy control for a quad-rotor UAV.” *Control Conference IEEE*, 2015.

[37] Domínguez-Navarro, J. A., et al. “Fuzzy-logic strategy control for switched reluctance machine.” 2018 Thirteenth International Conference on Ecological Vehicles and Renewable Energies (EVER). IEEE, 2018.

[38] Sastry, Shankar. Nonlinear systems: analysis, stability, and control. Vol. 10. Springer Science & Business Media, 2013.

[39] Y. Feng, Minghao Zhou, X. Zheng, F. Han and X. Yu, “Terminal sliding-mode control of induction motor speed servo systems,” 2016 14th International Workshop on Variable Structure Systems (VSS)., Nanjing, 2016, pp. 351-355.

[40] Guo, Xinchen, Z. Liang, and C. Li. “Finite time tracking control of mobile robot based on non-singular fast terminal sliding mode.” *Systems Science & Control Engineering* 6.1(2018):492-500.

[41] Van, Mien. “An enhanced robust fault tolerant control based on an adaptive fuzzy PID-nonsingular fast terminal sliding mode control for uncertain nonlinear systems.” *IEEE/ASME Transactions on Mechatronics* 23.3 (2018): 1362-1371.

[42] Mendel, Jerry M., et al. Introduction to Type-2 Fuzzy Logic Control: Theory and Applications. 2014.

[43] Li, Hongyi, et al. “Adaptive Sliding Mode Control for Interval Type-2 Fuzzy Systems.” *IEEE Transactions on Systems Man & Cybernetics Systems* 46.12(2017):1654-1663.

[44] Lü, Hui, et al. “Finite-Time Containment Control of Nonlinear Multi-Agent Systems with Non-Singular Terminal Sliding Mode.” 2018 *Australian & New Zealand Control Conference (ANZCC). IEEE*, 2018.

[45] Li, Shengbo, et al.“Nonsingular and Fast Terminal Sliding Mode Control Method.” *Information and Control* Volume 355, no.18, 2009.(Chinese)

[46] Zhao, Cheng, and L. Guo. “PID controller design for second order nonlinear uncertain systems.” *Science China(Information Sciences)*60.2(2017):022201.

[47] Van, Mien. “An enhanced robust fault tolerant control based on an adaptive fuzzy PID-nonsingular fast terminal sliding mode control for uncertain nonlinear systems.” *IEEE/ASME Transactions on Mechatronics* 23.3 (2018): 1362-1371.

[48] Zheng, Jinchuan , et al. “Robust motion control of a linear motor positioner using fast nonsingular terminal sliding mode.” *IEEE/ASME Transactions on Mechatronics* 20.4(2015):1743-1752.

[49] Nasiri, Mojtaba, Saleh Mobayen, and Quan Min Zhu. “Super-Twisting Sliding Mode Control for Gearless PMSG-Based Wind Turbine.” *Complexity* 2019 (2019).

[50] J. A. Moreno and M. Osorio, “Strict Lyapunov Functions for the Super-Twisting Algorithm,” *IEEE Transactions on Automatic Control*., vol. 57, no. 4, pp. 1035-1040, April 2012.

[51] Liang, Qilian, and Jerry M. Mendel, “Interval Type-2 Fuzzy Logic Systems: Theory And Design” ,IEEE Transactions on Fuzzy systems 8(5),pp. 535-550, 2000

[52] Wu, Dongrui, and Jerry M. Mendel. “Similarity measures for closed general type-2 fuzzy sets: overview, comparisons, and a geometric approach.” IEEE Transactions on Fuzzy Systems27.3 (2018): 515-526.

[53] Mendel, Jerry M., et al. Introduction to Type-2 Fuzzy Logic Control: Theory and Applications. 2014.

[54] https://images.app.goo.gl/wRLNE9G7wJvjGrX89

[55] https://images.app.goo.gl/eGg7gxuJXT2Miqd8A

[56] Sun, Zhe, et al. “Type-2 fuzzy sliding mode anti-swing controller design and optimization for overhead crane.” *IEEE Access* 6 (2018): 51931-51938.

[57] Rajhans, Akshay, et al. “Graphical Hybrid Automata with Simulink and Stateflow.” *Proceedings of the 21st International Conference on Hybrid Systems: Computation and Control (part of CPS Week). ACM*, 2018.

[58] Wang, Yongshuang, et al. “Fuzzy Sliding Mode Synchronous Control of Double-Container for Overhead Crane.” *2019 11th International Symposium on Advanced Topics in Electrical Engineering (ATEE). IEEE*, 2019.

Appendix A - Scientific Articles

Article: **Fuzzy Sliding Mode Synchronous Control of Double-Container for Overhead Crane.**

This article has been accepted and presented at the IEEE ATEE 2019 the 11th International Symposium on Advanced Topics in Electrical Engineering, March 28-30, Bucharest, Romania. The article has been published in IEEE Xplorer.

ATEE is the forum that stimulates active and effective exchange of information between researchers in various areas of theoretical and applied electrical engineering. Key leaders from private and state-owned companies involved in will also be in attendance.

THE 11th INTERNATIONAL SYMPOSIUM ON ADVANCED TOPICS IN ELECTRICAL ENGINEERING
March 28-30, 2019
Bucharest, Romania

Fuzzy Sliding Mode Synchronous Control of Double-Container for Overhead Crane

Yongshuang Wang[1,2], Octavian Adrian Postolache[1], Weimin Xu[2*], Shaohua Ye[3], Dongchen Ni[1,2] and Meisu Zhong[1,2]

1. ISCTE-University Institute of Lisbon, Lisbon, Portugal
2. Shanghai Maritime University, Shanghai, China
3. Xian Jiaotong University, Xian, China

*wmxu@shmtu.edu.cn

***Abstract*- The double-container overhead crane can grab two forty-inch containers at one time, greatly improving the efficiency of loading and unloading. However, the overhead crane system is unstable due to perturbation of system parameters and other uncontrollable factors. So, it is difficult to achieve synchronous control of twin-lift container. In order to deal with this problem, this paper proposes a synchronous control method for double containers of bridge crane, which based on the combination of mean deviation coupling synchronization control and fuzzy sliding mode control. The Takagi-Sugeno fuzzy control is used to estimate the uncertainty of the system effectively, which suppresses the chattering problem of the sliding mode control in the approaching stage. Finally, the stability of the controller proposed in this paper is proved by Lyapunov's theorem, and the effectiveness of the controller is demonstrated by using Matlab.**

***Keywords*: Bridge crane; Fuzzy control; Time-varying sliding mode; Synchronous control**

I. INTRODUCTION

The emergence of double-container overhead crane has greatly improved the loading and unloading efficiency of port automation terminals, but there are still many problems. The overhead crane system has the characteristics of time-varying and non-linearity. During its operation, the parameters of the system will be perturbed, and the system will be subject to uncertain disturbance. Due to the special nature of its work, the potential energy load driven by the two spreaders will vary in height. This makes it difficult to synchronize the control of the double-container overhead crane.

At present, there are few researches on the synchronous control of the potential energy load of the double-container overhead crane[1]. In order to solve the above problems, the combination of the synchronous control strategy and the tracking control strategy is used to control the system of double-container overhead crane. The synchronous control strategy is designed to eliminate the error between the double spreaders, while the tracking control strategy is designed to eliminate the tracking error of the single spreader. The main control categories of synchronous control of the motor are divided into mechanical coaxial and mechanical non-coaxial methods. However, because the mechanical coaxial control method has large mechanical loss and low control precision, this paper chooses the synchronous control method of mechanical non-coaxial. In recent decades, a variety of different synchronization control strategies have been proposed, including parallel strategy [2], master-slave strategy [3], virtual shaft control [4], coupling strategy [5] and so on. Among them, cross-coupling control [6] is widely used in industry, and its principle is to feed back the speed or position difference of two motors to the motor. The multi-axis synchronous control method based on adjacent cross-coupling proposed in reference[7] can make the tracking error and synchronization error converge in a short time. However, its proposed cross-coupling strategy can only reflect the difference between adjacent motors and cannot take care of the difference between all motor speeds. In view of this, the average deviation coupling control strategy proposed in [8] takes into account the speed difference of all running motors. Moreover, the control structure of this method is simple, and the response speed of the system is fast.

In reference[9], a nonlinear PID combined with improved cross-coupling two-axis synchronous controller is proposed to reduce the error caused by the misalignment of the two axes and improve the synchronization of the two axes. However, its proposed method of nonlinear PID control ignores the parameter identification of the system. If the system encounters load changes or is disturbed by external disturbances during operation, its control accuracy is low and its robustness is weak. Inspired by the reference [10], this paper explores a control method with high precision, insensitivity to parameter perturbation and strong robustness. Reference [11] proposes an adjacent cross-coupling control architecture with sliding mode control, which can converge the tracking error and synchronization error of the system. Reference [12] combines the ring-coupling control strategy with sliding mode control in the synchronous control system of multiple motors, but the system parameters in the equivalent control law need to be preset in advance, and the parameter perturbation is not taken into account. Double-container overhead crane synchronous control system is a kind of nonlinear system that is difficult to obtain accurately model. In view of this, the reference [13] proposed a fuzzy adaptive sliding mode variable structure control to track and

978-1-7281-0101-9/19/$31.00 ©2019 IEEE

control the aircraft. The algorithm is based on time-varying sliding mode control method, and the universal approximation theory of fuzzy system is selected. The uncertain parameters in the aircraft system model and the unknown function caused by external disturbance are effectively estimated, which improves the accuracy of system tracking.

Aiming at the requirements of the above-mentioned problems, the fuzzy sliding mode algorithm based on average deviation coupling is proposed to solve the above problems. The algorithm effectively suppresses the chattering problem of sliding mode control in the approaching stage and has a certain inhibitory effect on the uncertain disturbance. Finally, the effectiveness of the algorithm is demonstrated by Matlab simulation.

II. PROBLE FORMULATION

The double-container overhead crane consists of a system of double spreaders, spare wheel, lifting rope and drive motors (Figure 1). Each spreader system is equipped with a drive motor, a lifting rope and a spreader. The spreader is driven by an induction motor. During the operation of an overhead crane, if two drive motors produce changes in system parameters, they will not be at the same angle or position. This causes the double spreaders to not run synchronously, which can cause the container to collide and is very dangerous. Therefore, it is important to keep the two spreaders running at the same time, that is, keep the two drive motors running synchronously. Taking the spreader i as an example, when the rotor field is oriented, the spreader i drives the motor to rotate synchronously, and the nonlinear mathematical model in the d-q coordinate system can be written as [14]:

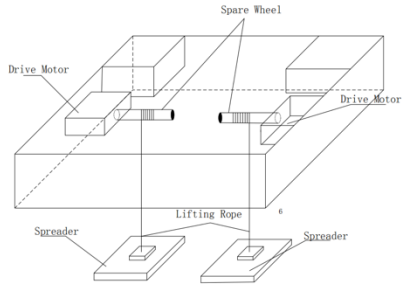

Fig.1 Double-container overhead crane structure diagram

$$\frac{d}{dt}\begin{bmatrix}\dot{\theta}\\ \psi_{dr}\\ i_{ds}\\ i_{qs}\end{bmatrix}=\begin{bmatrix}\mu(t)\psi_{dr}i_{qs}-\frac{1}{J}\left[B_m(\dot{\theta})\theta+G+\tau_f(\dot{\theta})+\tau_d(t)\right]\\ -\alpha(t)\psi_{dr}+\alpha(t)Mi_{qs}\\ -\gamma i_{ds}+\alpha(t)\beta(t)\psi_{dr}+n_p\dot{\theta}i_{qs}+\frac{\alpha(t)Mi_{qs}^2}{\psi_{dr}}\\ -\gamma i_{qs}+\beta(t)n_p\dot{\theta}\psi_{dr}-n_p\dot{\theta}i_{qs}+\frac{\alpha(t)Mi_{qs}i_{ds}}{\psi_{dr}}\end{bmatrix}+\frac{1}{\sigma L_s(t)}\begin{bmatrix}0&0\\0&0\\1&0\\0&1\end{bmatrix}\begin{bmatrix}u_{ds}\\u_{qs}\end{bmatrix} \quad (1)$$

Table1 Model variable representation

variable	Symbol
mechanical angular position	θ
d-axis rotor flux	ψ_{dr}
d-axis stator currents	i_{ds}
q-axis stator currents	i_{qs}
d-axis stator voltages	u_{ds}
q-axis stator voltages	u_{qs}
pole pair number	n_p
moment of inertia	J
nonlinear viscous drag coefficient	$B_m(\dot{\theta})$
external nonlinear perturbation torque	$\tau_d(t)$
the friction torque	$\tau_f(t)$
motor leakage inductance coefficient	$\mu_i(t),\beta_i(t),\alpha_i(t),\gamma_i(t)$

For the design of the controller and the smooth operation of the system, all the above parameters should be selected from the number in R.

The equation for the electromagnetically controlled torque T_c is described as:

$$T_c=\frac{3n_p\left(\psi_{dr}+\left(L_d-L_q\right)i_{ds}\right)i_{qs}}{2} \quad (2)$$

Where L_q and L_d are the inductances of the q-axis and the d-axis, respectively.

The model of the induction motor can be described as:

$$J\ddot{\theta}(t)+B_m\dot{\theta}(t)+G_i=T_c \quad (3)$$

By using the field-oriented mechanism with i_d^* =0 [15], we can obtain:

$$T_c=K_T i_{qs} \quad (4)$$

$$K_T=\frac{3n_p\psi_{dr}}{2} \quad (5)$$

In order to facilitate the design of the controller, the motor reference model is as follows:

$$J_r\ddot{\theta}_r(t)+B_{mr}\dot{\theta}_r(t)=K_{Tr}i_{qsi} \tag{6}$$

Where J_r is the moment of inertia, B_{mr} is the reference viscosity coefficient, θ_r is the reference rotation angle position, K_{Tr} is the reference electromagnetic torque coefficient, i_{qsi} is the reference control input.

The reference model of the motor obtained by equation (1)(6) as follows:

$$\ddot{\theta}_i=A(t)\dot{\theta}_i+L(t)i_{qs} \tag{7}$$

Where $A(t)=-B_{mr}/J_r$, $L(t)=K_{Tr}/J_r$, and B_{mr} and K_{Tr} are parameters of the system that change with time.

Based on the above motor reference model (7), the model parameters are estimated online using the principle of fuzzy control. Combined with the sliding mode control, the synchronization error e and the tracking error e_c between the two spreaders can be quickly converged. At the same time, the two spreaders can move synchronously to the desired position.

III. CONTROLLER DESIGN

The double-container overhead crane system is characterized by time-varying nonlinearity and strong coupling, and is a typical nonlinear system. The structure of the synchronous controller proposed in this paper is shown in Figure 2. The system is mainly composed of fuzzy sliding mode controller and mean deviation coupling controller.

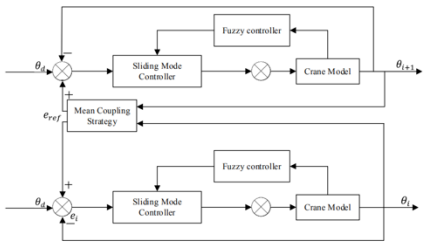

Fig.2 Controller structure diagram

The fuzzy control system is robust and insensitive to parameter perturbations. So, the basic idea of the control system is to use the fuzzy control method to fuzzify the control switching law and optimize the design of the control law, thereby further suppressing the chattering in the approaching stage of sliding mode control.

A. Sliding Mode Controller Design

The mean deviation coupling synchronization error of the spreader i is:

$$e_i(t)=\theta_i(t)-\frac{\sum_{j=1}^{n}\theta_j(t)}{n} \tag{8}$$

The tracking error of the spreader i is defined as:

$$e_{ref,i}(t)=\theta_d(t)-\theta_i(t) \tag{9}$$

By the mean deviation coupling error and tracking error of the spreader i, the sliding surface is defined as:

$$s(t)=c_1\dot{e}_{ref}(t)+c_2e_{ref}(t)+c_3\dot{e}_i(t)+c_4e_i(t) \tag{10}$$

Wherec_1、c_2、c_3、c_4 $\in R^+$.

Take the exponential approach law as follows:

$$u(t)=-\rho\mathrm{sgn}(s(t))-ks(t) \tag{11}$$

Where ρ∈ R+, $sgn(s(t))$ is a sign function. For the convenience of calculation, mark $sgn(s(t))$ as $sgn(s)$.

In order to suppress the chattering of the sliding mode in the approaching phase, it is considered to replace the symbol function with a saturation function. The saturation function is defined as follows:

$$sat(S)=\begin{cases}1 & S>\zeta\\ \dfrac{S}{\zeta} & |S|<\zeta\\ -1 & S<-\zeta\end{cases} \tag{12}$$

Where ξ∈ R+.

Consider Eq.11 as:

$$u(t)=-\rho sat\left(\frac{s(t)}{\zeta}\right)-ks(t) \tag{13}$$

Where ρ∈ R+, k∈ R+. The size of ρ determines the chattering of the sliding mode in the approaching phase, so ρ should not be too large.

For the convenience of calculation, mark $sat(s(t)/\zeta)$ as $sat(s)$.

We can obtain:

$$\begin{aligned}\dot{s}&=c_1\ddot{e}_{ref}+c_2\dot{e}_{ref}+c_3\ddot{e}_i+c_4\dot{e}_i\\&=c_1(\ddot{\theta}_d-\ddot{\theta}_i)+c_2(\dot{\theta}_d-\dot{\theta}_i)+c_3\ddot{e}_i+c_4\dot{e}_i\\&=c_1\ddot{\theta}_d+c_2\dot{\theta}_d+c_3\ddot{e}_i+c_4\dot{e}_i-c_1\ddot{\theta}_i-c_2\dot{\theta}_i\end{aligned} \tag{14}$$

$$\dot{s}=-\rho sat(s)-ks \tag{15}$$

Substituting (7) and (14) into (15), the control law can be expressed as:

$$\begin{aligned}&i_{qs}(t)=\\&L_1^{-1}(\theta_i,t)\left[\gamma_iB_{mr}k_{Tr}\left(c_1\ddot{\theta}_d+c_2\dot{\theta}_d+c_3\ddot{e}_i+c_4\dot{e}_i+\rho sat(s)+ks\right)\right]\\&-c_1\gamma_iB_{mr}k_{Tr}\dot{\theta}_iA(\theta_i,t)+c_2\gamma_iJ_rk_{Tr}\ddot{\theta}_i\end{aligned} \tag{16}$$

$$
\begin{aligned}
\dot{V}_1 &= s\left(\frac{1}{\gamma_i B_{mr} k_{Tr}} i_{qs}\left(\hat{L}_1\left(\theta_i,\delta_L^*\right)-\hat{L}_1\left(\theta_i,\delta_L\right)\right)\right.\\
&\quad +c_1\dot{\theta}_i\left(\hat{A}\left(\theta_i,\delta_A^*\right)-\hat{A}\left(\theta_i,\delta_A\right)\right)+\beta\left(\theta_i\right)-ks\\
&\quad \left.-\rho sat\left(\frac{s}{\alpha}\right)\right)+\eta_A^T\dot{\eta}_A+\eta_L^T\dot{\eta}_L\\
&= s\left(\frac{1}{\gamma_i B_{mr} k_{Tr}} i_{qs}\left(\hat{L}_1\left(\theta_i,\delta_L^*\right)-\hat{L}_1\left(\theta_i,\delta_L\right)\right)\right.\\
&\quad \left.c_1\dot{\theta}_i\left(\hat{A}\left(\theta_i,\delta_A^*\right)-\hat{A}\left(\theta_i,\delta_A\right)\right)-\rho sat\left(\frac{s}{\alpha}\right)-ks+\beta\left(\theta_i\right)\right)\\
&\quad -c_1\dot{\theta}_i\eta_A^T s\phi\left(\theta\right)-\frac{1}{\gamma_i B_{mr} k_{Tr}}\eta_L^T s\phi\left(\theta_i\right)i_{qs}\left(t\right)\\
&= s\left(c_1\dot{\theta}_i\left(\left(\delta_A^*\right)^T\phi\left(\theta_i\right)-\delta_A^T\phi\left(\theta_i\right)\right)-\rho sat\left(\frac{s}{\alpha}\right)-ks+\beta\left(\theta_i\right)\right.\\
&\quad \left.+\frac{1}{\gamma_i B_{mr} k_{Tr}} i_{qs}\left(\left(\delta_L^*\right)^T\phi\left(\theta_i\right)-\delta_L^T\phi\left(\theta_i\right)\right)\right)\\
&\quad -c_1\dot{\theta}_i\eta_A^T s\phi\left(\theta\right)-\frac{1}{\gamma_i B_{mr} k_{Tr}}\eta_L^T s\phi\left(\theta\right)i_{qs}\left(t\right)\\
&= s\left(c_1\dot{\theta}_i\eta_A^T\phi\left(\theta_i\right)+\frac{1}{\gamma_i B_{mr} k_{Tr}} i_{qs}\eta_L^T\phi\left(\theta_i\right)-\rho sat\left(\frac{s}{\alpha}\right)-ks+\beta\left(\theta_i\right)\right)\\
&\quad -c_1\dot{\theta}_i\eta_A^T s\phi\left(\theta\right)-\frac{1}{\gamma_i B_{mr} k_{Tr}}\eta_L^T s\phi\left(\theta\right)i_{qs}\left(t\right)\\
&= -\rho sat\left(\frac{s}{\alpha}\right)-ks+\beta\left(\theta_i\right)s\\
&\le\left(-\frac{\rho}{\alpha}-k+\beta\left(\theta_i\right)\right)|s|
\end{aligned}
$$

(36)

According to the fuzzy control theorem, it can be seen that the amount of beita is infinitely close to zero. ρ update as: $\rho=\varepsilon_0\left(-k+\beta\left(\theta_i\right)\right)\alpha$. When $\varepsilon_0>1$, $\dot{V}_1<0$ According to Lyapunov's law, the designed fuzzy sliding mode control system is globally asymptotically stable.

IV. Simulation and Results

In order to verify the usefulness of fuzzy sliding mode control for overhead crane systems, system model simulation was established by Simulink. The advantages of the control method are achieved by comparing the tracking error of the drive motor, the synchronization error and the position of the motor.

According to the control method proposed in this paper, two cases of fuzzy control and no fuzzy control are set, and the simulation of double-container synchronous control is carried out.

Case 1 Sliding mode control based on double-container overhead crane system with or without fuzzy control. The load G_1 of the container 1 is set to 2 N/m, the load $G_2$of the container 2 is set to 2 N/m, and the desired angle is θ = 10 rad. It can be seen from Fig. 3 that after the overhead crane system is controlled by the ordinary sliding mode, when the drive motor of the overhead crane reaches the specified value, the tracking error of the system has a 30% overshoot, which indicates that the system is unstable. The synchronization error converges to around $2*10^{-4}$rad. The normal sliding mode control system lacks good stability, so there is a sudden change in the synchronization error at 5 s. But the system under fuzzy control solves this problem. It can be seen from Fig. 4 that after the overhead crane system is controlled by the fuzzy sliding mode, the tracking error has no overshoot and smoothly converges to zero after 1s of operation. The synchronization error converges to around $0.3*10^{-4}$rad.

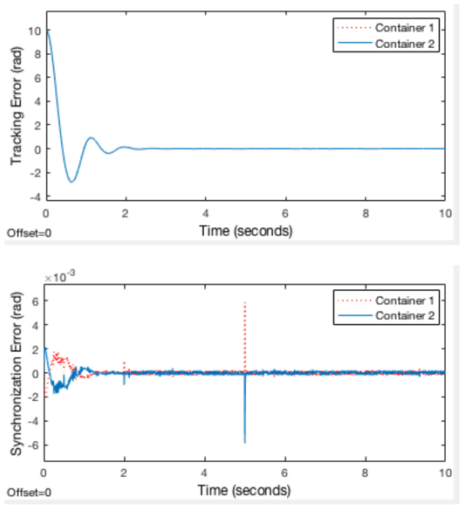

Fig.3 Tracking error and synchronization error after the system is controlled by sliding mode

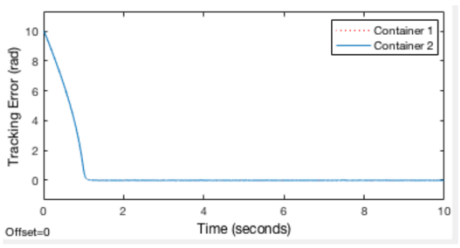

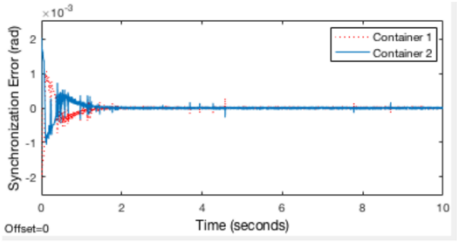

Fig.4 Tracking error and synchronization error after the system is controlled by fuzzy sliding mode

Case 2 Since the tracking error is more proof of the tracking performance of the system, the change of the synchronization error better proves the synchronization performance of the system. Therefore, in the simulation of the robustness of the system, this article chooses the synchronization error to prove. When the system parameters change, the robustness of the system is reflected by the synchronization error of the drive motors of the two spreaders. This simulation compares the robustness of the system with or without fuzzy control. The load G_1 of the container 1 is set to 2 N/m, the load $G_2$of the container 2 is set to 2 N/m, and the desired angle is $\theta = 10$ rad. At 5s, the viscosity coefficient B of the drive motor of the spreader is abruptly changed to two-thirds of the original, that is, $B^{`} = 2B/3$. After 5 s, the value of the synchronization error have changed. Figure 5 shows the synchronization error of the double spreader based on the common sliding mode control. Figure 6 is a partial enlarged view of the synchronization error after the viscosity coefficient is changed. It can be seen that the synchronization error hardly converges to zero after the system parameters are changed. This shows that the system is less robust. Figure 6 shows the synchronization error of the double spreader based on the fuzzy sliding mode control. Figure 8 is a partial enlarged view of the synchronization error after the viscosity coefficient is changed. Due to the addition of fuzzy control, the robustness of the system is enhanced. After changing the system parameters, the convergence of the synchronization error has not changed. It can be seen that the system has little change before and after 5 s.

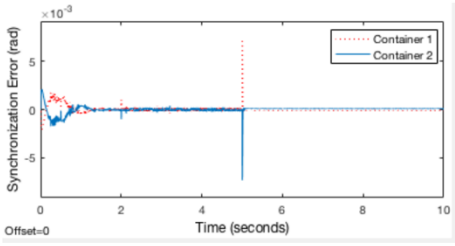

Fig.5 Synchronization error after the system is controlled by sliding mode

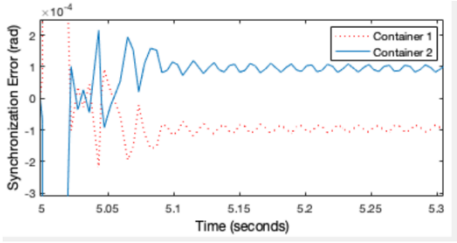

Fig.6 Partial enlargement after changing the viscosity coefficient

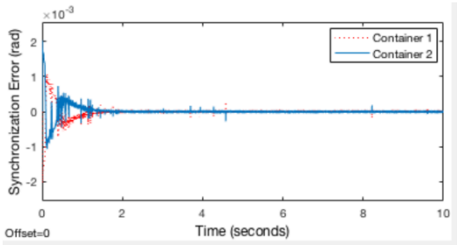

Fig.7 Synchronization error after the system is controlled by fuzzy sliding mode

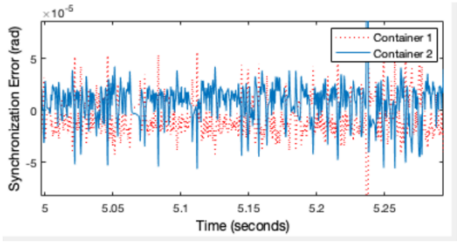

Fig.8 Partial enlargement after changing the viscosity coefficient

As can be seen from Figure 3 and Figure 4 above, the system using fuzzy control has a shorter settling time and a higher control accuracy of the synchronization error. It can be seen from Fig. 5 and Fig. 7 that when the system parameters change, the system using fuzzy control is more robust and almost unaffected.

Table2 Comparison between sliding mode control and fuzzy sliding mode control

	Tracking error convergence time	Synchronization error	Robustness
Sliding mode control	2.2s	$2 * 10^{-4}$rad	Weak
Fuzzy sliding mode control	1.1s	$0.3 * 10^{-4}$rad	Strong

V. CONCLUSION

This study demonstrates the effectiveness of the fuzzy sliding mode control scheme based on the mean deviation coupling on the synchronous control of the overhead crane. It solves the problem of parameter uncertainty and estimates system parameters online. Through the simulation results of the synchronization error, it can be seen that the improved sliding mode control has the characteristics of small steady-state error and strong robustness. However, the response speed of the system has not accelerated, and improvements are needed in subsequent studies.

REFERENCES

[1] X. Lai and D. Zhu. "Synchronization Control of Double Container Crane Based on Sliding Mode Control."*Control Engineering*, 2007(s3).145-147.

[2] He, Zelong , J. Bai , and C. Ma . "Conductance through a. parallel-coupled double quantum dot with a side-coupled quantum dot system." *Modern Physics Letters B*31.09(2017):1750095.

[3] Chen, Wu Hua , Z. Wang , and X. Lu . "On Sampled-Data Control for Master-Slave Synchronization of Chaotic Lur'e Systems." *IEEE Transactions on Circuits and Systems II: Express Briefs* 59.8(2012):515-519.

[4] Andert J. , et al. "Virtual shaft: Synchronized motion control for real time testing of automotive powertrains." *Control Engineering Practice* 56(2016):101-110.

[5] Zhao, D. Z. , C. W. Li , and J. Ren . "Speed synchronization of. multiple induction motors with adjacent cross-coupling control." *IET Control Theory & Applications* 4.1(2010):119-0.

[6] C. Chen and L. Chen, "Robust Cross-Coupling Synchronous Control by Shaping Position Commands in Multiaxes System," *IEEE Trans. on Indus.Elect.*, vol. 59, no. 12, pp. 4761-4773, Dec. 2012.

[7] Zhao, Wei , X. M. Ren , and S. Wang . "Parameter Estimation-Based Time-Varying Sliding Mode Control for Multi-Motor Driving Servo Systems." *IEEE/ASME Transactions on Mechatronics* (2017):1-1.

[8] L. Li, L. Sun, and S. Zhang, "Mean deviation coupling synchronous control for multiple motors via second-order adaptive sliding mode control," *ISA Trans.*, vol. 62, pp. 222–235, 2016.

[9] P. R. Ouyang, T. Dam, and V. Pano, "Cross-coupled PID control in position domain for contour tracking,"*Robotica,* vol. 33, no. 6, pp. 1351–1374, 2015.

[10] S. Dzung, H. Duy, and T. Seo, "Nonlinear adaptive control based on fuzzy sliding mode technique and fuzzy-based compensator," *ISA Trans.*, vol. 70, pp. 309–321, 2017.

[11] G.Zhong, Z.Zhi, and H.Deng, "Precise position synchronous. control of multi-axis servo system,"*IEEE Trans. on Indus. Elec., IEEE Trans. on Indus. Elec.,* vol. 64, pp.3707-3717,[5] 2017

[12] L. B. Li, L. L. Sun, S. Z. Zhang, and Q. Q. Yang, "Speed. tracking and synchronization of multiple motors using ring coupling control and adaptive sliding mode control," *ISA Trans.*, vol. 58, pp. 635–649, 2015.

[13] Mao, Xiang , H. Zhang , and D. Han . "T-S fuzzy control for a quad-rotor UAV." *Control Conference* IEEE, 2015.

[14] X. U. Wei-min and X. U. Pan, "Robust adaptive sliding mode synchronous control of double-container for twin-lift overhead cranes with uncertain disturbances," Control and Decision 2016,vol. 31, no. 7, pp. 1192–1198, 2016.

[15] D. Zhao, W. Ni, and Q. Zhu, "A framework of neural networks based consensus control for multiple robotic manipulators, " *Neurocomputing,*vol. 140, pp.8-18,2014.

[16] A. Sabanovic, "Variable Structure Systems With Sliding Modes in Motion Control—A Survey," in *IEEE Trans. Indus. Infor.*, vol. 7, no. 2, pp. 212-223, May 2011.

[17] H. Ji, X. Liu, Z. Song, and Y. Zhao, "Time-varying sliding mode guidance scheme for maneuvering target interception with impact angle constraint,"*Journal of the Franklin Institute*., Volume 355, no.18, pp,9192-9208 ,2017.

[18] K. D. Young, V. I. Utkin and U. Ozguner, "A control engineer's guide to sliding mode control," Proceedings. 1996, *IEEE International Workshop on Variable Structure Systems.*, pp. 1-14., 1996.

[19] J. A. Moreno and M. Osorio, "Strict Lyapunov Functions for the Super-Twisting Algorithm," *IEEE Transactions on Automatic Control.*, vol. 57, no. 4, pp. 1035-1040, April 2012.

[20] Y. Feng, Minghao Zhou, X. Zheng, F. Han and X. Yu, "Terminal sliding-mode control of induction motor speed servo systems," *2016 14th International Workshop on Variable Structure Systems (VSS).*, Nanjing, 2016, pp. 351-355.

[21] J. A. Moreno and M. Osorio, "Strict Lyapunov Functions for the Super-Twisting Algorithm," *IEEE Transactions on Automatic Control.*, vol. 57, no. 4, pp. 1035-1040, April 2012.

[22] J. Xu, Z. Guo and T. H. Lee, "Design and Implementation of Integral. Sliding-Mode Control on an Underactuated Two-Wheeled Mobile Robot,"'*IEEE Transactions on Industrial Electronics*, vol. 61, no. 7, pp. 3671-3681, July 2014.

[23] J. Yang, S. Li and X. Yu, "Sliding-Mode Control for Systems With Mismatched Uncertainties via a Disturbance Observer," *IEEE Transactions on Industrial Electronics*., vol. 60, no. 1, pp. 160-169, Jan. 2013.

[24] W. Zhao and X. Ren, "Parameter estimation-based coupling control for generalized cascade systems with guaranteed cost," *J. Franklin Inst.*, vol. 354, no. 4, pp. 1696–1721, 2017.